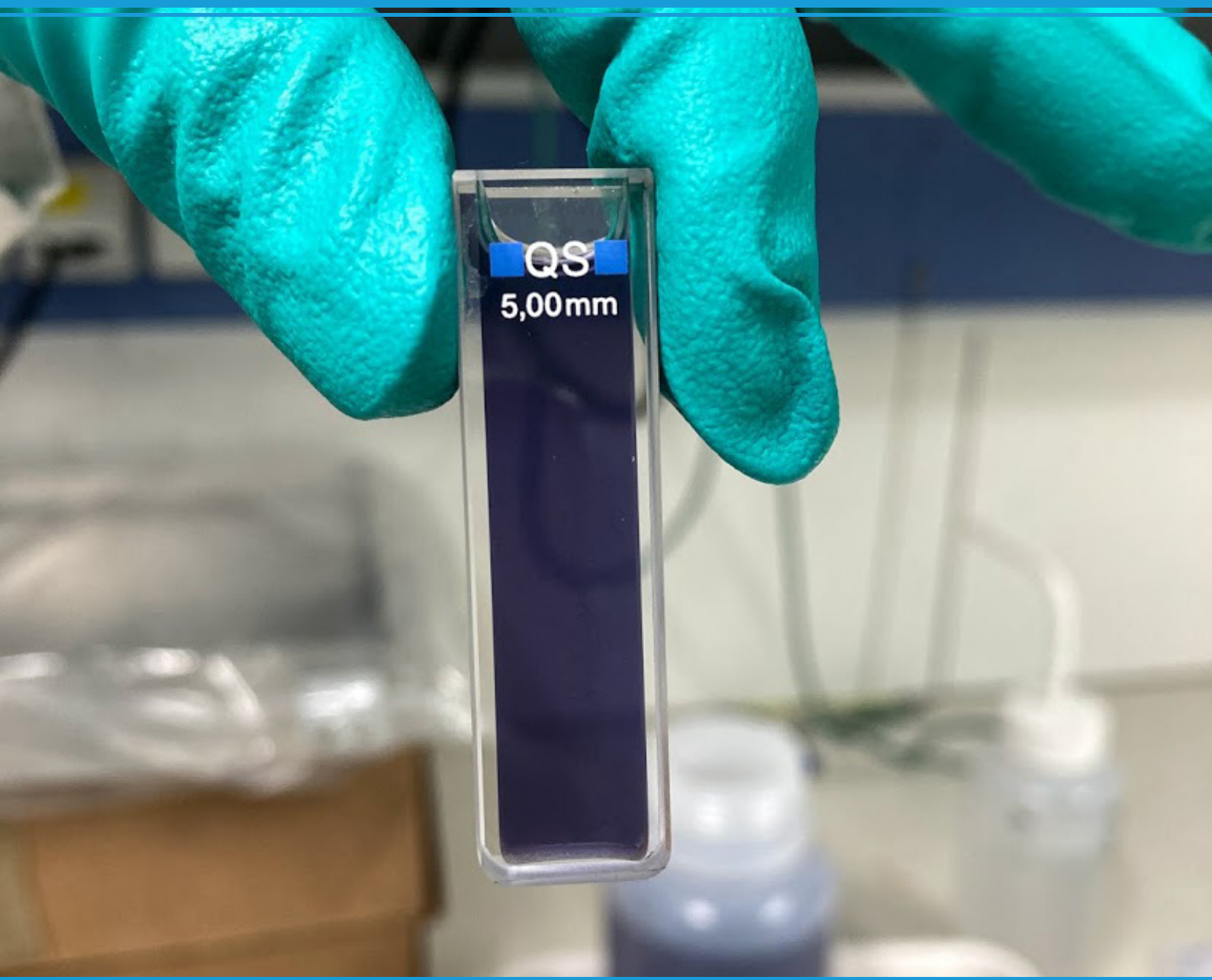


The effects of formate ion concentration on the complexation of Cr(III) in aqueous Cr(III) electrolytes from $\text{Cr}_2(\text{SO}_4)_3$ salts.

MSc Thesis Department of Material Science and Engineering



Master Thesis

The effects of formate ion concentration on the complexation of Cr(III) in aqueous Cr(III) electrolytes from $\text{Cr}_2(\text{SO}_4)_3$ salts.

Department of Material Science and Engineering at Delft University of Technology

Anouk van Lottum

March 26, 2021

Thesis committee:

Prof.dr.ir. J.M.C. Mol, TU Delft (Chairman)

M. V. E. Ankora, TU Delft

Dr. P. Dey, TU Delft

Dr. P. Taheri, TU Delft



Acknowledgment

Turning a master thesis into a successful project is not an easy task to accomplish. It was a special year with a lot of uncertainties, and there were many hurdles to overcome. Writing your thesis entirely from home in your room, without having coffee breaks at the university, small chitchats in the corridors and conducting experiments in quiet laboratories, was not always easy. However, when I started, I could not have imagined that the project would have ended in this field of expertise, providing me with the knowledge I possess now.

Throughout the year, I had the help of many people, too many to thank individually. First of all, I want to thank Maxine Ankora for all our weekly meetings, hours of instructions in the lab and her supervision. Secondly, I want to thank Arjan Mol for the supervision throughout the year being the chair of my project and offering me the opportunity to do my thesis work within the Corrosion Technology and Electrochemistry group at TU Delft. Although all our meetings were virtual, except for the first one, it was nice to have the supervision available.

Next, I want to thank Agnieszka Kooijman for her help in the lab, and small talks during my thesis, since the university was a quiet place during the summer break and throughout this year with covid-19. I also want to thank Alberto Ferrari for answering all my questions on DFT that helped me understand the theory and the implementation of DFT in my thesis, especially in the beginning.

Last but not least, I would especially like to thank my roommates, friends, and family for all the support throughout the year. This year has been an emotional rollercoaster, but these people have always offered a listening ear in difficult and happy times. Thank you all!

Anouk van Lottum, Delft, March 2021

Abstract

Trivalent chromium (Cr(III)) is one of the most promising non-toxic replacements for hexavalent chromium (Cr(VI)) coatings in the steel packaging industry. The application of a chromium layer to packaging steel is essential for providing a protective layer on the steel packaging's external surface area, which prevents corrosion during its use. However, the deposition process of Cr-metal from Cr(III) solution cannot produce a deposit thicker than 10 μm with sufficient corrosion and wear resistance without the application of a complexing agent.

This study provides both an experimental research as an comparative computational model. Experiments are set up to analyze the effect of the formate ion (HCOO^-) concentration as a complexing agent in $\text{Cr}_2(\text{SO}_4)_3$ electrolytes, which results are compared to the output of the used computational model. The results provide insights in the initial composition of species in plating electrolytes, which is essential for the determination of the deposition mechanism from Cr(III) electrolytes to improve the electroplating process.

Ligand exchange and bonding with HCOO^- in chromium complexes is studied with Ultraviolet-visible light (UV-VIS) spectroscopy and Attenuated Total Reflectance Fourier InfraRed spectroscopy (ATR-FTIR) at various concentrations of HCOO^- . Additionally, computational modelling is performed with Density functional theory (DFT) to predict the spontaneous character of various ligand substitutions, and simulations of spectroscopic spectra are performed as a reference to mimic the experimentally observed data.

It was found that ligand exchange with HCOO^- in $\text{Cr}(\text{SO}_4)_3$ solutions occurs spontaneously within two days at elevated temperatures at the analysed concentrations. The experimental data shows, there is a transition point in the complex formation between the ratio of $[\text{Cr}^{3+}]:[\text{HCOO}^-]$ respectively is $[1]:[1.61]$ and $[1]:[3.32]$. This indicates that the complex formation decreases past the ratio of $[\text{Cr}^{3+}]:[\text{HCOO}^-] = \text{c.a.}[1]:[3]$ and that the concentration at which the most chromium-formate complexes can be observed is within the range of $[\text{Cr}^{3+}]:[\text{HCOO}^-] = [1]:[1.61]$ to $[\text{Cr}^{3+}]:[\text{HCOO}^-] = [1]:[3.32]$. The formation of chromium-formate complexes is beneficial for the deposition process, as addition of formate increases the amount of chromium deposited on the steel surface. Furthermore, it is found that the presence of SO_4^{2-} , originating from the chromium salt, is beneficial for the ligand exchange of HCOO^- . Also, the bonding of formate to chromium is found to be as monodentate binding.

Contents

Acknowledgement	i
Abstract	iii
1 Introduction	1
2 Scientific motivation and research approach	4
2.1 Scientific motivation	4
2.2 Research questions	4
2.3 Research approach	5
2.3.1 UltraViolet Visible-light Spectroscopy	6
2.3.2 Attenuated Total Reflectance- Fourier Transform Infra-Red spectroscopy	9
2.3.3 Computational modelling	12
2.4 Thesis outline	13
3 Chemistry of Cr(III) in electrolytes	14
3.1 Chromium complexation in aqueous solutions	14
3.2 Quantum mechanical understanding of metal-ligand interactions	15
3.3 Ligand exchange mechanisms and characterisation	17
3.4 Effect of ligand exchange on the field splitting energy	18
3.5 Addition of formate as complexing agent	21
4 Process and operation conditions affecting solution chemistry	23
4.1 Electroplating basics	23
4.2 Temperature, pH and concentration	23
4.3 Kinetics of species in plating electrolytes and diffusion layer	24
5 Density-functional theory (DFT) computational calculations	27
5.1 Definition of a functional in DFT	27
5.2 Basis set	29
5.3 Geometry optimization & single point energy	30
5.4 Include solvent effects	30
5.5 Spectroscopic studies with DFT	32
6 Materials and methods	34
6.1 Materials	34
6.2 Methods	34
6.2.1 Ultra Violet visible spectroscopy (UV-VIS)	34
6.2.2 Attenuated Total Reflection ATR-FTIR	35
6.2.3 DFT Computational studies with ORCA	35
7 Results and discussion	38
7.1 Changes in the solution chemistry of $\text{Cr}_2(\text{SO}_4)_3$ solutions in addition of NaHCOO	38
7.1.1 UV-Vis experiments	38
7.1.2 ATR-FTIR experiments	41
7.2 Modelling of ligand substitution with DFT calculations	44
7.2.1 Point energy calculations	44
7.2.2 Molecular orbitals and bandgap	47

7.2.3	Polarizability	48
7.2.4	Simulated IR-spectra	49
7.2.5	Simulated UV-Vis spectra	53
7.3	Effect of formate and sulphate on $[\text{Cr}(\text{H}_2\text{O})_6]^{3+}$	57
8	Conclusions	60
9	Recommendations	64
A	Appendix: Background figures	75
B	Appendix: ATR-FTIR results	76
C	Appendix: DFT results	77

List of Figures

2.1	Chromium ion vs formate ions ratio [1]:[1] - [1]:[3] (water molecules are left out for convenience)	5
2.2	Visualisation focus area of the research techniques used in this study	6
2.3	UV-Vis spectra of 0.05 mol/L ⁻¹ CrCl ₃ solutions in addition of formic acid 0.025-0.1 mol/L ⁻¹ [1]. Line 1 fresh solution, line 2-6 represent solutions in addition of formic acid 0.025-0.1 mol/L ⁻¹	8
2.4	Explanation of possible shifts in the position and hight of λ_{Max} in UV-Vis spectra	8
2.5	Visualisation of ATR-FTIR (θ , incoming beam angle)[2]	9
2.6	FTIR spectra of Uranyl(VI)ion complexation with formate[3]	11
2.7	Overview of different systems using specific chromium salts: system 1 Cr ₂ (SO ₄) ₃ , system 2 Cr(ClO ₄) ₃ and system 3, where no anions are surrounding the Cr ion, only H ₂ O molecules. Also system 1 and 2 contain H ₂ O molecules, but these are left out for convenience	12
3.1	a) Hybridization of Cr(III) b) Octahedral symmetry	15
3.2	Splitting of the d orbitals with octahedral symmetry(CC BY-NC-SA)[4]	15
3.3	d_{xy}, d_{xz}, d_{yz} less destabilized orbitals and dx^2dy^2 and dz^2 destabilized orbitals with ligands on the axes(CC BY-NC-SA)[4])	15
3.4	a) Tanabe and Sugano diagram of d^3 transition metal, with the selected transitions for Cr(III) complexes[5] b) correlation diagram for d^3 transition metals created using the work of Lever[6]	16
3.5	Ligand substitutions reactions mechanisms with their accompanied change in volume of the first coordination sphere[7]	17
3.6	Difference inner and outer-sphere complex related to the bonding with a surface[8]	18
3.7	Electronic configurations of chromium cations in octahedral and tetrahedral coordination[9]	19
3.8	cis and trans isomers in octahedral symmetry, with A & B being different ligands[10]	20
3.9	Meridional(mer) and facial (fac) isomers in octahedral symmetry, with A & B being different ligands[10]	21
3.10	Chemical structure of formic acid and sodium formate[11]	21
4.1	Visualisation of interfacial area and bulk solution of a negatively charged metal in aqueous solution	24
4.2	Reaction of the hexaaqua ion of Cr ³⁺ undergoing dissociation and continuously condensation by means of hydroxo bridges[12]	25
5.1	Jacob's Ladder describing the different type of functionals[13]	27
5.2	Effect of d-polarization function added to a p orbital CC-BY-SA-3.0[14]	29
5.3	Substitution reaction of H ₂ O by HCOO ⁻ in Cr ³⁺ complex, visualized with Avogadro software	30
5.4	Difference between explicit and implicit solvation models[15]. ΔG , the free energy of solvation is calculated according to equation 15, H is the Hamiltonian of an system which is the operator corresponding to the total energy of that system . .	31
5.5	Theory behind implicit solvation models visualized, using slides from University of Helsinki[16], the cavity shape is defined according to figure 5.6	31
5.6	Visualisation of defining the cavity surface with Van der Waals surface, Solvent-Accessible Surface and Solvent-Excluded surface[17]	32
7.1	UV-Vis spectra of Cr ₂ (SO ₄) ₃ at pH 2.45 and room temperature, legend shows different ratios of [Cr ³⁺]:[HCOO ⁻]	38
7.2	Shift in the position of λ_{Max} of the second transition peak in Cr ₂ (SO ₄) ₃ solutions. Legend shows different ratios of [Cr ³⁺]:[HCOO ⁻]	39

7.3	Shift in the position of λ_{Max} of the first transition peak in $\text{Cr}_2(\text{SO}_4)_3$ solutions. Legend shows different ratios of $[\text{Cr}^{3+}]:[\text{HCOO}^-]$	39
7.4	Collected ATR-FTIR spectra of $\text{Cr}_2(\text{SO}_4)_3$ solutions with four ranges	41
7.5	Expanded FTIR spectra of the 3900 - 2500 cm^{-1} range	41
7.6	Expanded FTIR spectra of the 1800- 1500 cm^{-1} range	41
7.7	Expanded FTIR spectra of the 1500- 1200 cm^{-1} range	42
7.8	Expanded FTIR spectra of the 1200- 900 cm^{-1} range	43
7.9	Overview chromium-formate complexes used in the DFT calculations	44
7.10	Results DFT point energy calculations PW91 and CPCM solvation model	45
7.11	Results DFT point energy calculations PW91 and SMD solvation model	45
7.12	DFT point calculations of reactions 22 till 27 with PW91 and CPCM solvation model, in these reactions a hydroxide group is present in the complex, but a H_2O molecule will be substituted.	46
7.13	DFT point calculations of reactions 28 till 33 with PW91 and CPCM solvation model	47
7.14	Difference between HOMO en LUMO in Cr^{3+} complexes, simulated with functional PW91 and SMD solvation model with medium water	48
7.15	Simulated IR spectra PW91 CPCM(water)	50
7.16	Simulated IR spectra PW91 CPCM(water)	50
7.17	Simulated IR spectra PW91 CPCM(water)	50
7.18	Simulated IR spectra PW91 CPCM(water)	50
7.19	Simulated IR spectra PW91 CPCM(water)	51
7.20	Simulated IR spectra PW91 CPCM(water)	51
7.21	Simulated IR spectra PW91 CPCM(water)	51
7.22	Simulated IR spectra PW91 CPCM(water)	51
7.23	Simulated IR spectra PW91 CPCM(water)	52
7.24	Experimental ATR-FTIR spectra of $[\text{Cr}^{3+}]:[\text{HCOO}^-] = [1]:[1.21]$	52
7.25	Simulated absorption spectra of $[\text{Cr}(\text{H}_2\text{O})_6]^{3+}$ with PW91 CPCM(water), without the presence of HCOO^- molecules.	54
7.26	Simulated absorption spectra of $[\text{Cr}(\text{H}_2\text{O})_5(\text{HCOO})]^{2+}$ with PW91 CPCM(water)	54
7.27	Simulated absorption spectra of <i>cis</i> - $[\text{Cr}(\text{H}_2\text{O})_4(\text{HCOO})_2]^+$ with PW91 CPCM(water)	55
7.28	Simulated absorption spectra of <i>trans</i> - $[\text{Cr}(\text{H}_2\text{O})_4(\text{HCOO})_2]^+$ with PW91 CPCM(water)	55
7.29	Simulated absorption spectra of <i>mer</i> - $[\text{Cr}(\text{H}_2\text{O})_3(\text{HCOO})_3]$ with PW91 CPCM(water)	55
7.30	Simulated absorption spectra of <i>fac</i> - $[\text{Cr}(\text{H}_2\text{O})_3(\text{HCOO})_3]$ with PW91 CPCM(water)	55
7.31	Simulated absorption spectra of $[\text{Cr}(\text{H}_2\text{O})_2(\text{HCOO})_4]$ with PW91 CPCM(water)	56
7.32	Simulated absorption spectra of $[\text{Cr}(\text{H}_2\text{O})(\text{HCOO})_5]$ with PW91 CPCM(water)	56
7.33	Simulated absorption spectra of $[\text{Cr}(\text{HCOO})_6]$ with PW91 CPCM(water)	56
7.34	Experimental UV-Vis spectra of $[\text{Cr}^{3+}]:[\text{HCOO}^-] = [1]:[1.61]$	56
7.35	UV-Vis spectra of $\text{Cr}(\text{ClO}_4)_3$ in addition of SO_4^{2-} (no pH adjustment), legend defines the ratio of $[\text{Cr}^{3+}]:[\text{SO}_4^{2-}]$	57
7.36	Shift in the position of λ_{Max} of the second transition peak in $\text{Cr}(\text{ClO}_4)_3$ solutions, legend defines the ratio of $[\text{Cr}^{3+}]:[\text{SO}_4^{2-}]$	58
7.37	Shift in the position of λ_{Max} of the first transition peak in $\text{Cr}(\text{ClO}_4)_3$ solutions, legend defines the ratio of $[\text{Cr}^{3+}]:[\text{SO}_4^{2-}]$	58
A.1	Range of water exchange rate constants and mean lifetime (H_2O) for primary shell water molecules on aqua metal ions at 25 °C (the dotted line represents Taube's inert/labile boundary[7]	75
A.2	Visualisation of solvation-shells around metal-ion[7], X can be an example of additional compounds introduced in the system	75

B.1	ATR-FTIR Data of (incorrect) first batch $\text{Cr}(\text{OH})\text{SO}_4$ solutions in addition of NaHCOO for comparison of similar results	76
C.1	Results DFT point energy calculations BP86 reaction 16 till 21	77
C.2	Vibrational spectra analysis of chromium-formate complexes	77
C.3	Vibrational spectra analysis of chromium-formate complexes	78
C.4	Results TD-DFT with B3LYP of a) $[\text{Cr}(\text{H}_2\text{O})_6]^{3+}$ b) $[\text{Cr}(\text{H}_2\text{O})_5(\text{HCOO})]^{2+}$ c) <i>trans</i> - $[\text{Cr}(\text{H}_2\text{O})_4(\text{HCOO})_2]^+$ d) <i>cis</i> - $[\text{Cr}(\text{H}_2\text{O})_4(\text{HCOO})_2]^+$ e) <i>fac</i> - $[\text{Cr}(\text{H}_2\text{O})(\text{HCOO})_3]$ f) <i>mer</i> - $[\text{Cr}(\text{H}_2\text{O})(\text{HCOO})_3]$ g) $[\text{Cr}(\text{H}_2\text{O})_2(\text{HCOO})_4]^-$	78

List of Tables

2.1	Expected bonds in vibrational spectra of $\text{Cr}_2(\text{SO}_4)_3$ electrolytes in addition of NaHCOO	11
6.1	$\text{Cr}_2(\text{SO}_4)_3$ solutions in addition of HCOONa	34
6.2	$\text{Cr}(\text{ClO}_4)_3$ solutions in addition of Na_2SO_4	35
7.1	Isotropic polarizabilities of molecules in $\text{Cr}(\text{III})$ electrolytes of this study	48
C.1	DFT point calculations of reactions 16 till 21 with PW91 and PB86 and CPCM solvation model	77
C.2	DFT point calculations of reactions 16 till 19 with PW91 and PB86 and SMD solvation model	77
C.3	DFT point calculations of reactions 22 till 27 with PW91 and PB86 and CPCM solvation model	78
C.4	DFT point calculations of reactions 28 till 33 with PW91 and PB86 and CPCM solvation model	78

1 Introduction

Over the years, the demand for packaging materials increases due to economic welfare increase and changing living standards. In particular, the need for metal packaging materials increases due to European environmental standards and the recycling opportunities of metals[18]. Steel packaging materials are more frequently recycled compared to other packaging materials such as plastics. Since 2017, 82,5 per cent of the steel packaging materials were recycled, compared to only 42 per cent of the plastics[19]. Besides the improved environmental effects such as lower carbon emissions, the use of recycled metal saves up to 70% in energy[19]. In addition, metals are not consumed during their life cycle and can be re-used several times during recycling[20].

Steel is one of the predominantly used metals for packaging. The main advantages of steel over alternative materials are the unique strength, formability and durability of the material[21]. Therefore, steel is a suitable and widely used packaging material for final user product, such as food & beverage, cosmetics and healthcare[22]. Despite the promising advantages of steel as a packaging material, the material is vulnerable to corrosion[23]. The packaging material's internal surface is in contact with the packed content, for example, canned food or soda drinks. As a result, corrosion will occur, if no protection is adopted in the steel packaging. This protection is needed to prevent the packaging's degradation and counteract contamination of the packaged substance by corrosion products. To protect the steel packaging, a protective layer of chromium is applied to the steel packaging's whole external surface area. Electrodeposition of a thin duplex coating composed of chromium and chromium oxide to the external steel surface is a widely applied method to construct this protective layer[24]. This protective layer results in increased corrosion resistance. Furthermore, the chromium coating improves the adhesion for an additional protective organic polymer topcoat, which functions as a barrier layer to obtain better corrosion protection. Finally, the coating increases the wear resistance, hardness and provides an attractive bright appearance for consumers[25].

Traditionally, the deposition of a chromium layer on packaging steel is applied by electrodeposition from aqueous hexavalent chromium (Cr(VI)) baths. One company employing this electrodeposition process is Tata Steel. The process is well-known as Electro Chromium Coated Steel (ECCS). However, studies carried out in the late 19th century already showed severe health issues caused by the use of hexavalent chromium, particularly for the health conditions of employees working with this material. Only a few years ago, strict European REACH regulations on hexavalent chromium were set up, which oblige the packaging industry to adjust their processes and shift towards a safer alternative[26]. New alternatives to the use of hexavalent chromium need to be investigated. The alternative should be non-toxic while being as competitive as the traditional ECCS in terms of providing corrosion resistance and durability of the material[26].

Trivalent chromium (Cr(III)) is one of the most promising research directions for a non-toxic replacement for hexavalent chromium[19]. Commercial electroplating with trivalent chromium is already applied since the mid- 1970s for decorative coatings[27]. However, decorative coatings have decreased mechanical properties and a reduced corrosion resistance and are therefore not suitable as functional hard chromium coating in the packaging industry[28]. Studies carried out on trivalent chromium show a possibility to improve the mechanical properties and corrosion resistance and thereby make trivalent chromium suitable as a functional coating. Although trivalent and hexavalent chromium coatings are both mainly composed of chromium, the deposition process, electrolyte composition and characteristics are different. Unlike most other metals

that can be electroplated, trivalent chromium cannot be deposited from an aqueous solution containing only chromium ions[29]. Additional chemical compounds, for example complexing agents or conducting salts, are required for successful deposition of a coating.

This study focuses on formate (HCOO^-), which is a common complexing agent for trivalent chromium. After the dissolution of sodium formate (NaHCOO) in aqueous solution, sodium (Na^+) and formate dissociate and an equilibrium of formate and formic acid (HCOOH) forms depending on the pH of the solution[30]. The pKa value of the equilibrium between $\text{HCOO}^-/\text{HCOOH}$ is 3.45[30]. Therefore, at pH values below 3.45 more formic acid will be present in the electrolytes. It has been found that in the addition of sodium formate to the electrolyte, chromium carbides are introduced into the deposit creating a deposit which is characterised by an amorphous structure [31, 32, 33]. In the electrolytes, the formate ion is the only carbon containing species. Therefore, the layer composed from chromium carbides (chromium and carbon) indicates that the formate ion must play an active role in the deposition process of trivalent chromium. However, the exact reaction mechanism and how formate ion concentration influences the deposition process and species in solution is unknown. Before the reaction mechanism of Cr(III) can be determined, it is of great importance to know the initial species participating in the deposition process. Therefore, the main goal in this thesis is to investigate the effect of formate ion concentration on the complexation of Cr(III), to be able to determine the initial complexes participating in the deposition of a chromium layer.

The creation of Cr(III) electrolytes is possible from different chromium salts, for example CrCl_3 , $\text{Cr}_2(\text{SO}_4)_3$ and $\text{Cr}(\text{NO}_3)_3$ are observed in relevant studies on chromium and formate[34, 27, 35, 36]. The type of chromium salt defines the anions that will be present in the investigated system. In this study the focus lies on $\text{Cr}_2(\text{SO}_4)_3$ solutions, since these are used and studied by Tata Steel. In a study of Wijenberg et al. the electrodeposition of a mixed chromium metal-carbide-oxide coatings from a trivalent chromium-formate electrolyte of $\text{Cr}_2(\text{SO}_4)_3$ is studied without a buffering agent[27]. Investigating a similar system as Wijenberg et al. is considered promising, since successful results were achieved for the development of a chromium metal-carbide-oxide coatings. The specific system investigated does not only contain formate as complexing agent and Cr(III) and SO_4^{2-} from the chromium salt, but also conducting salts are supplemented to the electrolyte to increase the conductivity of the plating bath. A common conducting salt used by Tata Steel is sodium sulphate (Na_2SO_4). When $\text{Cr}_2(\text{SO}_4)_3$ is used as chromium salt and Na_2SO_4 is used as conducting salt, sulphate ions (SO_4^{2-}) are extensively present in the electrolyte. Therefore, the goal in this thesis is to not only investigate the effect of formate ion concentration in $\text{Cr}_2(\text{SO}_4)_3$ electrolytes, but also investigate the effect that sulphate might have on the complexation process.

The role of formate as a complexing agent has been studied earlier by Zeng et al.[37][1] in Cr(III) solutions from CrCl_3 . However, experimental studies on the effect of complexing agent concentration and the bonding between chromium and formate is limited, especially for solutions created with $\text{Cr}_2(\text{SO}_4)_3$. The reduction mechanisms of Cr(III) have been studied by Voys et al.[38] and Del piana et al.[36] with and without the addition of a complexing agent. It is observed by Del piana that the ratio of complexing agent vs. chromium influenced the reduction mechanism. However, there is no information on how the concentration of complexing agent is related to the active chromium-formate complexes in the electrolytes. In this study, the goal is to investigate the effect of complexing agent (formate ion) concentration on the complexes formed in the electrolyte. This information is considered critical for the determination of the deposition mechanism of Cr(III)-complexes.

This thesis includes experimental studies with UV-Vis and FTIR to study the effect of formate ion concentration on the ligand substitutions in chromium-formate complexes. In addition, Density Functional Theory (DFT) calculations are performed to study the spontaneous or unspontaneous character of a ligand substitution reaction with point energy calculations, and Time-dependend DFT (TDDFT) and frequency analysis are performed to generate spectroscopic spectra as an attempt to mimic the experimental spectra conducted in this work.

2 Scientific motivation and research approach

In this chapter, the scientific motivation and research approach of this study will be discussed. This study's experimental techniques will be addressed separately in the research approach, explaining each technique extensively with some scientific background and important parameters to consider. At the end of this section, the thesis outline will be explained.

2.1 Scientific motivation

Electro-deposits of chromium are applied to a wide range of products to improve durability by enhancing corrosion and wear resistance[39]. As packaging steel is continuing to play an essential role in achieving climate goals[19], the protection of this substrate steel cannot be neglected. However, the deposition process of trivalent chromium is too little understood to be successfully used as functional chromium coating. It is difficult to deposit a layer thicker than 10 μm [34] at a good quality due to the decreasing efficiency of the plating bath, especially when no complexing agents are added[40]. Therefore, creating a better understanding of Cr(III) in aqueous solutions and the effect of possible complexing agents is considered critical for the development of a non-toxic replacement for hexavalent chromium[19].

It is observed that by the addition of sodium formate, carbides are introduced in the deposit[31, 32, 33]. Since sodium formate is the only possible source of these carbides, it is expected that sodium formate plays a dominant role in chromium's deposition process and that it participates in the electrolytes' initial composition of species that become deposited. However, how the formate ion concentration affects the initial composition of species in the plating bath and what this composition is, is unknown. Before the reaction mechanism of Cr(III) can be fully understood, the chromium's initial and final form needs to be determined to backtrack the steps in between. Research has been performed on the microstructure and characteristics of a deposit of Cr(III). However, the connection between the electrolytes' composition and the formed deposits from similar electrolytes is missing. To determine the reduction mechanism of Cr(III) it is considered critical to consider the initially formed complexes and the effect of complexing agent concentration since it is expected that the addition of a complexing agent is not beneficial at all concentrations.

These uncertainties show this project's relevance, investigating the effect of formate ion concentration on the complexation of the Cr(III) ion to complement the currently available studies on the plating process from trivalent chromium.

2.2 Research questions

This thesis aims to provide new insights into the complexation behaviour of Cr(III) ions in aqueous solutions made of chromium sulphate as Cr(III) salt and sodium formate additions as a complexing agent. The use of chromium sulphate as trivalent chromium salt and the addition of conducting salts, which also often include sulphate, causes sulphate ions to be present in the system of interest. From other studies it is observed that sulphate can bond to chromium[41], which might suggest that sulphate is able to affect the complex formed with chromium. However, according to Mandich, the tendency to bond to chromium is higher for formate than sulphate, but it does not provide information about the possible effects of both species in the same electrolyte[29]. Therefore, it is considered essential to determine the possible effect of sulphate on chromium complexation with formate, as both species will be included in plating electrolytes.

Another effect that is important to consider is the pH of the electrolytes. From other complexation studies with, for example, Uranyl and formate, it is observed that the electrolyte's pH influences the complexation in the solutions[42]. Besides, one of the common problems occurring during the plating process from Cr(III) electrolytes is an increase of the local pH around the electrode as a result of hydrogen evolution[43]. As this is the area the chromium metal will be deposited, understanding the effect that pH might have on the complex formed is important for understanding the reaction mechanism. Therefore, it is important to consider the effect of pH in the system. In this study experiments are conducted at similar pH to exclude possible pH effects on the complexes formed and make sure the results are comparable.

The research questions of this project are listed below:

- What is the effect of the formate ion concentration on the possible complexation and ligand substitution reactions in Cr(III) electrolytes?
- Is the effect of formate ion concentration different in the presence of sulphate, originated from the Cr-salt?
- Can DFT computational studies be used in predicting complexion and substitution reactions?

2.3 Research approach

This thesis's research approach will be considering individual complexes of chromium ions with their molecules in their surrounding, and how these interact. The study will be carried out in three parts, firstly the effect of the formate ion concentration will be tested in electrolytes originating from $\text{Cr}_2(\text{SO}_4)_3 \cdot 15\text{H}_2\text{O}$ as chromium salt. The notation of the 15 H_2O molecules in the chemical equation of this hydrated salt will be ignored through the report for convenience. The first step will be creating aqueous solutions from this chromium salt and adding sodium formate in a specific range of concentrations, where the formate and chromium ion have a specific ratio towards each other, visualized in figure 2.1. This approach is chosen, as it is expected that a certain amount of formate molecules can bind to the metal ion to form a chromium-formate complex. However, the amount of formate molecules that can form a coordinate covalent bond with the chromium ion in this complex is unknown. Therefore, the bonding and effect of ligand exchange will be studied with spectroscopic techniques.

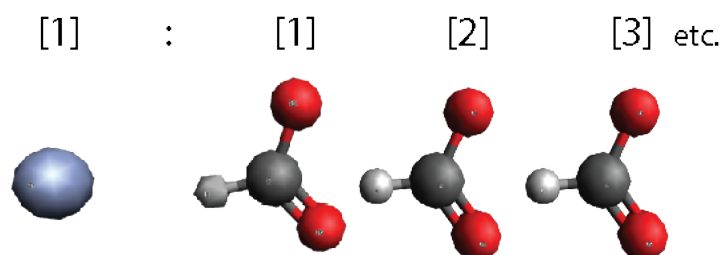


Figure 2.1: Chromium ion vs formate ions ratio [1]:[1] - [1]:[3] (water molecules are left out for convenience)

Chromium is a first row transition metal, and the oxidation state of 3+ (Cr(III)) accommodates three electrons in its d-shell. Spectroscopic techniques are well suited to investigate solutions of transition metals since the promotion of an electron to an excited state, called a

transition, in the d-shells of these metals often occur in the visible light region[44]. Individual molecules of formate or sulphate show no transitions in this region. Therefore, the transitions in the visible light range can fully be attributed to the chromium complex.

The exchange of species surrounding the chromium ion in solution affects the observed transitions due to the system's changed energy. This change in energy can indicate a change of species connected to the Cr-atom. **UltraViolet Visible-light (UV-Vis) spectroscopy** is a technique suitable to study the transitions in the visible light and near visible light region. Therefore, this technique is suitable to study the effect of formate ion concentration on possible changes of species surrounding the Cr-atom. As UV-Vis only gives information on alterations around Cr-atom environment, other techniques need to be considered providing more information in the bonding with formate.

Formate is an organic group of which the vibrations of the bonds can be well studied in the infra-red light range. Free formate in solution and formate connected to a larger molecule, for example, a chromium complex, vibrate at a different frequencies. Equation 1 gives the relation between wavelength λ , c speed of light and ν the velocity (frequency). According to equation 1 a higher frequency is observed at a lower wavelength.

$$\lambda = c/\nu \quad (1)$$

As a result, formate connected to a chromium ion and formate free in solution will show absorption peaks at different wavelengths. Therefore, the effect of formate concentration on bonding between formate and chromium can be well studied with **Fourier Transform Infra-Red spectroscopy**.

The specific complex formed and ligand substitution reactions in solutions containing chromium and formate are unknown. Therefore, the ligand substitution reactions will also be studied by simulating the possible exchange reactions with Density Functional Theory (DFT) calculations. The benefits of using computational modelling is that it can help understand the spectroscopic studies' experimental outcome of this study. Figure 2.2 gives an overview of the three main research techniques used in this study and the focus of the specific techniques. Subsequently, the following three subsections will provide more extensive information on how these techniques going to be used and what parameters need to be considered when conducting the experiments.

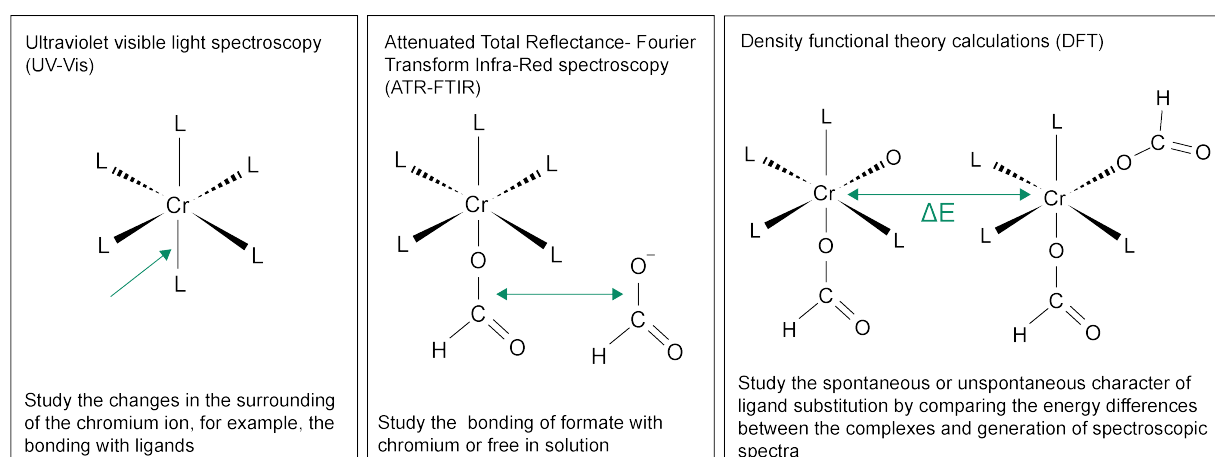


Figure 2.2: Visualisation focus area of the research techniques used in this study

2.3.1 UltraViolet Visible-light Spectroscopy

In UV-Vis, the solution of interest is investigated in a compartment (cuvette) with a known path length for the light. Light with a specific wavelength, mainly in the visible light region, passes through the compartment filled with the solution of interest, and energy from the light is used to promote an electron from a bonding or non-bonding orbital into one of the empty anti-bonding orbitals[45]. The measurement's output is a spectrum where absorption peaks can be observed, representing electron transitions. The x-axis shows the wavelength at which the absorption peaks are measured. The y-axis shows the measured absorption of the species. This is according to the Lambert-Beer's law given in equation 2, where A is the absorbance, ϵ is the molar absorption coefficient ($M^{-1}cm^{-1}$), c the molar concentration (M) and l the path length (cm) of the cuvette used in the experiment. Equation 3 shows the relation between the wavelength and the energy. In this equation E is the energy, h the Planck's constant, c the speed of light and λ the wavelength of the light. It can be observed that the wavelength and energy are inversely proportional.

$$A = \epsilon cl \quad (2)$$

$$E = hc/\lambda \quad (3)$$

According to equation 2, a solution with a higher concentration shows an increased absorption value. Therefore, in this study, the electrolytes investigated have similar chromium concentrations. In case different concentrations are used, the absorbance values will be converted to molar absorption coefficient for the comparison.

Other parameters that might affect the UV-Vis measurements are temperature and pH. Firstly the effect of temperature is discussed. According to Lever 1968, the UV-Vis spectra of some materials are temperature dependent[6]. As a result, a shift in the absorbance maximum (λ_{Max}) to higher or lower values can be observed, depending upon whether the slope of $dE/d(Dq)$ is positive or negative[6]. The variable Dq is the octahedral crystal field parameter, which is connected to the charge of the metal, the distance of ligands and metal, and the radial electron density of the d-electrons[6, 44]. This variable will be discussed more extensively in chapter 3. It is also possible that $dE/d(Dq)$ is independent of temperature. In this study, it is chosen to perform all experiments at room temperature. Therefore the effect of temperature on the experimental results can be neglected.

Secondly, the effect of pH on the observed UV-Vis spectra. As the system's pH increases or decreases, species in solution can become protonated or deprotonated. Especially if the molecule of interest has functional groups with exchangeable protons like hydroxy, amines, or carboxylates, the spectrum will change if the pH is adjusted[46]. Besides, it is possible that by adjusting the pH value, the equilibrium of the system shifts at which another chromium-formate complex becomes favourable. In this study, it is chosen to perform all experiments at a pH of 2.45 to make sure the results are comparable. This value is chosen as it is in-between experimentally found pH values of 2.3-2.8 performed by Tata Steel[24].

At constant concentration, temperature and pH, the shift in λ_{Max} is expected to be caused by changes in the chromium complex, related to an increase or decrease of energy in complex. According to equation 3, a complex with higher energy, λ_{Max} is found at lower wavelengths. These differences in energy are caused by the change in species surrounding the chromium ion. Why and how the wavelength is affected by the species surrounding the chromium ion is de-

scribed in more depth in chapter 3.2.

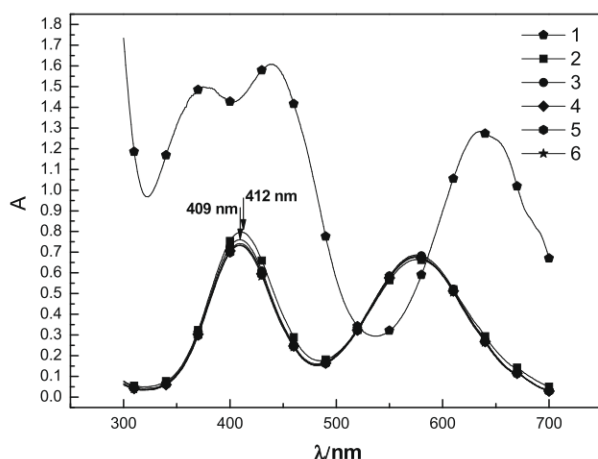


Figure 2.3: UV-Vis spectra of 0.05 mol/L^{-1} CrCl_3 solutions in addition of formic acid $0.025\text{-}0.1 \text{ mol/L}^{-1}$ [1]. Line 1 fresh solution, line 2-6 represent solutions in addition of formic acid $0.025\text{-}0.1 \text{ mol/L}^{-1}$

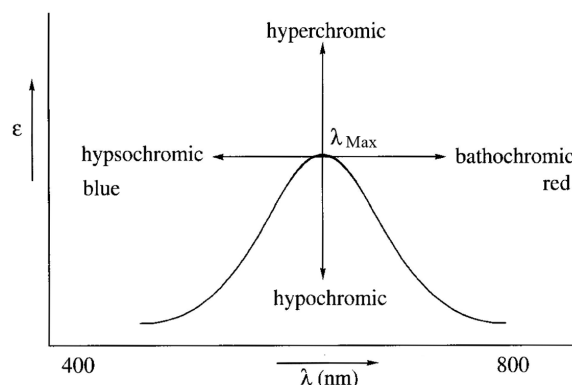


Figure 2.4: Explanation of possible shifts in the position and height of λ_{Max} in UV-Vis spectra

In figure 2.3, a spectra of CrCl_3 solutions is given. Line 1 presents the spectra of a fresh solution of CrCl_3 and lines 2-6 represent solutions with the addition of formate in various concentrations[1]. The range that is collected is 300-700 nm, in which two transition peaks can be observed. The first observed peak is in the 550-600 nm range and the second peak is in the 400-450 nm range. In studies where formate is added to Cr(III) electrolytes, a shift of the peaks in the spectra can be observed[1]. This shift is often described with the following terms: **hypsochromic** or **bathochromic** and **hyperchromic** or **hypochromic**. A visualisation of these shifts is given in figure 2.4. In this study the focus mainly lies on the hypsochromic or bathochromic shift, as this shift is correlated with a higher or lower energy complex and a change in the band gap of the d-orbitals. A red bathochromic shift, is connected to a lower energy complex and a smaller splitting in the d-orbitals. The blue hypsochromic shift is connected to a higher energy complex and a smaller splitting in the d-orbitals. How exactly a change in the d-orbitals is correlated to UV-Vis spectra is explained in section 3

In this study, only the interpretation of the first two transition peaks of Cr(III) are included. As often, the third transition peak is observed outside the visible light spectrum and in the low ultraviolet range of the spectrum ($<280 \text{ nm}$). One method of interpretation of the UV-Vis spectra is by studying the allowed transitions in the d-orbitals with a **Tanabe Sugano diagram**, which is described more extensively in section 3.2. However, in this section, some other scientists' theories on the transition peaks in the UV-Vis spectra of coordinated transition metals are discussed.

Firstly, it can be concluded that there is no general agreement on the origin of the observed peaks[47]. However, the opinions of various authors may find the point of agreement in attributing the second band (400-450 nm) to the coordination of electrons[47].

Secondly, an interesting assumption taken by Mead is that origin of the first band and the

second band could not be attributed to the same cause[47]. However, Mead sees no support for the theory of Lifschitz and Rosenbohm, where the first band was attributed to the metal ion and the second to the coordinated groups. The hypothesis that is proposed by Mead is that the differences in the two bands represent different states of excitation of the coordination electrons[48]. As in the large majority of cases, both observed absorption bands were influenced by changing the metal or one or more of the co-ordinated ligands[48].

Mead observed that in stable complexes, for example, in Cr^{3+} , plotting of the λ_{Max} at the progressive replacement of oxalate ions by ethylenediamine produces regular shifts in the positions of λ_{Max} [48]. Therefore, in this study λ_{Max} will be plotted with an increasing ratio of formate to see if a regular change can be observed. When a regular shift in λ_{Max} can be observed this can indicate a substitution of multiple HCOO^- groups to the Cr^{3+} ion.

Thirdly, Tsuchida's main conclusion explains the shift of λ_{Max} in the first band by postulating that the electron transitions are more or less depressed by the negative field of the surrounding species[47]. Therefore, molecules with large dipole moments or anions with larger polarizabilities must bring larger depressions and give a larger shift[47]. The type of this shift, bathochromic or hypochromic, depends on the initial species and replacing species in the substitution reaction. It is expected that anions in a solution with higher polarizability, which is a measurement of ease to distort the electron cloud of an atom, will have more overlap of electron clouds and cause more electron-electron interactions. The differences in polarizability between this study's anions will be calculated and discussed in chapter 5.

Finally, the complexes connected to species situated far apart in the **spectrochemical series**, which is the general order of ligands strength[49] discussed in section 3, have broader and less symmetrical first bands than those containing only one kind of ligand[47]. Considering this last statement, if one of the H_2O molecules in $[\text{Cr}(\text{H}_2\text{O})_6]^{3+}$ complex is replaced by HCOO^- it is expected that the band gets slightly wider. It is not precisely determined yet where formate is placed in this order, but it is expected to be close to H_2O , as the nature of bonding is by an oxygen atom. At the end of this study, the relative position of formate, sulphate and water will be determined.

2.3.2 Attenuated Total Reflectance- Fourier Transform Infra-Red spectroscopy

In spectroscopy studies, UV-Vis only addresses a specific range of the light spectrum around 300–800 nm to study species at molecules and complexes' size. If the information on the type of bonds or functional groups in the molecule is required, Fourier-Transform Infrared spectroscopy (FTIR) can be used. In this study, Attenuated Total Reflection- Fourier Transform Infra-Red spectroscopy (ATR-FTIR) is used. The ATR accessory operates by measuring the changes that occur in an internally reflected beam. The crystal must be in direct contact with the sample[2]. An evanescent wave, visible in figure 2.5 is created, penetrating the sample a few microns to derive its chemical information[2].

A variety of materials can be used as ATR crystal, and typical examples include diamond, ZnSe (Zinc Selenium), KRS-5 (thallium iodide and thallium bromide mixed optical crystal), Silicon and Ge (Germanium)[50]. The type of crystal effects parameters such as the infra light's penetration depth into the sample or the intensity of the peaks[50]. Equation 4 shows how the penetration depth is related to the crystal's refractive index. In this equation, dp is the penetration depth of the infrared beam, n_1 is the refractive index of the crystal, n_2 is the refractive index of the sample, λ is the wavelength in air, and θ is the angle of incidence of the infrared

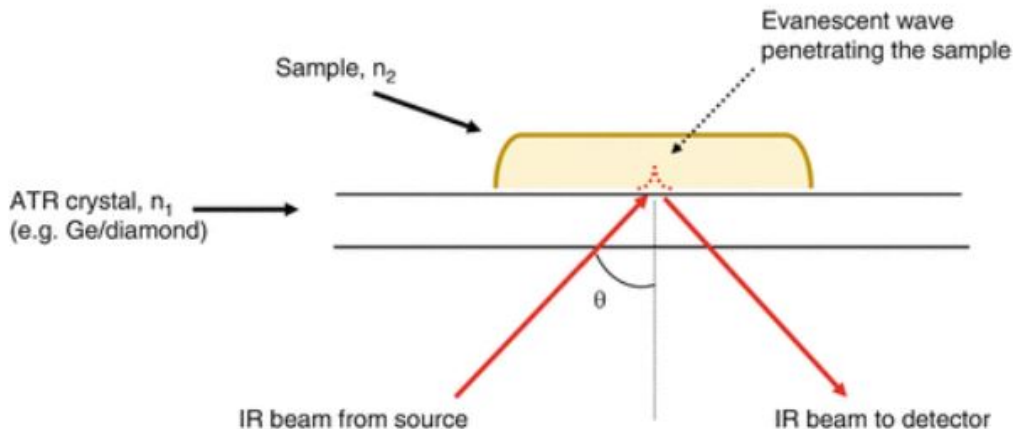


Figure 2.5: Visualisation of ATR-FTIR (θ , incoming beam angle)[2]

beam. According to equation 4, the penetration depth of the infrared light is proportional to the wavelength λ and is related to the crystal's material by n_1 . As a result, an increase of the crystal's refractive index will lead to a decrease in penetration depth and generate a weaker peak intensity[50].

$$dp = \frac{\lambda/n_1}{2\pi\sqrt{\sin^2\theta - (n_2/n_1)^2}}[50] \quad (4)$$

Two aspects to consider in the choice of crystal are the pH of the electrolytes and the crystal's solubility in water. Since the electrolytes used in this study are acidic 2.45, not all crystals are suitable in this range as this will damage the crystal. The crystal used in this study is a Germanium crystal, which is suitable in the acidic pH range and insoluble in water. The high refractive index of Germanium will cause a smaller penetration depth and measurement will show a lower intensity than when, for example, a ZnSe crystal is used. As a result, the measurement will mainly contain information on the interface between the crystal and the sample.

ATR-FTIR can be used to study the infrared range of the light spectrum around 4000-400 cm^{-1} (2500-25000 nm). The light used in this range of wavenumbers provides the energy at which stretching or bending of specific molecule groups can be observed, providing an idea of the molecule groups present in the material. As ATR-FTIR is sensitive for changes in the concentration, according to 2, it is important to investigate all solutions at similar chromium content. Also the effect of temperature is considered. According to Topala, the shape of the FTIR spectra of Ribavirin (antiviral agent) is influenced by a temperature change, they observe that with increasing temperature vibrational bands broad[51]. When the temperature of the compounds changes in the range 24 - 175 $^{\circ}\text{C}$, the half-width of the C=O, C-O, OH absorption bands in the IR spectra increases, the bands are shifted at higher wavenumbers and for C-O symmetrical, C-O asymmetrical bands are shifted at lower wave numbers. Similar bonds will be observed in this study. As the shifts observed are small (max 2 cm^{-1}), it is not expected that a small difference in temperature will effect the outcome of this study. However, all experiments of this study will be conducted at constant temperature (room temperature). In addition, the

experiments in this study will be conducted in two-fold to guaranty the reproducibility of the data.

A method to start analysing FTIR spectra is by assuming that the spectrum can be divided into two regions. The region below 1500 nm is called the fingerprint region, which is unique for each material[52]. The region above 1500 nm is the bond region, which can again be divided into regions of peaks corresponding to single, double and triple bonds. In this study mainly the the region above 1200 nm will be used for the interpretation of the data, since the single and double carbon bond of the formate groups will be visible in this region. In the spectra, the peak width, height and position are of interest for interpreting the data.

Table 2.1 gives the type of bonds in combination with their origins, which are expected to be present in the collected spectra with ATR-FTIR. The pKa value of $\text{HCOO}^-/\text{HCOOH}$ is 3.45[30]. Therefore, at the pH of 2.45, more HCOOH will be present in the electrolytes. By the addition of formate to the electrolytes, it is expected that more peaks can be observed in the spectra then without the addition of NaHCOO . The new peaks will correspond to the carbon-oxygen single and double bonds and a carbon-hydrogen single bond. With increasing formate ion concentration, the peaks corresponding to these bonds will increase due to the functional groups' rising concentration in the electrolyte.

Type of bond	Originating from
C-O	$\text{HCOO}^-/\text{HCOOH}$
S-O	SO_4^{2-}
H-O	$\text{H}_2\text{O}/\text{HCOOH}$
C-H	$\text{HCOO}^-/\text{HCOOH}$
C=O	$\text{HCOO}^-/\text{HCOOH}$
S=O	SO_4^{2-}

Table 2.1: Expected bonds in vibrational spectra of $\text{Cr}_2(\text{SO}_4)_3$ electrolytes in addition of NaHCOO

Comparable work performed with this technique in studying Cr(III) complexation with formate seems limited. However, a comparative study by Lucks et al., who studied the structural and photochemical behaviour of the complexation of uranyl(VI) ion with formate is found[3]. In figure 2.6 the results of their FTIR study can be observed, where the middle black line corresponds to the IR spectra in the presence of uranyl(VI) and formate in the pH range of 2.0 to 4.5[3]. In figure 2.6 it can be observed that there is a splitting of c.a 292 cm^{-1} between the COO^- modes of the U-formate series. This increased larger spectral splitting $\Delta(v_{\text{as}}-v_{\text{s}})$ of the COO^- modes around 1314 and 1608 cm^{-1} is a clear indication of uni coordination in uranyl(VI) formate[3]. In contrast, another study by Lucks et al. on uranyl(VI) acetate, a succinate small splitting value of c.a. 70 cm^{-1} was observed which is typical of bi-coordination[42]. It is found that the splitting in the symmetrical and asymmetrical vibration of V_{COO^-} goes according equation 5, where $\Delta v_{\text{a-s}}$ ionic is approximately $160\text{--}170 \text{ cm}^{-1}$ [53]. According to Ab initio molecular orbital calculations of Nara et al. the differences in the observed $\Delta v_{\text{a-s}}$ are attributed to changes in the CO bond length and the OCO angle[54]. The relation between the splitting of the V_{COO^-} modes and the type of binding is applied in multiple studies on metal ions[42, 53, 54, 55], and is considered very useful for this study.

$$\Delta v_{\text{a-s}}(\text{Unidentate}) > \Delta v_{\text{a-s}}(\text{Ionic}) > \Delta v_{\text{a-s}}(\text{Bridging}) > \Delta v_{\text{a-s}}(\text{Bidentate})[53] \quad (5)$$

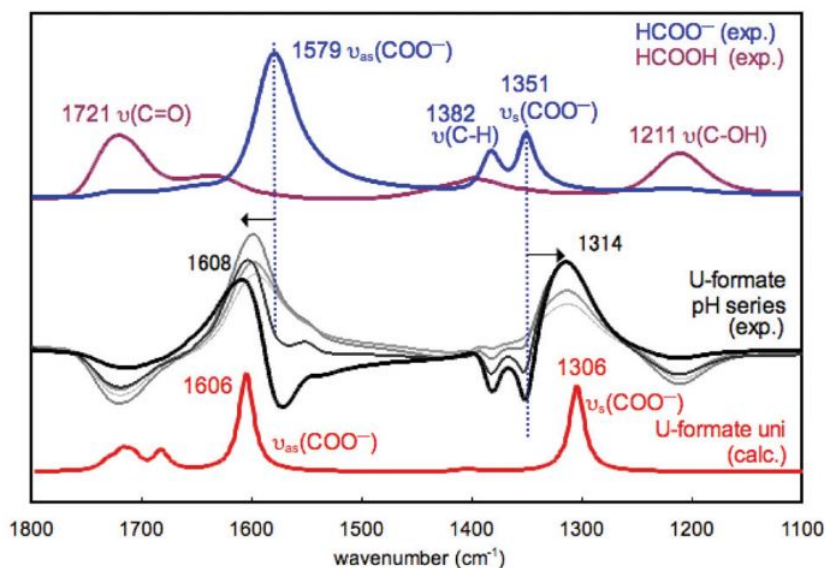


Figure 2.6: FTIR spectra of Uranyl(VI)ion complexation with formate[3]

In this study, there are two main focus points in interpretation of the data. First, the focus will be on the studying the expected shift in the vibrational modes of C-O, C=O (double-bonded) and C-H, as a result of the bonding between formate and chromium. Secondly, the splitting between ν_{ass} and ν_{s} of COO^- will be studied in the chromium-formate electrolytes as this splitting can provide information on the bonding between formate and chromium ions.

It is expected that formate only binds the Cr^{3+} ion by its oxygen atom with free electrons. Therefore, it is expected to observe a splitting of ν_{ass} and ν_{s} which is larger than 150 cm^{-1} according to Lucks and higher than $160\text{-}170 \text{ cm}^{-1}$ according to Nara to confirm the monodentate binding[3, 42, 53].

2.3.3 Computational modelling

Besides the presented spectroscopic techniques, the ligand substitution reactions will also be studied by simulating the possible exchange reactions with Density Functional Theory (DFT) calculations. The benefits of using computational modelling to simulate this study's different systems are that it can help understand the spectroscopic studies' experimental outcome. Besides, it can be used to study a specific individual system from which the structure is known. This can not be explored experimentally, as the experimental electrolytes will always have a large number of (different) complexes and the structure of these complexes is not always determined. However, a drawback of DFT is that the system described and calculated can differ from the real experimental composition, and that attention to both systems' comparability needs to be paid.

The DFT calculations in this study are used to predict the spontaneous or unspontaneous character of different ligand substitutions reactions and specific spectroscopic characteristics of the complexes. This data can be used as a comparison for the experimental data. The structure of the complex is one of the input parameters in DFT and should be known. Therefore, the calculations are performed considering a chromium-water system where only water molecules initially surround the chromium ion, as there is an overall agreement of the existence and structure of this $[\text{Cr}(\text{H}_2\text{O})_6]^{3+}$ complex. However, it should be mentioned that assuming a chromium-

water system with only water molecules as ligands is expected to be different from reality. In solutions created from $\text{Cr}_2(\text{SO}_4)_3$ as chromium salt, it is expected that sulphate will also be incorporated in the complex. However, this assumption is considered necessary due to the uncertainties in the chromium-sulphate complexes' chemical structure.

Therefore, to test if it is legitimate to address the complexation of the molecules in $\text{Cr}_2(\text{SO}_4)_3$ electrolytes as an complex with only H_2O ligands, solutions of $\text{Cr}(\text{ClO}_4)_3$ are used as a reference. The difference between these chromium salts is the type of secondary molecule introduced in the system, perchlorate ions instead of sulfate ions. Figure 2.7 gives an overview of the differences between $\text{Cr}_2(\text{SO}_4)_3$ and $\text{Cr}(\text{ClO}_4)_3$ as chromium salt and a system where no anions are present. The difference between perchlorate and sulfate is that perchlorate's tendency to bind to chromium is much lower than sulfate's tendency. Therefore, the chromium atoms in the solutions created with $\text{Cr}(\text{ClO}_4)_3$ are expected to be complexed with only water molecules. As a result, an experimental solution created with perchlorate, system 2 is considered to be similar to system 3 (figure 2.7).

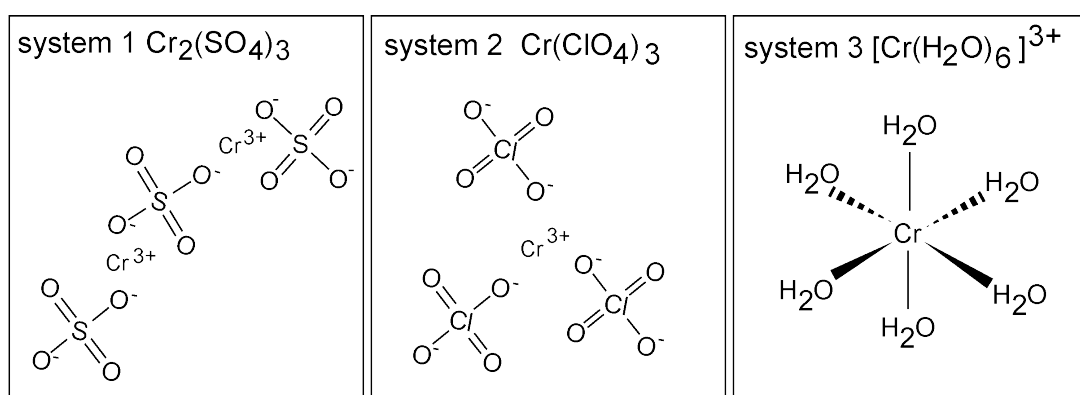


Figure 2.7: Overview of different systems using specific chromium salts: system 1 $\text{Cr}_2(\text{SO}_4)_3$, system 2 $\text{Cr}(\text{ClO}_4)_3$ and system 3, where no anions are surrounding the Cr ion, only H_2O molecules. Also system 1 and 2 contain H_2O molecules, but these are left out for convenience

In the DFT calculations of this study's two other important assumptions are taken. Firstly, it is assumed that the chromium complexes consist of one chromium atom coordinated with six ligands. Secondly, it is assumed that the ligands present in the complex are mainly water molecules and no hydroxide groups. This assumption is based on the electrolytes' low pH 2.45 used in this study. According to a theory calculations of Phuong, at the pH of 2.5, 93.15% of fresh trivalent chromium solutions will contain $[\text{Cr}(\text{H}_2\text{O})_6]^{3+}$ and only 6.85% will contain $[\text{Cr}(\text{H}_2\text{O})_5(\text{OH})]^{2+}$ [56]. Therefore, it is expected that most complexes will include H_2O instead of HO^- .

2.4 Thesis outline

The outline in this thesis consists of nine chapters; the first chapter introduces the subject of this thesis. The second chapter presents the research approach of this thesis and informs the reader with the background information and applicability of the spectroscopic research techniques used in this study. In the third chapter the reader will be informed with all necessary background information and current literature on the chemistry of Cr(III) electrolytes. The fourth chapter provides the basics of electroplating and operating conditions that affect the solution chemistry. Chapter five explains the basics and maths behind DFT calculations, which are extensively used

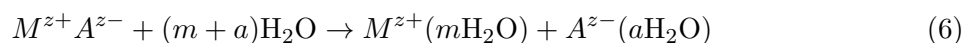
in this study. Chapter six describes all material and methods used in this study. Next, chapter seven discusses and interprets the experimental results of this study. Finally, chapter eight and nine accommodate the conclusions and recommendations of this work.

3 Chemistry of Cr(III) in electrolytes

In this chapter, the chemistry of the chromium(III) ions in the electrolytes will be explained to provide the reader with necessary background information. First, the complexation of chromium in an aqueous solution is addressed. In this subsection, the complex's specific symmetry is explained, which is related to the molecular orbital configuration of the complex. Secondly, information about the possible electron transitions is provided, with Tanabe Sugano diagrams, which is necessary for understanding the electron transitions observed in UV-Vis. Next, an introduction to the ligand exchange mechanism and the characteristics of ligand exchanges is given to explain the chromium complexes' specific observed behaviour. Subsequently, the effect of ligand exchange on the splitting in the d-orbitals (Dq) is explained, which can be directly related to a shift in UV-Vis spectra. In the last subsection, formate's chemical structure and the effect of different anions on the complexation of Cr(III) in aqueous solutions is discussed.

3.1 Chromium complexation in aqueous solutions

Electroplating electrolytes are created by adding a metal salt to an aqueous solution, often in combination with additional compounds, for example conducting salts, brighteners or **complexing agents** (a substance capable of forming a complex compound with another material in solution). A wide range of initial chromium salts can be observed in studies on trivalent chromium electrolytes and deposits. However, the following salts are observed the most in similar studies: CrCl_3 , $\text{Cr}_2(\text{SO}_4)_3$ and $\text{Cr}(\text{NO}_3)_3$. The focus of this study is mainly on $\text{Cr}_2(\text{SO}_4)_3$ as chromium salt since Tata Steel's research is also conducted with this type of chromium salt. As a result, the comparability between this study and Tata steels research is increased. The addition of conducting salts and brighteners is not included in this study, and only the addition of sodium formate as a complexing agent is considered. This section will inform the reader on the geometry of chromium in aqueous solutions and explain why this specific geometry is favoured.



The overall dissolution process of a salt goes according to equation 6. After dissolving a trivalent chromium salt, for example, $\text{Cr}_2(\text{SO}_4)_3$ in an aqueous solution, the salt is first separated in Cr^{3+} and SO_4^{2-} ions, and then secondly, an interaction with the water molecules occurs[57]. During dissolution, these processes occur simultaneously. In general, every system strives towards a state of minimal energy and dissolved metal ions in solution can form complexes with ligands to lower their energy state. A ligand also called a complexing agent, is an ion or molecule with a free electron pair to bind with a central metal atom to form a **coordination complex**. The influence of ligands on the energetic ordering of transition metal d-orbitals is of great fundamental importance in understanding the behaviour, structure, reactivity and spectroscopic transitions of transition metal complexes[58]. Regardless of the nature of the metal-ligand interaction, the connection between the two is practically a lewis acid or lewis base reaction. In this case, the Cr(III) metal ion acts as the Lewis acid (electron-pair acceptor) in the interaction, and the ligand acts as Lewis base (electron pair donor)[45, 58]. The simplest ion that chromium forms in aqueous solutions is the **hexaqua ion** $[\text{Cr}(\text{H}_2\text{O})_6]^{3+}$, one chromium atom, hexavalently coordinated with six water ligands. The Cr(III) ion has three electrons in its 3d shell, by accepting the lone pair of electrons of six water molecules the complex fills the empty d shells, the 4s shell and 4p shell, lowering its energy state. This type of bonding is called d^2sp^3 **hybridization** and visualised in figure 3.1a. The most favourable energy configuration

to take for Cr(III), in most instances, is an octahedral symmetry. This is visualised in figure 3.1b.

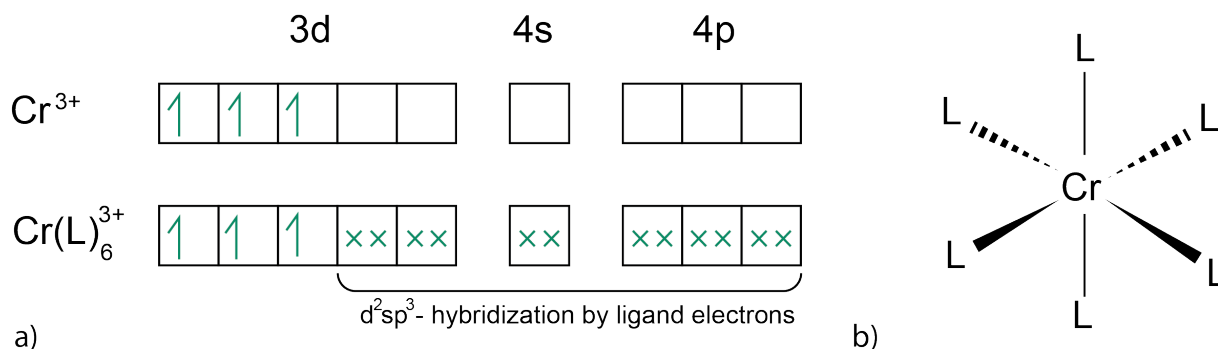


Figure 3.1: a) Hybridization of Cr(III) b) Octahedral symmetry

3.2 Quantum mechanical understanding of metal-ligand interactions

It is mentioned before that the transitions observed in the d-orbitals can be observed with UV-Vis experiments. However, before these transitions can be studied, some fundamental knowledge on the specific ordering of the d-orbitals is considered necessary. The octahedral arrangement in a Cr(III) complex of six negative charges around a metal ion causes the five d-orbitals to split into two sets of orbitals, t_{2g} and e_g corresponding to different energies levels.

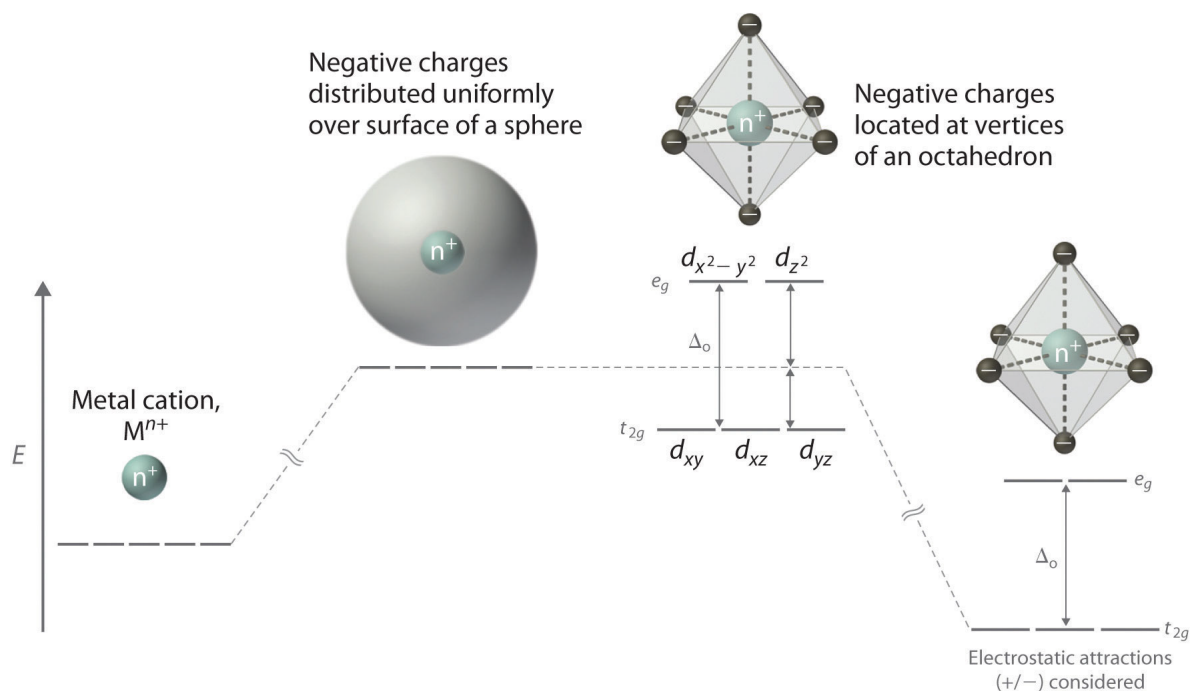


Figure 3.2: Splitting of the d orbitals with octahedral symmetry(CC BY-NC-SA)[4]

In figure 3.2 this is visualised, it can be observed that the energy increases as the negative charges distribute uniformly over the surface of a sphere. Subsequently, the negative charges located at the vertices of an octahedron, and the d-orbitals split in two sets. In figure 3.3, the

orbitals are visualised on an octahedral arrangement. Those d-orbitals that point toward the ligand groups dx^2dy^2 and dz^2 are destabilised by the negative charge of the ligands and move to a higher energy level (e_g). The d orbitals pointing away d_{xy} , d_{yx} and d_{xz} , are less stabilised and stay at a lower energy level[4].

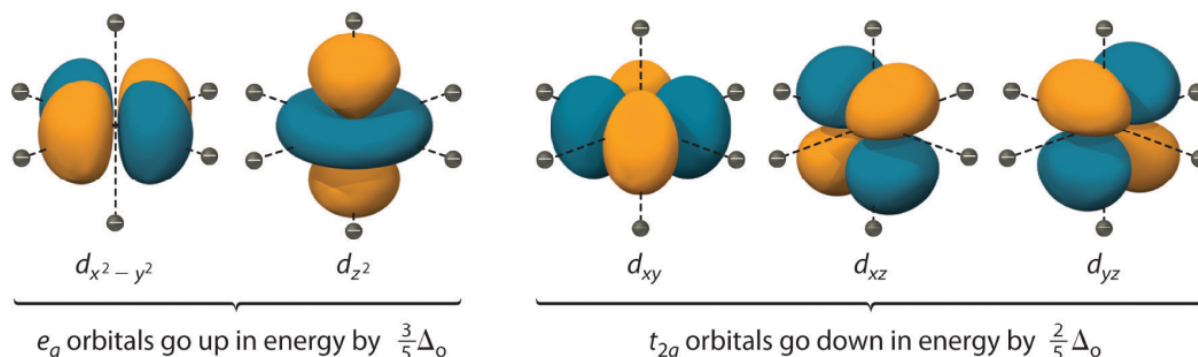


Figure 3.3: d_{xy} , d_{xz} , d_{yz} less destabilized orbitals and dx^2dy^2 and dz^2 destabilized orbitals with ligands on the axes(CC BY-NC-SA)[4])

In an octahedral symmetry, the ordering of the molecular d-orbitals with $d(x^2 - y^2)$ and $d(z^2)$ at higher energy levels, and d_{xy} , d_{xz} and d_{yz} at lower energy levels is qualitatively the same, regardless of the type of ligands present in the complex[6]. However, the extent of the splitting between the t_{2g} orbital set (HOMO) and the e_g orbital set (LUMO), called the crystal field splitting energy ΔO , visible in figure 3.2 is affected by ligand exchange[10].

In figure 3.4a, the Tanabe Sugano diagram for d^3 transition metal complexes is shown, these diagrams can be used for quantitative interpretation of electronic absorption spectra[6]. In figure 3.4a, it can be observed that there are eight possibilities to promote an electron to from the ground state 4A_2 . However, not all these electron transitions are possible since there are two main rules which the electron transitions have to obey. The first rule, also called the **spin rule**, says that allowed transitions must involve the promotion of electrons without a change in their spin[59]. The second rule, called **Laporte rule**, states that if a molecule has a centre of symmetry, transitions which only involve the redistribution of the electrons in a given subshell, for example d-orbitals, are forbidden[59]. Cr(III) has three electrons in its d-shell, and therefore a spin multiplicity (amount of unpaired electrons +1) of 4. Taking into consideration the spin selection rule, we can only expect transitions between the ground state 4A_2 and 4T_2 , 4T_1 and the other 4T_1 excited state, as these are spin allowed.

Although all three transitions presented above are spin allowed, two of them are Laporte forbidden, and can not occur according to this rule. However, experimentally, chromium solutions appear to be coloured; this is only possible if the d-d transitions are occurring. This is only allowed by vibronic coupling and as a result, the transitions will be less intense than Laporte allowed transitions[6]. According to Lever 1968, hexavalently coordinated complexes with organic ligands with spin allowed and Laporte forbidden transitions show a molar extinction coefficient of 10^2 - $10^3 M^{-1}cm^{-1}$. On the contrary, spin allowed and Laporte allowed molecules transitions have a molar extinction coefficient of 10^3 - $10^6 M^{-1}cm^{-1}$ [6]. The first two transitions discussed in section 2.3.1, correspond to Laporte forbidden transition occurring in the Cr(III) complex. This explains the low absorption values found in these transition peaks. In our experiments it is expected to find similar low absorption peaks, corresponding to the d-d transitions, which are going to be used for the interpretation. It is also possible to observe a part of third higher

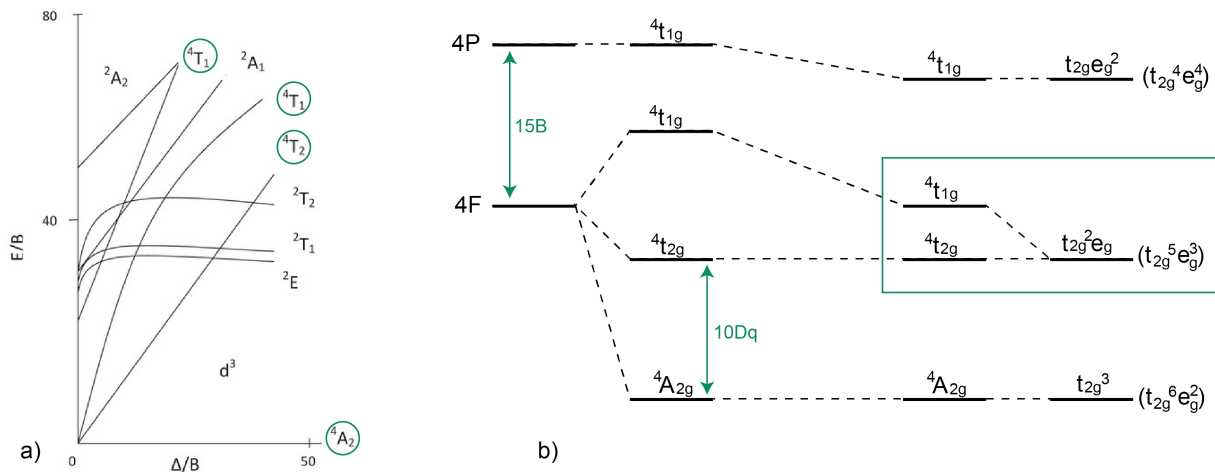


Figure 3.4: a) Tanabe and Sugano diagram of d^3 transition metal, with the selected transitions for Cr(III) complexes[5] b) correlation diagram for d^3 transition metals created using the work of Lever[6]

absorption peak at boundary of low wavelengths, corresponding to a electron excitation from the metal to the ligand. This peak will not be included in interpretation of the data, as it is often out of the range of the spectrum.

In rectangle in figure 3.4b it can be observed that ${}^4T_{2g}$ and ${}^4T_{1g}$ correspond to the same transition ($t_{2g}^2 e_g$), but can be observed at different energies. This is the reason two absorption peaks can distinguished in UV-Vis spectra of d^3 transition metals. The difference in energy is caused by the difference in experienced repulsion, due to overlapping of the shells[6]. According to this statement, the difference between the first and the second peak it is expected to be caused by repulsion of overlapping shells.

In figure 3.4, B is one of the Racah parameters, which describes the inter electronic repulsion among the electrons in the d-orbitals and is an approximation of the bond strength between the ligand and metal[44, 60]. In this same figure, $10Dq$ is the octahedral crystal field parameter, which accounts for the charge of the metal, the distance of ligands and metal and the radial electron density of the d-electrons[6, 44]. In figure 3.4a it can be observed that energy of the first transition is linearly dependent on the crystal field splitting. It can also be observed that the second transition the energy is non linear related to the crystal field splitting. Therefore, it is expected that a shift in the first peak will be easier to relate to a change in the crystal fields splitting, which is related to ligand exchange. How the ligand exchange is related to the crystal field splitting will be discussed in the following section.

In general, chromium complexes are kinetically inert complexes, due to the absence of electrons in the E_g type of d-orbitals and have a considerable ligand field stabilisation energy. Therefore ligand substitution reactions occur very slowly. This inertness, is overall not beneficial for the electroplating process, as high activation energies are needed for dehydration of the Cr(III) molecule. This dehydration of the Cr atom is required before chromium metal can be deposited on the surface[57]. During the process of dehydration the bonds between the water molecules and the chromium atom need to be broken, which requires energy. In general, the strength of the bond between the chromium atom and the ligand is related to the crystal field splitting, and a higher splitting leads to stronger bonds between the ligands and metal[61][4].

3.3 Ligand exchange mechanisms and characterisation

In this thesis, it is expected that a ligand exchange occurs upon the addition of formate to Cr(III) electrolytes. However, with which ligand and how this reaction is happening is unknown. Therefore in this subsection, first, the possible exchange mechanisms and characteristics of ligand exchange are explained. Next, the effect of ligand exchange on the field splitting energy is explained, which can be related to the UV-Vis experiments.

Ligand substitution can go according to a **dissociative** or **associative** mechanism. In the associative mechanism, the new ligand B interrupts the complex and forms an intermediate where an extra ligand is present. Subsequently, the intermediate loses its initial ligand A, forming a new complex. In the dissociative mechanism, the initial complex firstly loses a ligand to form an intermediate with only five ligands instead of six in this case. Continuously, the new incoming ligand B reacts with the intermediate[10]. Both mechanisms can be observed in figure 3.5, and also, a third option is visible, which is the interchange mechanism. This mechanism is similar to the associative and dissociative pathways, except that no distinct intermediates are formed[62]

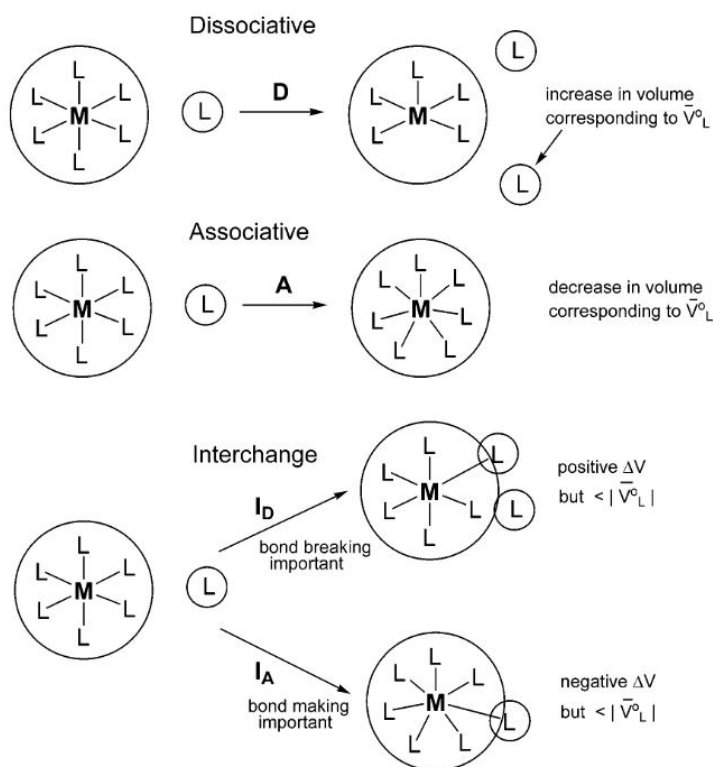


Figure 3.5: Ligand substitutions reactions mechanisms with their accompanied change in volume of the first coordination sphere[7]

The specific mechanism in Cr(III) complexes is uncertain as both the associative or dissociative character of ligand substitution are proposed in different studies[7, 63], Schonle2014, Dei1997. According to Dalal, most of the ligand displacement takes place through the interchange route rather than purely associative or dissociative[64]. It has to be concluded that there is no conclusion on the substitution mechanism for Cr(III), and that the mechanism depends on characteristics of the complex, such as the type of ligands.

In figure 3.5, it can be observed how the volume change is related to the ligand exchange mechanism. Studying this volume change is one method for studying the ligand exchange

mechanisms and can be performed with a UV spectrophotometer equipped with high-pressure cells[65]. It is found that the ΔV for $[\text{Cr}(\text{H}_2\text{O})_6]^{3+}$ water exchange reactions is negative, indicating an associative mechanism for Cr(III)[7, 66]. However, if one hydroxide group is present in the complex $[\text{Cr}(\text{H}_2\text{O})_5(\text{OH})]^{2+}$, the ΔV has changed to positive values indicating a dissociative mechanism[67, 66]. Therefore, it needs to be considered that the ligands present in Cr(III) complex affect the ligand exchange mechanism, and both mechanisms are possible in this study. The determination of the exchange mechanism of formate as a ligand will not be determined in this study, as it is out of the scope of this thesis, but will be a recommendation for further research. However, explaining both the reaction mechanism is considered useful to consider possible intermediates before the ligand substitution has occurred in the experiments presented in this study.

According to Dei et al., it is generally accepted that complex formation by metal ions proceeds by a mechanism in which the rate-determining step is the change from an **outer-sphere** to an **inner-sphere complex**. The first step will be the formation of the outer-sphere complex between the metal ion and ligand[67], continuously the ligand might be included in the inter sphere. This makes the ligand exchange a time depended process. A visualisation of the difference between an inner and an outer-sphere complex is given in figure 3.6. Although, the difference in an inner and an outer-sphere is presented in relation with a surface, the theory behind is similar. In the inner sphere complex the oxygen atom of the ligand is directly bonded to the metal ion, and at the outer-sphere mechanism the oxygen atom is connected with the metal ion with a H_2O molecule in-between. It is expected that the strong bonds between H_2O and Cr in the $[\text{Cr}(\text{H}_2\text{O})_6]^{3+}$ complex make it difficult for a ligand to enter the inner sphere complex. Therefore, it suggested the presence of a ligand with weaker bonds in the inner-sphere complex, also correlated with a lower crystal field splitting, would enhance and shorten the time scale of the ligand substitution.

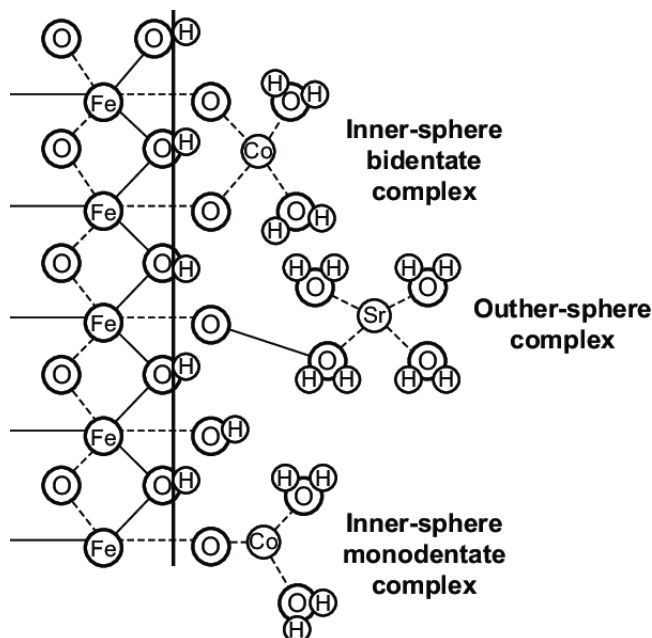


Figure 3.6: Difference inner and outer-sphere complex related to the bonding with a surface[8]

As mentioned before ligand exchange is a time dependent process. The exchange of ligands can be classified as **labile** when the half-life is one minute or less, or **inert** if the reaction time is longer, according to Taube[68]. In appendix A, the range of water exchange rates and mean lifetime for primary shell water molecules on aqua metal ions can be observed. The dotted line is the boundary between labile and inert presented by Taube[7]. It can be observed that Cr(III) shows a lifetime in the scale of years at 25 degrees Celsius, which can also be a problem for investigating these solutions, as it requires a long time scale for the experiments.

To conclude, the labile character of the Cr(III) complex is not beneficial for the deposition process due to the inertness of the $[\text{Cr}(\text{H}_2\text{O})_6]^{3+}$ complex. It has been observed that without the addition of complexing agents, no Cr(III) deposits can be obtained[34]. Secondly, it is also expected the complexation in the addition of complexing agents takes time before the composition in the plating bath is improved due to the slow ligand substitution in the $[\text{Cr}(\text{H}_2\text{O})_6]^{3+}$ complex. It is suggested that a ligand with weaker bonds in the inner-sphere complex, also correlated with a lower crystal field splitting, would enhance and shorten the time scale of the ligand substitution. Therefore, the creation of a complex with a less labile character than the $[\text{Cr}(\text{H}_2\text{O})_6]^{3+}$ would lower the energy needed for dehydration and would improve the reduction of the chromium complexes. It is expected that a chromium complex where formate is included is less labile than the $[\text{Cr}(\text{H}_2\text{O})_6]^{3+}$ complex, which could result in an improved deposition of chromium metal. Therefore, a high concentration of chromium-formate complexes is expected to be beneficial for the deposition process of trivalent chromium.

3.4 Effect of ligand exchange on the field splitting energy

It is of importance to understand how ligand exchange in Cr(III) electrolytes results in a change of the spectroscopy studies, to be able to draw some conclusions out of the experimental data. In most cases where a high crystal field splitting energy is observed, complexes tend to be inert[62]. It is essential to consider that even thermodynamically unstable complexes can be kinetically inert. Therefore, it is possible that the observed complex might not be the complex with the lowest energy, if not enough time is given for the substitution to occur.

In electrolytes where sodium formate is added to Cr(III) solutions, it is observed that there is a change in the chemistry of the molecule accompanied by a shift in the UV-Vis spectra[1]. According to Bennet et al. the first peak in UV-Vis spectra in Cr(III) complexes is a direct measure of the ligand field splitting parameter $10Dq$ [69]. Whereas, the second peak depends on Dq and the Racah parameter B , which describes the effects of electron-electron repulsion within the metal complexes[69]. Therefore, it is considered that a shifts in first peak of the UV-Vis spectra can be related to increase or decrease of the field splitting energy. To be able to explain eventual shifts in the UV-Vis spectra, the parameters that can affect the splitting between the d-orbitals need to be defined .

In literature, factors that can affect the field splitting energy are the following[4]:

- The charge on the metal ion
- Spin pairing energy
- The nature of the ligand
- Geometry of the complex

Firstly, the charge on the metal and **spin pairing energy** will be discussed. The spin pairing energy is the energy needed to paired electrons in the molecular orbitals. These are

connected with the distribution of the electrons and distortion of the complex. In the case of Cr^{3+} (inert) the d-orbitals have empty e_g orbitals, in a Cr^{2+} complex, one electron will be positioned in the e_g orbital distorting the complex away from its octahedral symmetry, which results in higher energy level and a complex being more labile[70]. The distribution of electrons of Cr^{2+} and Cr^{3+} in octahedral and tetrahedral symmetry are visualised in figure 3.7. Also the difference between a high and low spin complex can be observed. If the pairing energy is less than the crystal field splitting energy, ΔO , then the next electron will go into the d_{xy} , d_{xz} , or d_{yz} orbitals due to stability forming a low spin complex. It is assumed that the complexes in this study have a chromium atom with a charge of 3+ with three unpaired electrons in its d-shell. Therefore, the charge of the metal is not expected to influence the field splitting energy. Also the e_g orbitals are expected to be used for ligand bonding, therefore it is not considered possible to go from a Cr^{3+} to a Cr^{2+} complex without losing a ligand.

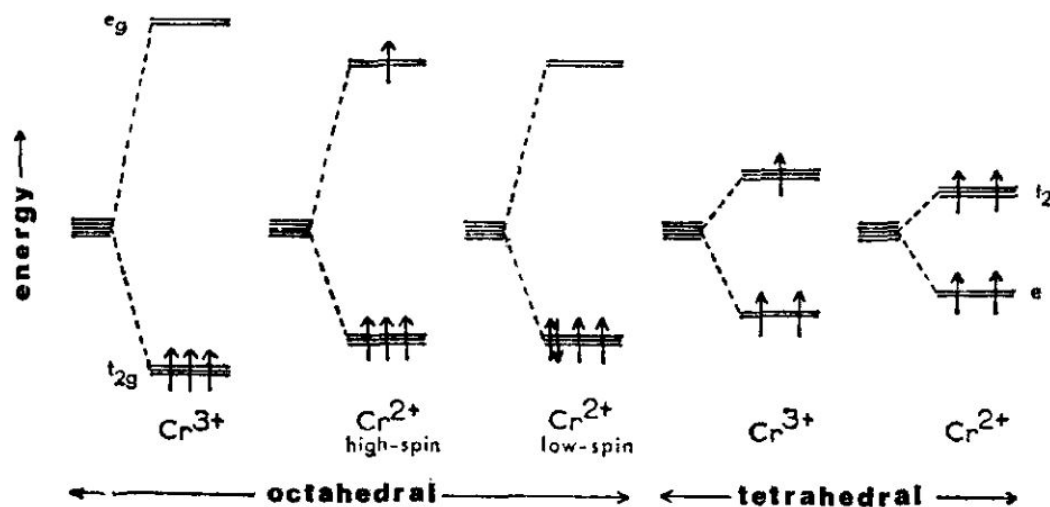


Figure 3.7: Electronic configurations of chromium cations in octahedral and tetrahedral coordination[9]

Secondly, the nature of the ligand in the complex also affects the crystal field energy. Ligands can be strong, intermediate or weak field ligands[61]. It can be observed that in chemically similar ligands, for example, $F > Cl > Br > I$ (halogens), smaller more localized charges interact stronger with the d-orbitals[4]. Therefore, F has larger field splitting energy (ΔO) than I^- . The general order of ligands strength is called the **spectrochemical series**. In this series it can be seen that weak ligands give a lower ΔO and stronger field ligands give a larger ΔO . It is not precisely determined yet where formate is placed in this order is, but it is expected to be close to H_2O , as the nature of bonding is by an oxygen atom. According to this order, it can be expected that H_2O will produce a larger ΔO than SO_4^{2-} . Different spectrochemical series can be found, some more extended than others, an example of a series for Cr(III) complexes is given in the following order:

- $I^- < Br^- < \text{OCrO}_3^{2-}$ (chromate) $< Cl^- \approx \text{SCN}^- < F^- \approx \text{SSO}_3^{2-}$ (thiophosphate) $\approx \text{Urea(O)} < \text{OCO}_2^{2-}$ (carbonate) $< \text{OCO}_2\text{R}^-$ (carboxylate) $< \text{ONO}^- \approx \text{OH}^- < \text{OSO}_3^{2-}$ (sulfate) $< \text{ONO}_2^-$ (nitrate) $< \text{O}_2\text{CCO}_2^{2-}$ (oxalate(bidentate)) $< \text{H}_2\text{O} < \text{NCS} < \text{glycine} \approx \text{EDTA}^{4-} < \text{pyridine} \approx \text{NH}_3 < \text{en} < \text{SO}_3^{2-} < \text{bipy} < \text{o-phen} < \text{NO}_2 < \text{PPh}_3 < \text{Cp} < \text{CN}^- < \text{CO}$ [71]

Finally, the geometry of the complex affects the splitting of the d-orbitals. It can be observed in figure 3.7, that the the splitting in the d-orbitals in an octahedral geometry of Cr^{3+} has a

larger splitting than the tetrahedral geometry. The positioning of three unpaired electrons in octahedral symmetry at T_{2g} , compared to two electrons in T_{2g} and one in e_g makes octahedral highly more favourable than tetrahedral. Therefore, Cr^{3+} is only expected to be present in octahedral geometry in our experiments.

Depending on the specific complex, ligand substitution is possible till a certain ratio of metal-ion vs ligand-molecules. This means that even in an octahedral complex, it might not be favourable to replace all ligands of type A with type B, as this will not fit. Besides, there is also a possibility to have **geometric isomers** in a molecule with the same amount of A and B ligands. In figure 3.8 and 3.9 four different types of isomers in octahedral symmetry are visualised which are included in this study. *cis*- $[Cr(H_2O)_4(HCOO)_2]^+$ and *trans*- $[Cr(H_2O)_4(HCOO)_2]^+$ both have two ligands of type B, located next to each other or at opposite sides of the molecule and *mer*- $[Cr(H_2O)_3(HCOO)_3]$ and *fac*- $[Cr(H_2O)_3(HCOO)_3]$ both have three ligands of type B. It is expected that isomers of *mer*- $[Cr(H_2O)_3(HCOO)_3]$ and *trans*- $[Cr(H_2O)_4(HCOO)_2]^+$ will experience less repulsion of the electrons in their $HCOO^-$ group as these are orientated further apart, than the $HCOO^-$ groups in the isomers *Cis*- $[Cr(H_2O)_4(HCOO)_2]^+$ and *fac*- $[Cr(H_2O)_3(HCOO)_3]$. As a result, *trans*- $[Cr(H_2O)_4(HCOO)_2]^+$ and *mer*- $[Cr(H_2O)_3(HCOO)_3]$ might have a lower energy configuration than *Cis*- $[Cr(H_2O)_4(HCOO)_2]^+$ and *mer*- $[Cr(H_2O)_3(HCOO)_3]$. However, this is not experimentally proven.

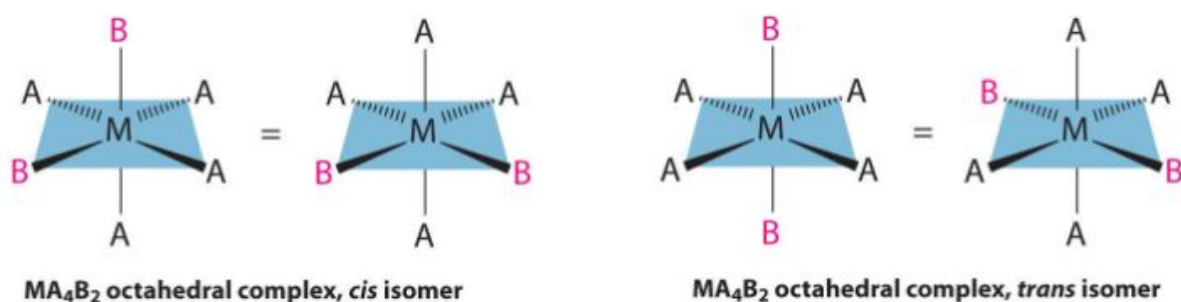


Figure 3.8: cis and trans isomers in octahedral symmetry, with A & B being different ligands[10]

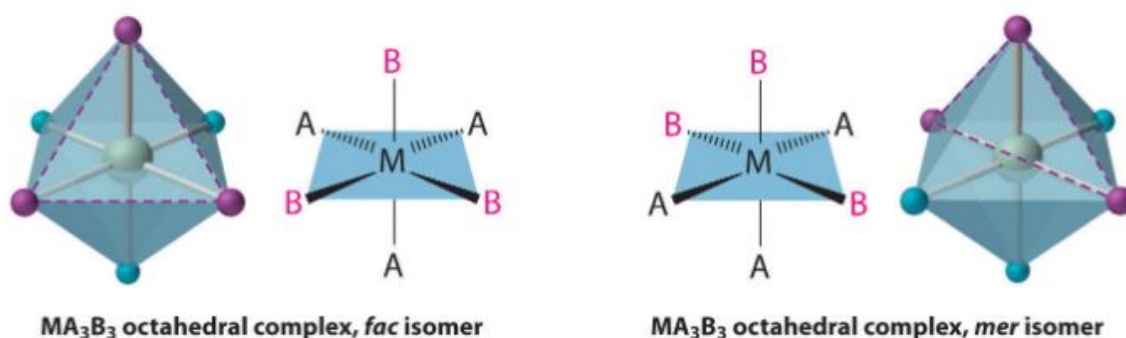


Figure 3.9: Meridional(*mer*) and facial (*fac*) isomers in octahedral symmetry, with A & B being different ligands[10]

To conclude, it is expected that the nature of the ligand exchange has the largest effect on the field splitting energy. Therefore, a shift in the UV-Vis spectra's first peak can be related

to ligands exchange with a different nature. However, the pH and temperature of the solutions compared need to be kept constant. It is expected that all geometries of chromium-formate complexes are octahedral. This will cause the same splitting between the orbitals, even with different ligands. It is expected that the distortion of the octahedral symmetry caused by different ligands in the complex is small and therefore, will not cause a large shift in the UV-Vis spectra.

3.5 Addition of formate as complexing agent

In this study, the addition of sodium formate as a complexing agent for Cr(III) plating electrolytes is studied, as it is proved that formate increases the amount of deposited Cr-metal from trivalent chromium solutions[27] and simultaneously introducing chromium carbides in the deposit[31, 32, 72]. Formic acid or formate is an organic molecule with the following chemical notation ($\text{HCOOH}/\text{HCOO}^-$) and structure visible in figure 3.10. After the dissolution of sodium formate in an aqueous solution, sodium and formate will decompose, and the equilibrium between formic acid and formate will establish depending on the solution's pH[30]. It has been mentioned before that the pKa value of the equilibrium between HCOO^- and HCOOH is 3.45[30]. Therefore, in solutions with a pH lower than 3.45, formic acid will be dominant.

It was mentioned before that in the addition of formate, the deposition of Cr-metal was improved. One possible explanation for this improved deposition is the formation of a complex between Cr^{3+} and HCOO^- . This complex might be related to the lower activation energy needed for the dehydration of the water molecules. Dehydration of the water molecules is necessary before the chromium-metal can be deposited on the substrate[1], but this will be explained more in depth in chapter 4.

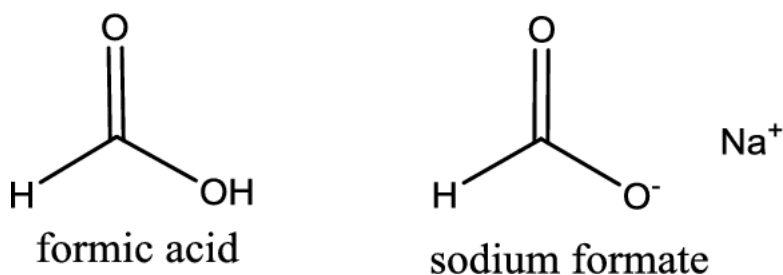


Figure 3.10: Chemical structure of formic acid and sodium formate[11]

In this study, till now it was assumed that the initial state of the Cr(III)-complex consists of Cr^{3+} coordinated with six H_2O molecules as ligands. However, in aqueous solutions with other ligands, with a stronger affinity than H_2O this is expected to be not true. In reality, species, for example, nitrate, sulphate and chloride will be included in the electrolytes, as these are often included in common chromium salts, or conducting salts. It is experimentally proved that some of these species, actively participate in the complexation of Cr(III) in aqueous solutions. According to Mandich[29], the tendency of an anion to participate ligand exchange goes according to the following order:

- **Oxalate > Glycinate > Tartarate citrate > Gluconate > Acetate > Monochloracetate > Formate > Sulfate > Chloride > Nitrate > Perchloride**

Considering this order, it is expected that if enough formate is available, it is likely that in most complexes, ligand exchange with formate will occur even in solutions containing sulfate.

However, the amount of formate molecules that can replace a water molecule is undetermined yet. According to this order to participate in ligand exchange, a chromium perchlorate salt can be used if a large concentration of $[\text{Cr}(\text{H}_2\text{O})_6]^{3+}$ is needed, since the tendency of perchlorate to participate in the complexation is lower than that of H_2O [36].

Formate is a relatively large molecule, compared to H_2O . Therefore, it is likely that it is impossible to substitute all H_2O molecules in a complex if the coordination of six ligands is maintained. It is observed that coordination number of a metal ion is often influenced by the relative sizes of the metal ion and the surrounding ligands[73]. However, no other coordination numbers than six are found for Cr(III) and according to Brown in coordination for Cr(III) is invariably six[73]. It is expected that coordination number different than six, only occurs during associative or dissociative substitution of a ligand.

4 Process and operation conditions affecting solution chemistry

In this section, an introduction is given to the general basics of electroplating to inform the reader of the process and the operating conditions that could influence the studied electrolytes. Subsequently, the parameters pH, concentration and temperature are discussed more extensively. At the end of this section, the diffusion of chromium complexes from the bulk of the solution to the metal interface is discussed, with the hurdles that accompany this process.

4.1 Electroplating basics

Electrochemical deposition of metals and alloys involves the reduction of metal ions from aqueous, organic or fused-salt electrolytes[57]. In the deposition process, a substrate material is coated with a thin layer of another metal by electrolysis, to improve the surface characteristics, such as, corrosion or wear resistance of the metal substrate[57]. The deposition process of metal ions from an aqueous solution into the lattice can be presented with the following equation, where z electrons are provided from an external power source.



In general, electroplating is conducted in an electrochemical cell where the anode is positively charged, the cathode (to be plated metal) is negatively charged, and these electrodes are submerged in an electrolyte. The application of voltage with an external power source is the driving force for the reduction-oxidation reaction to occur at the electrodes. Typically, this reaction goes according to equation 8. In this reaction from left to right, electrons are consumed, which is called reduction, from right to left electrons are liberated, which is called oxidation[57].



At the cathode, the metal molecules from the solution are reduced and deposited on the substrate, simultaneously at the anode, a counter-reaction is occurring to balance out the flow of electrons[57]. This counter-reaction can be dissolving of the anode to balance the loss of metal ions in the electrolyte or another oxidation reaction, for example, the evolution of hydrogen ions from the electrolyte to hydrogen gas. However, in this second example, it is essential to supplement the electrolyte with ions of the material to be deposited to maintain the concentration and keep the deposition process going[57].

4.2 Temperature, pH and concentration

Within the plating bath, the temperature, pH and concentration are operation conditions that need to be regulated and kept constant at their desired values. Effective regulation of process operation conditions is essential for the plating bath's performance. It is proven that in general electroplating, a deviation of more than 5 °C from the optimal plating temperature is sufficient to harm the quality of the deposit[57]. Whether this is also the case for Cr(III) electrolytes is not specified due to the limited studies on these electrolytes and will also not be investigated in this study. However, all solutions in this study will be tested at constant temperature, in this study for convenience this is chosen to be room temperature.

Secondly, regulation of the pH in the plating bath is important for the solution chemistry, especially for the concentration of specific molecules or complexes, as it is found that too high pH can poison the plating bath. The primary purpose of pH control in electroplating is to keep the pH within a specific range, that fulfils the desired performance, for example, deposition speed and optimum quality of deposit[74]. This optimum pH value is found to be dependent on

the type of metal ions, solvent and any other additives added to the electrolyte. Deviation of this optimum pH could give rise to precipitation of hydroxides out of the electroplate solution, dissolution of the freshly deposited metal or inclusion of undesired species in the deposit[75, 76].

On the other hand, it is also observed that the formation of specific complexes is influenced by the pH of the solution[3]. However, if the complexes in Cr(III) electrolytes are also dependent on pH is not proven. The complexes Lucks et al. observed at different pH values showed a significant difference (min. 10 cm^{-1}) in the FTIR spectra between the pH range of 0.8-3.7[42]. Therefore it is expected, a difference of minimal 10 cm^{-1} in the wavenumbers is a significant indication to suggest the formation of a new complex in this study.

Finally, the concentration of chromium and other additives is of influence on the layer characteristics. It is observed in different studies, that the concentration of formate affects the final composition of the deposit[1, 40]. However, what effect an increase of formate concentration has on the electrolytes' chemistry is undetermined yet, showing the relevancy of this project. In this study the effect of the optimal concentration will not be tested in relation to the quality of the final deposit. However, this study will give better insights on the expected optimal concentration for of formate for the deposition process.

4.3 Kinetics of species in plating electrolytes and diffusion layer

The metal-solution interface is in this scope, the most important component of an electrochemical cell, as this is the crucial part where the deposition of the metal is occurring[57]. Immediately after immersion of a metal in an aqueous solution, the system shifts to a new equilibrium configuration. The exchange of charge carriers (ions and electrons) across the metal-solution inter-phase is constant at equilibrium[57]. In electroplating, a current is applied to the metal, which gives the surface a negative charge. The negatively charged surface attracts positively charged ions M^+ , for example, a positively charged chromium complexes from the solution, and repels negatively charged ionic species[57]. Therefore, a gradient exists in the species observed from the interface to the bulk of the solution[57, 77]. Different models can be used to predict the charges distribution in the interface region. A standard method to describe the interface region is the inner and outer Helmholtz planes which are both within the diffusion boundary layer[57]. The inner Helmholtz layer designates a monolayer on the electrode of adsorbed solvent molecules (e.g. H_2O) or other ions from the electrolyte. The outer Helmholtz layer consists of the positively charged hydrated ions of the electrolyte attached to the inner Helmholtz layer. These two layers form the boundary between the bulk solution and metal interface. Figure 4.1 provides a visualisation of this process.

Before chromium metal can be deposited on the surface, a chromium complex must diffuse from the bulk of the electrolyte to the surface and penetrate the Helmholtz layers. This process is accompanied by **dehydration**, where the ions strip off their hydration shells and are incorporated in the lattice of the solid[77]. The transport through the boundary layers and the stripping of hydration shells requires activation energy, which an external voltage source must supply[77]. In this study, the effect of externally applied voltage on the complexation and plating from Cr(III) is not included. However, this study's primary goal is to obtain better insights on the electrodeposition process of Cr(III). It is expected that the presence of formate in the inner-sphere complex of Cr(III) is beneficial for the dehydration of the other water ligands. This is caused by expected distortion of the octahedral symmetry of the complex.

One of the practical problems during electroplating is an increased pH of the electrolyte. It is mentioned before that regulation of the pH is essential. However, an increase in the pH can

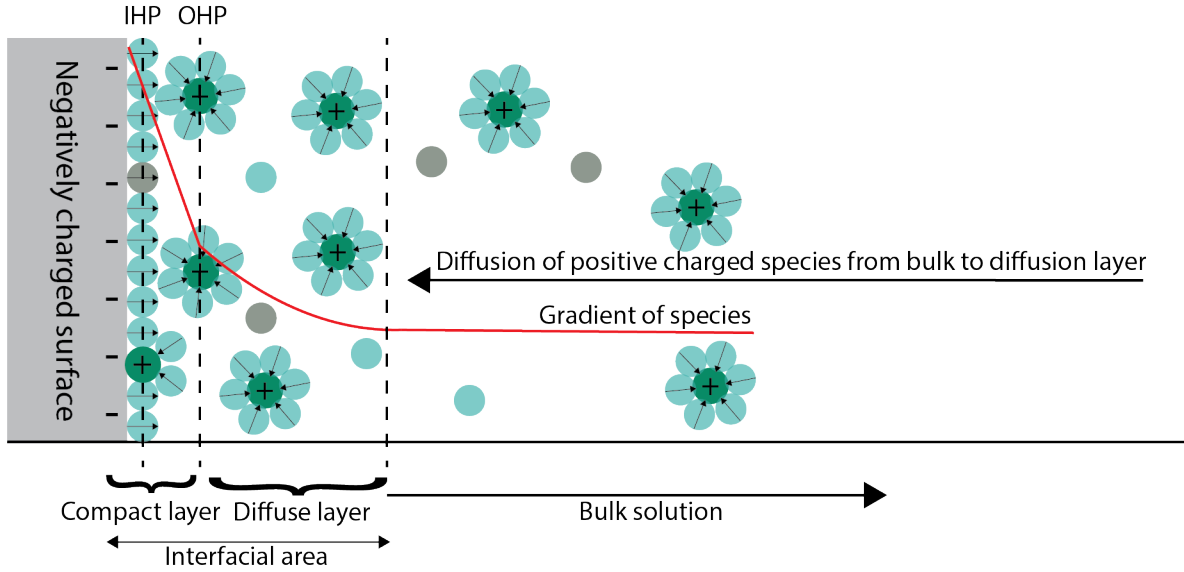
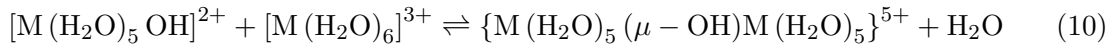
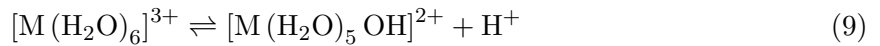


Figure 4.1: Visualisation of interfacial area and bulk solution of a negatively charged metal in aqueous solution

also only occur in the diffusion layer, making it complicated to control. It is observed that in solutions of Cr-Ni alloys with trivalent chromium, the bulk of the electrolyte could still have a pH value of 2, while the diffusion layer around the electrode could reach a pH value of 4[78]. In studies of Hong et al and Wijenberg et al. even a pH increase up to 8.2 and 8.4 is observed at the cathode[27, 79]. This increase of pH can occur if the rate of hydrogen ions transported by the current is lower than the number of hydrogen used in the deposition reaction[57, 74]. The increased pH of the diffusion layer can lead to precipitation of hydroxides as a continued process of olation at which polymerization can occur[78]. **Olation** is the process by which metal ions form polymeric oxides in an aqueous solution. In equation 9 and 10 this process of olation in metal ion complexes is visualized, which starts by displacement of one water molecule by a neighbouring complex[12]. The μ -OH, in equation 10, presents the hydroxide ligand that bridges the two metals complexes. This process is reversible, but the long times required to return to the original complexes lead to the conclusion that dealation is extremely slow[78]. In this study, it is expected that olation reactions will not occur since the pH is kept at 2.45, and no voltage is applied, which can cause an increase of the pH. However, in electroplating at industrial scale this problem still exists.



To conclude, a pH increase in the diffusion layer is expected to be detrimentally for the plating processes. However, more extensive research is necessary to investigate the possible effect of a pH increase on the complexation of Cr(III). Since the control of the diffusion layer pH's is difficult, it might be helpful to study if the chromium-formate complexes also similarly undergo olation as presented in equation 4.2. Since the process of olation occurs by bridging two hydroxide groups, it is expected that $HCOO^-$ ligand(s) could hinder the olation process. Investigating this behaviour is out of the scope of this study. However, if chromium-formate

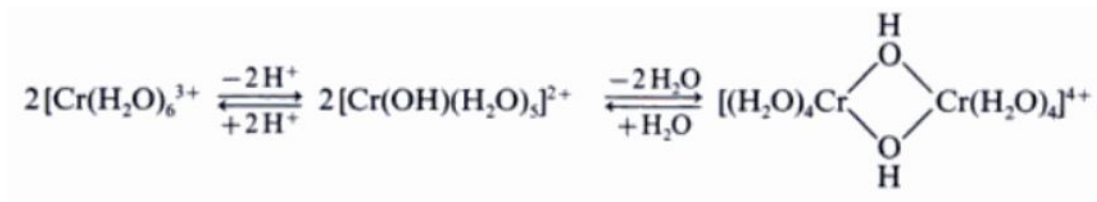


Figure 4.2: Reaction of the hexaaqua ion of Cr^{3+} undergoing dissociation and continuously condensation by means of hydroxo bridges[12]

complexes have a lower tendency to undergo olation, this work's insights on creating a high concentration of chromium-formate complexes could be of use in preventing olation in the electrolytes in case of a pH increase at the cathode.

In this study, the pH is maintained at 2.45 to prevent processes as olation to occur, as the goal of this study is to investigate the initial composition complexes. However, the possible effect of a hydroxide group in the complex is included in the ligand substitution simulations of chapter 7.2.

5 Density-functional theory (DFT) computational calculations

This section aims to familiarize the reader with the density functional theory and provide a background for understanding the experiments performed in this study. In general, in computational modelling, a system is described by a set of mathematical equations and variables. With the use of a computer, a solution is searched within the described system[80]. DFT is such a set of mathematical equations, which established itself as a well-reputed way to compute the electronic structure of many-body systems in most branches of chemistry, physics and materials science[81]. In one sentence, the goal of DFT is to obtain an approximate solution to the Schrödinger equation of a many-body system[82]. In 1964, Piere Hohnberg and Walter Kohn came up with a different approach to calculate the system’s electronic structure, instead of the well-known wave function theory by Schrödinger[82]. Their new approach was called the Density Functional Theory (DFT). The fundamental property used in DFT calculations is the electron density, which is represented by only three input variables[83].

Before DFT calculations can be performed, two main choices need to be considered: What type of functional and basis set to use? Both aspects will be explained in this section. In addition, the execution of geometry optimization and the implementation of solvent effects are explained. At the end of this section, the explanation is given on how DFT can generate spectroscopic data as a comparison for the experimental conducted experiments.

5.1 Definition of a functional in DFT

In the last 50 years, different functionals for DFT are developed by multiple scientists. The density functional theory is the method of addressing the problem, but a functional is the way how the electron density, which is the primary input variable in DFT, is specifically addressed and calculated. Equation 11 presents the density functional theory’s main structure, where the goal is to minimize the energy by inserting a trail electron density (n)[83].

It can be observed that the energy is depending on the interaction of the electron density with the nuclei integrated over all space. The part Honhnberg and Kohn proved is that there is a universal functional $F[n(\vec{r})]$ of the density, which contains the rest of the energy term, for example, kinetic energy and the electron-electron interaction[83].

$$E = \min_n \left\{ \int V_{\text{nuclei}}(\vec{r})n(\vec{r})dV + F[n(\vec{r})] \right\} [83] \quad (11)$$

In 1965 Kohn and Sham separated the energy functional into different components, visible in equation 12[82]. In this equation, the energy is described as a functional of different functions depending on the electron density. T_{ni} is the kinetic energy of non interacting electrons, V_{ne} is the nuclear-electron interaction, V_{ee} is the electron-electron repulsion and ΔV_{ee} and ΔT_{ne} are correction terms on the kinetic energy and electron interaction.

$$E[\rho(r)] = T_{\text{ni}}[\rho(r)] + V_{\text{ne}}[\rho(r)] + V_{\text{ee}}[\rho(r)] + \Delta T[\rho(r)] + \Delta V_{\text{ee}}[\rho(r)][83] \quad (12)$$

Functionals vary from very simple to very complex, and can be divided in different levels of complexity[84]. In figure 5.1 the Jacob’s ladder can be observed, which visualises the different groups of functionals with increasing accuracy and computational cost.

Then if we take the simplest DFT functional, the Local Spin-Density Approximation (LSDA), as an example, the components presented in equation 12, can be recognized in equation 13. The kinetic energy T_{KS} is calculated by the method of Kohn-Shan, and V_{en} and V_{ee} are also familiar in this equation. The new terms appearing are the ϵ_x and ϵ_c which are the exchange and

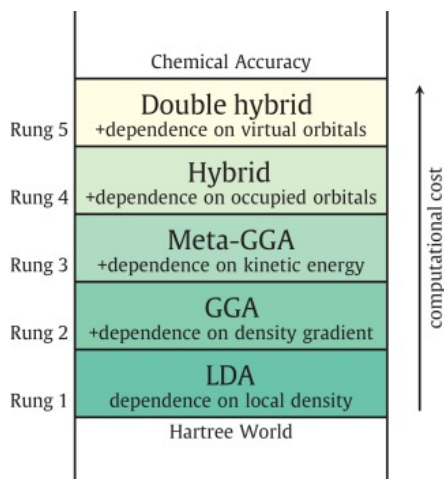


Figure 5.1: Jacob's Ladder describing the different type of functionals[13]

correlation energy terms. In DFT calculations, these exchange and correlation energy terms are defined in multiple ways by different scientists, creating a set of functionals, which are all slightly different in calculated the minimum energy. So within a different rung of the Jacob's ladder, multiple functionals exist which are slightly different in their exchange and correlation terms, but way of describing the electron density in the DFT calculations is similar.

$$\text{Energy} = T_{\text{KS}} + V_{\text{ne}} + V_{\text{ee}} + \int d^3\vec{r}\rho(\vec{r}) \{\varepsilon_x[\rho(\vec{r})] + \varepsilon_c[\rho(\vec{r})]\} \quad [83] \quad (13)$$

LDA functionals typically, overbind molecules by about 30 kcal/mol, which is an unacceptable error for chemical applications[84]. Therefore, the functionals in this rung are not considered not accurate enough for our applications. On the next rung in the Jacob's ladder are generalized gradient approximations (GGAs), which are formulas that use both the density and its gradient at each point[84]. Most GGA functionals are constructed in a way that they add a term to the known LSDA method. In equation 14, it can be observed that a second term $\Delta\varepsilon_{x/c}$ is added, which describes the density gradient.

$$\varepsilon_{x/c}^{GGA}[\rho(r)] = \varepsilon_{x/c}^{LSD}[\rho(r)] + \Delta\varepsilon_{x/c} \left[\frac{|\nabla\rho(r)|}{\rho^{4/3}(r)} \right] \quad [83] \quad (14)$$

After introducing GGA functionals, meta-GGA and hybrid functionals are developed, which introduces more terms to the energy equation. In the meta-GGA's, a dependence on the kinetic energy (τ) is included in the exchange-correlation potential as a second derivative term. Continuously, in the hybrid functionals, GGA is mixed with some exact exchange[84]. However, by including an exact exchange, which does not depend on the electron density alone but also on the density matrix, the computational cost is increased[84].

In this thesis, the main functionals used are the Generalized Gradient Approximation functionals (GGA). The error in these group of functionals is lower than the LDA functionals, and the the overbinding errors are decreased from 30 kcal/mol to 5–10 kcal/mol[84]. According to Rappoport, the error is only slightly improved if Meta-GGA's are chosen[84]. Hybrid functionals are typically accurate to 3–5 kcal/mol, however they require a higher computational cost. Besides the smaller error, complexes of 3d elements are better described by GGA/meta-GGA functionals, while hybrid functionals yielded somewhat smaller deviations from the experiment for 4d and 5d element compounds[84]. Since Cr(III) is a 3d transition element it is expected

that GGA functionals are a reasonable choice. These functionals are considered the best balance of accuracy and computational cost in this study.

The calculations in this thesis are performed using the basic GGA's named by their inventors, BP86(Becke-Perdew), PW91(Perdew-Wang), PBE (Perdew–Burke-Ernzerhof), and one hybrid functional(B3LYP). The BP86, PBE and PW91 functional chosen for their low computational cost and are often observed in similar studies[27, 37, 85]. The B3LYP functional is chosen as it is a popular often observed functional[86], and only has a small percentage of exact exchange. This is important as functionals with a high percentage of exact exchange are probed to be problematic in calculating transition metal compounds and yield to unreliable spin split setting[84]. In this study one hybrid functional is tested, to see if the results between the GGA's and hybrid functional are comparable.

5.2 Basis set

Besides the functional, also a basis set is needed for the calculation. The basis set defines a set of functions that are used to represent the system and turn the partial differential equations into algebraic equations suitable for implementation on a computer[87]. The primary function of a basis set is to define the basis of orbitals included in the calculation.

In general, two types of basis sets can be found: Slater-type orbitals (STO) and Cartesian Gaussian-type orbitals (GTO)[84, 87]. In this study, only gaussian-type basis sets are used, which are less accurate than Slater-type but take less computational time and are easier to solve[87]. The most important aspect of choosing a basis set is choosing the number of functions that are included in a basis set[87]. The smallest basis set employs only enough functions for a minimum description of the neutral atoms occupied orbitals and is called a minimum or Single Zeta (SZ) basis set[87]. In a double-zeta basis set, two times as many STOs or GTOs are used as the number of core and valence atomic orbitals and in a triple-zeta three times.

According to Rappoport, a general rule in choosing the basis set is that the basis set's error must be smaller than the error produced in the functional[84]. It is described earlier that the error in the GGA functionals is between 5-10 kcal/mol. Therefore, the goal is to choose a basis set with an error comparable to or smaller than 10 kcal/mol. It is expected that a Triple Zeta basis set will be suitable for the calculations in this study for open-shell first-row transition metals like Cr(III)[88].

Next, if the amount of valance atomic orbitals to include in the calculation is determined, there is a possibility to include polarization and diffuse functions in the basis set. Adding these kind of functions is another way to expand the basis set and obtain more accurate results. The diffusion and polarization functions serve a different purpose when added to the system, but if implemented correctly both these functions can to improve the model's accuracy.

Polarization functionals are used to add more angular flexibility in forming the valence molecular orbitals by adding, for example, a d-polarization on top of the p orbitals visible in figure 5.2[14]. In the case of an octahedral symmetry, it is expected that the orbitals are mainly oriented on the axes. Therefore, it is expected no angular flexibility of the orbitals is needed. However, if different ligands are attached to the Cr(III) ion in the complex, there may be a distortion in the complex. According to Jensen, the bonding in transition metals is dominated by s- and d-orbitals, which suggests that f-type functions are the first polarization functions needed, but p-type polarization functions are also likely to be important[89]. To what extent a polarization functional will achieve better results in our type of system is not precisely de-

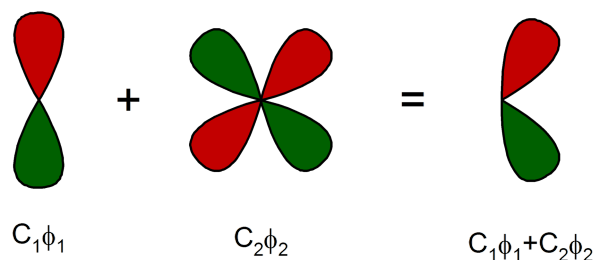


Figure 5.2: Effect of d-polarization function added to a p orbital CC-BY-SA-3.0[14]

terminated. However, as the bonding with ligands is expected to occur by d, s and p orbitals a polarization functional will be implemented in this study.

The incorporation of diffuse functions in the basis set is recommended if the system investigated contains noncovalent or long-range interactions[90]. In this study, a solvent environment is investigated, and it is intended to look beyond the length scale of bond-lengths, for example, to the excited states. Therefore, the implementation of diffuse functionals is crucial in our system to improve the calculations' accuracy.

To conclude, in this study, different basis sets will be tested and compared based on the differences in energy and calculation time. Finally, a basis set will be selected that includes diffuse functions and represents the doable balance between calculation time and accuracy for the time of this project.

5.3 Geometry optimization & single point energy

After choosing a functional, basis set and the defining the input coordinates of all atoms, the charge and multiplicity of the molecule, the system's geometry can be optimized by performing a DFT calculation. In this thesis coordinated complexes of Cr^{3+} are studied on their ligand substitution reactions. The optimized geometry of a complex is found at the minimum Gibbs free energy of that complex. To be able to compare different single-point energies of the complexes, the atoms at both sides of the reaction must be equal. Therefore, the substitution of a ligand in Cr^{3+} complexes is studied using both sides of the chemical equation. An example of this is given in figure 5.3. The driving force for the reaction is calculated by subtracting E2 from E1, providing the difference in energy ΔE between both sides of the equation.

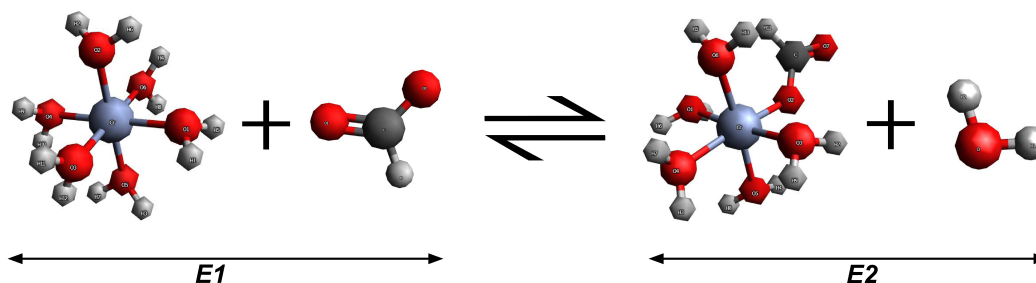


Figure 5.3: Substitution reaction of H_2O by HCOO^- in Cr^{3+} complex, visualized with Avogadro software

5.4 Include solvent effects

Initially, the single point calculations are executed for a single molecule in a vacuum, without accounting for solvent effects. In general there are two main groups of solvent models to include for solvent effects: implicit and explicit. The explicit solvent model considers all molecular details of each solvent molecule, while implicit models the solvent is treated as a continuous medium[16]. A visualisation of both models is given in figure 5.5. In addition, there is also the possibility to use a hybrid model, where the first (and second) solvation sphere is addressed explicitly while the rest is treated implicitly[16]. The relatively high computational cost of explicit solvent models has resulted in implicit solvent models remaining popular[91].

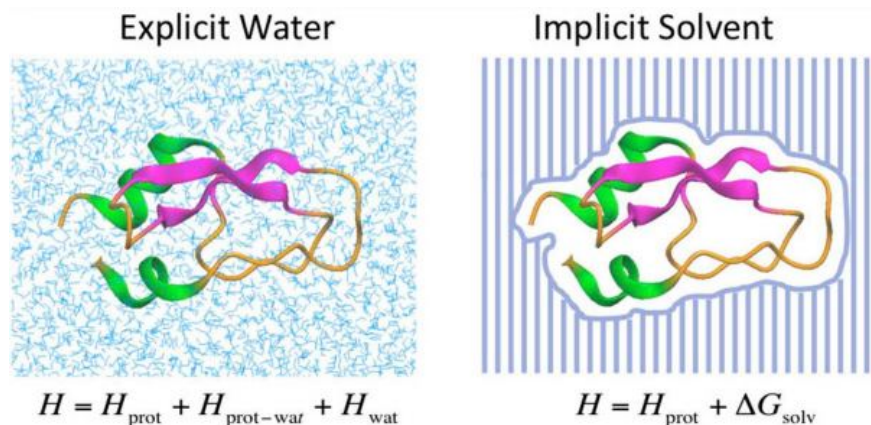


Figure 5.4: Difference between explicit and implicit solvation models[15]. ΔG , the free energy of solvation is calculated according to equation 15, H is the Hamiltonian of an system which is the operator corresponding to the total energy of that system

Two types of implicit solvation models which are available in ORCA 4.0.2 are implemented in this study. These solvent models are developed, as it is almost impossible to create a system considering each solvent molecule as a separate molecule for calculating the solvent effects due to the rise of a very high computational cost. The implementation of solvent models in this study is expected to be critical for creating meaningful results, as it is expected that the DFT calculations performed in a vacuum will be far from realistic. Therefore, in this study a solvation model will be implemented. It should be mentioned that all solvation models are simplifications to reduce computational costs[92]. In addition, in a solvent model a medium is chosen for the calculation. In this study, water is chosen, since a large percentage of the electrolytes used in this study will consist of water. However, it should be mentioned that within the possibilities this choice is the best, but it is not perfect, as other anions will be present in the experimental electrolytes.

The conductor-like polarizable continuum model (CPCM) and the Universal solvation model (SDM) are the solvation models which are used in this study. The main equation used to calculate solvent effects is the free energy of solvation given in equation 15. The free energy of solvation is defined by the ΔG_{cav} which is the free energy to create a solute cavity, ΔG_{disp} which contains the van der Waals interaction between solute and solvent and ΔG_{elec} which contains the electric component defining the polarisation between solute and solvent. In some examples, the ΔG_{hb} is included, which is the hydrogen bonding term.

$$\Delta G_{\text{solv}} = \Delta G_{\text{cav}} + \Delta G_{\text{disp}} + \Delta G_{\text{elec}} (+\Delta G_{\text{hb}}) [16] \quad (15)$$

The solvation models are built from a few parts, the solute molecule, possibly supplemented

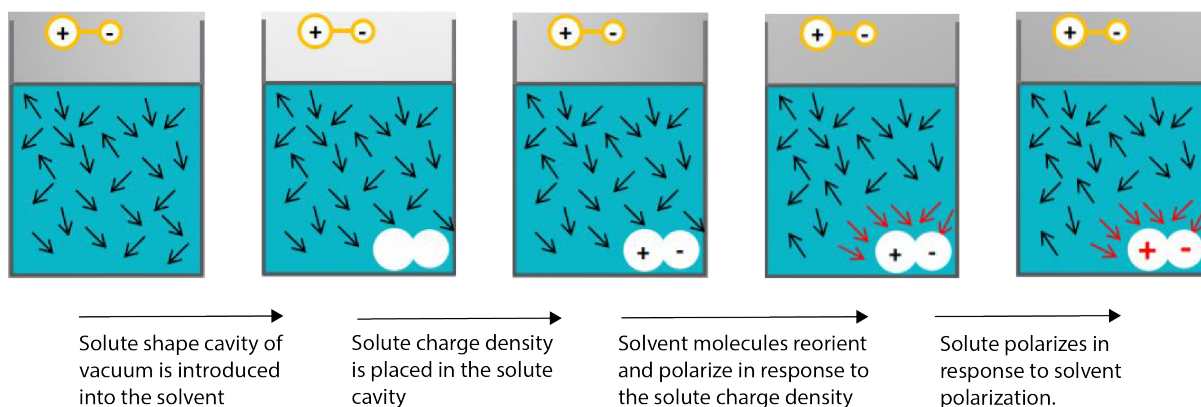


Figure 5.5: Theory behind implicit solvation models visualized, using slides from University of Helsinki[16], the cavity shape is defined according to figure 5.6

by some solvent molecules, which is placed into a void cavity within a continuous medium mimicking the solvent[93, 94]. Figure 5.5 provides a visualisation of this method. In different continuum models, the shape and size of the cavity, which is defined from Van der Waals surface, Solvent-Accessible Surface, Solvent-Excluded Surface can be different[92]. The Van der Waals surface is defined from the Van der Waals radii, which is the radius of a imaginary hard sphere representing the distance of closest approach for another atom. The solvent-accessible surface is defined from the center of the ideal solvent molecule (probe), and is all the area the molecule can come into contact with. On the contrary, the solvent excluded surface is the area, the ideal solvent model can not come into contact with. A visualisation of the cavity shape defined from these three parameters is given in figure 5.6.

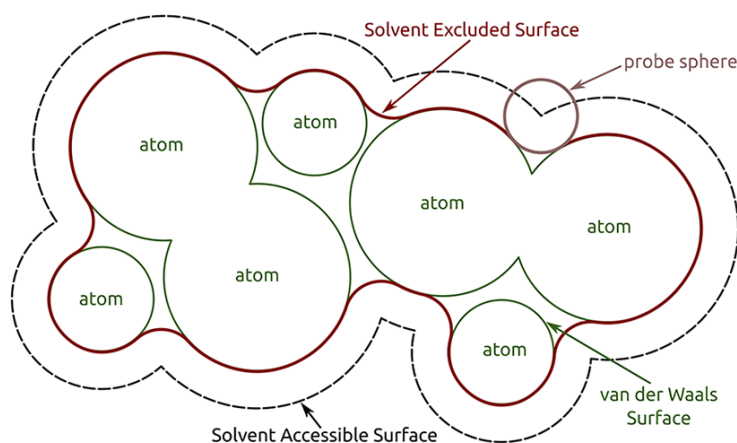


Figure 5.6: Visualisation of defining the cavity surface with Van der Waals surface, Solvent-Accessible Surface and Solvent-Excluded surface[17]

The SDM method[94] differs from the CPCM model[93] in calculating the cavity-dispersion term. The CPCM model only uses the area, while the SMD model uses the full solute electron density. According to Zhang, the SMD model is significantly better than other on force field-based implicit solvents models, but it is not as good as the explicit solvent model[91]. The SMD model still lacks explicit hydrogen bonding and most likely overestimates the strength of salt bridges if present[91]. The CPCM solvation model has a similar methodology comparable

to the SMD model but is not addressed in their study. According to the study of Sillanpää et al., the complexation energies with ligands are in general overestimated in the conductor-like solvation model, but the trends are reproduced correctly. Therefore it is likely that the energy of solvation will also be overestimated in our study. However, for this study's purpose, the implicit solvation models CPCM and SMD are expected to be sufficient to investigate the effect of ligands exchange as all complexes are investigated with the same solvation model and compared among each other. In further research an improvement could be made on including an explicit solvation model considering other species in the electrolyte for example an excess of HCOOH, HCOO⁻ and SO₄²⁻.

5.5 Spectroscopic studies with DFT

In this study, a significant focus is on investigating the spectroscopic characteristics of Cr(III) electrolytes in the addition of formate with UV-Vis and FTIR experiments. The possibility of predicting spectroscopic characteristics with DFT is considered a great benefit for the interpretation of the experimental data[95]. In this study, an attempt is made to simulate infrared spectra and UV-Vis spectra with the ORCA software[96]. The execution of frequency analysis to simulate infrared spectra is simple to implement in ORCA by including a frequency command in the input line. After the frequency calculation there should be no imaginary frequency on the optimized geometries, which means the geometries are the minimum points on their potential energy surface[97].

The simulation of UV-Vis spectra requires more additional calculations to be executed before the spectra can be predicted. Characterization of excited states can be performed by tackling an eigenvalue problem by either solving the Schrödinger equation using a multiconfigurational ansatz or the single-particle Kohn–Sham equations in the time-dependent formalism of the density functional theory (TD-DFT)[98]. In this study, the second example TD-DFT, is used. Two main drawbacks of this procedure are: 1) Large molecules/complex systems require a large set of KS orbitals, which makes Casida's equation (an eigenvalue problem for solving the excited states) unfeasible[98]. 2) High energy excitations are usually not adequately described due to the lack of well converged high energy virtual KS orbitals[98]. As this study's systems are relatively small complexes (less than 25 atoms) and only the lowest transitions are of interest, it is not expected that this approach will result in problems. However, in ORCA, the basic settings used TD-DFT with a simplified Tamm-Dancoff density functional approach, which simplifies the eigenvalue problem and speeds up the calculation two to three orders of magnitude in the excited state part at an only minor loss of accuracy[99]. The calculated excited states in TD-DFT can be used to generate electronic spectra, for example, UV-Vis spectra[99].

It should be mentioned that TD-DFT is found to give substantial errors[97] especially in large π -systems[100]. Although the bonding between Cr(III) and the ligands in octahedral symmetry is expected to be of σ -bonds character, it is expected that the metal-ligand bonding in our study and the open-shell character of the complexes is sensitive for errors. This is expected since our study structures are not as straightforward as calculating low-lying excited states in closed-shell systems. To what extent TD-DFT results are considered realistic will be checked with the available experimental data on Cr(III) complexes.

6 Materials and methods

6.1 Materials

In this study, two sets of chromium solutions are prepared from different chromium salts. Table 6.1 gives the solutions created with the chromium sulphate hydrate $\text{Cr}_2(\text{SO}_4)_3 \cdot 15\text{H}_2\text{O}$ salt supplied by Tata Steel, and table 6.2 the solutions created with $\text{Cr}(\text{ClO}_4)_3 \cdot 6\text{H}_2\text{O}$. The concentration of the $\text{Cr}_2(\text{SO}_4)_3 \cdot 15\text{H}_2\text{O}$ salt is tested with ICP-MS to determine the exact chromium content. Testing of the salt is necessary since the hydrated salt can have a different number of water molecules. In the end, the amount of chromium in the created solutions is corrected to 18.58 g/L.

Two stock solutions of 18.58 g/L chromium and 100 g/L SO_4^{2-} are created, one without the addition of NaHCOO and one with the ratio $[\text{Cr}]:[\text{HCOO}^-] = [1]:[9.7]$. The pH of both stock solutions is adjusted to 2.45 and stored at elevated temperatures of 40 degrees Celsius to prevent a deposit in the solutions to form. From these two stock solutions, new solutions with ratios in the range of c.a.[1]: [1 to 7.5] of $[\text{Cr}]:[\text{HCOO}^-]$ are created all in two-fold. The solutions used in this study are given in table 6.1.

Solution	Ratio Cr	Ratio HCOO^-	Cr [M]	HCOO^- [M]
1	1	0	0.3573	0
2	1	0.4	0.3573	0.1442
3	1	0.74	0.3573	0.2885
4	1	1.11	0.3573	0.4327
5	1	1.48	0.3573	0.5769
6	1	2.96	0.3573	1.1539
7	1	4.44	0.3573	1.7308
8	1	5.93	0.3573	2.3078
9	1	7.41	0.3573	2.8847

Table 6.1: $\text{Cr}_2(\text{SO}_4)_3$ solutions in addition of HCOONa

Table 6.2, presents the set of solutions created with chromium perchloride ($\text{Cr}(\text{ClO}_4)_3$) as chromium salt. Due to the salt's highly hydrophilic character, the amount of chromium salt needed for the stock solution of 15 g/L is weighted in a glove box. The use of a glovebox prevents a mass increase of the chromium salt by attracting water before the correct amount for the stock solution is weighted. Subsequently, six solutions in addition to sodium sulphate with ratios 1-6 are created in threefold. A prior screening was conducted using a UV-Vis spectrometer to ascertain the range of concentration, at which it was feasible to test the electrolytes (absorption value between the 1-2). After two days, the solutions are screened to see if a change in the spectra can be observed. However, no changes were observed after two days. Therefore, the solutions were placed at elevated temperatures of 70 degrees Celsius for one week to speed up the chromium complexes' complexation.

6.2 Methods

6.2.1 Ultra Violet visible spectroscopy (UV-VIS)

The UV-Vis spectra were collected with Shimadzu UV-2600 equipment with the Lab Solutions software. The chromium solutions are investigated in a cuvette of Quartz glass with a 2 mm path length for the chromium sulphate solutions and a 5 mm path length for the chromium perchloride

Solution	Ratio Cr	Ratio SO ₄	Cr [M]	SO ₄ ²⁻ [M]
1	1	1	0.2885	0.2885
2	1	2	0.2885	0.5770
3	1	3	0.2885	0.8654
4	1	4	0.2885	1.1539
5	1	5	0.2885	1.4424
6	1	6	0.2885	1.7309

Table 6.2: Cr(ClO₄)₃ solutions in addition of Na₂SO₄

solutions at the applied scan range of 800-280 nm and data interval 1 at room temperature. All the chromium sulphate solutions' pH values are corrected to 2.45 (error marge of 0.01) with sulphuric acid. The solutions from Cr(ClO₄)₃ are not pH corrected. A background measurement of distilled water was collected before conducting the Cr(III) electrolytes measurements, as a large percentage of the electrolyte consists of distilled water. Between each measurement, the quartz glass was rinsed three times with distilled water and all the droplets were removed before the new solution was pipetted in the cuvette. The chromium sulphate solutions are created in two-fold, and chromium perchloride solutions in three-fold to exclude eventual errors. Also, the measurements are repeated to exclude eventual errors in the measurements if no comparable data was observed in similar solutions. Two possible explanations that can cause deviation between the measurements are a not properly cleaned quartz glass or air bubbles at the cuvette's inside surface.

6.2.2 Attenuated Total Reflection ATR-FTIR

The FTIR spectra were collected with a Thermo-Nicolet Nexus equipped with a liquid-nitrogen cooled mercury-cadmium-telluride (MCT) detector and an ATR accessory. The ATR accessory operates by measuring the changes that occur in an internally reflected infrared beam when the beam comes into contact with the sample. A pipet is used to apply a portion of the sample to the ATR germanium crystal, and it was ensured that the liquid completely covered the crystal. A background measurement of distilled water was collected before each measurement, as a large percentage of the electrolyte contains distilled water. The ATR crystal was carefully cleaned before and between each analysis. First with isopropanol and secondly with distilled water (at room temperature). All the spectra were collected at constant room temperature and repeated three times to exclude eventual errors in the measurements. In addition, all solutions are created and tested in two fold to ensure the reproducibility of the data. The range of measurements was fixed at 4000 to 650 cm⁻¹ where peaks corresponding to the stretching or bending of specific functional groups can be observed.

6.2.3 DFT Computational studies with ORCA

DFT calculations are performed with ORCA 4.2.0, an ab initio, DFT, and semi-empirical SCF-MO package developed by Frank Neese et al. [96]. In this thesis, chromium (III) complexes are investigated with H₂O, SO₄²⁻ and HCOO⁻ as possible species participating in ligand exchange. Chromium is a first-row transition metal, and the complexes formed are characterised by their open-shell with six ligands orientated in an octahedral symmetry. The open-shell and charge of the complex require the electrons to be unevenly distributed in the molecular orbitals. Therefore an unrestricted ORCA calculation will be used, allowing three electrons extra in the spin-up orbitals than the spin-down orbitals.

All investigated structures are built using the Avogadro software[101], and the geometry is pre-optimised before a .xyz coordination file was generated as input for ORCA. Basic information about the basis set, functional, computational task, xyz coordinates, charge and multiplicity of the molecule needed for ORCA calculations, can be selected via the simple input feature line in a notepad file. An example of an input command will be the following:

- ! UKS (Unrestricted calculation) BP86 (functional) Def2-TZVP (Basisset) opt (optimization) freq (frequency analysis)
- * xyzfile 3 (charge) 4 (multiplicity) file.xyz (name of the file with xyz coordinates)*

Consequently, the command manager is used to execute the calculation by calling ORCA and referring to the input file with the specifics on the calculation. The output is generated in an .out file and can be studied with notepad as raw data. or visualised with a DFT visualisation program, for example Avogadro[101]. In this study both the raw data and Avogadro is used for studying the results of the calculations.

The functionals BP86 and PW91 will be used for optimizing the complex structures and calculating the point energies. The QZVP basis set was found to produce an error smaller than the chosen functional BP86 and PW91. However, the large computational cost and long calculation times make it difficult to implement this basis set for the calculations in this study. Therefore, a triple zeta functional is chosen, which produces a slightly larger error. The addition of diffusions to the basis set is considered critical for this study. Therefore the basis set Def2-TZVP[102] is chosen for the calculations, which has two diffuse functionals and one polarization functional.

First, all structures are optimized in a vacuum, then with the CPCM solvation model and finally with the SMD solvation model. All solvent models will use water as a medium. Subsequently, the total point energies of the chemical equation's left side will be subtracted from the right side. If the energy difference is negative, the equilibrium will shift to the chemical equation's right side, and this side will be favoured. If positive, the species at the left side of the chemical equation will be favoured. Next, all the energy differences of the complexes with 1 - 6 HCOO⁻ groups and the different isomers will be compared to see up to and including when it is spontaneous to replace a H₂O molecule by a HCOO⁻ molecule.

Subsequently, the simulated spectra will be generated using the PW91 functional. The optimized structures from the point energy calculations will be used for performing a additional frequency analysis. To execute this command 'Freq' will be included in the input-file. The results of the IR spectra will be visualized using the Avogadro software[101].

Next, the UV-Vis spectra will be calculated using the PW91 functional, ensuring comparability in the data obtained during this study. On the ORCA software tutorial site, the minimal basis set suggested for this type of calculations is Def2-TZVP. The high computational cost of the TD-DFT calculation is compensated with the RIJCOXS approximation, recommended from the ORCA library[103]. This approximation is stated to increase the speed without affecting the results drastically. The procedure is essentially linear scaling such that large and accurate calculations become possible with high efficiency[104]. With the RIJCOXS approximation, the problem is addressed by performing 2 electron integrals. The first integration is done numerically on a grid, and the second (involving the coulomb singularity) is performed analytically[104].

The observed errors are of c.a. 1 kcal/mol in the total energies, which can be reduced using a larger grid than default or by running the final SCF cycle without this approximation[104].

However, the error in the range of 1 kcal/mol is considered accurate enough for this studies purpose. Finally, the results obtained in the TD-DFT calculations will be studied using the raw-data in a notepad file and visualizing the spectra with the Avogadro software[101].

7 Results and discussion

This section is divided into three subsections. Firstly the experimental results of $\text{Cr}_2(\text{SO}_4)_3$ electrolytes are discussed. It is expected that these solutions are closest to electrolytes used in industrial applications by Tata Steel and their experiment[24, 27]. Secondly, the results of the DFT calculations on the substitution of H_2O by HCOO^- is presented. In these calculations, SO_4^{2-} is not included due to the uncertainties in the chemical structure of chromium complexes with SO_4^{2-} . The last part of this section contains the experimental data of $\text{Cr}(\text{ClO}_4)_3$ electrolytes in addition of SO_4^{2-} . These experiments are performed for comparability between the simulated DFT data to experimental data.

7.1 Changes in the solution chemistry of $\text{Cr}_2(\text{SO}_4)_3$ solutions in addition of NaHCOO

The results of UV-Vis and ATR-FTIR experiments are presented in this subsection. The UV-Vis data is used to study chromium-ligand connections on the molecular scale and ATR-FTIR data is used to study the bonds and functional groups in the molecule. It should be noted that both techniques give different information on the chemical structure of the molecules and need to be addressed separately.

7.1.1 UV-Vis experiments

The collected UV-Vis measurements are shown in figure 7.1. In the range of 280-800 nm, two clear peaks can be distinguished, and a third peak can be observed just out of this range below 280 nm. Due to limitations of available cuvettes and unstable measurements below this range, this third peak is excluded from the interpretation. In figure 7.1, the absorption values (A) are converted into the molar absorption coefficient ϵ according to the Beer-Lambert law of equation 2.

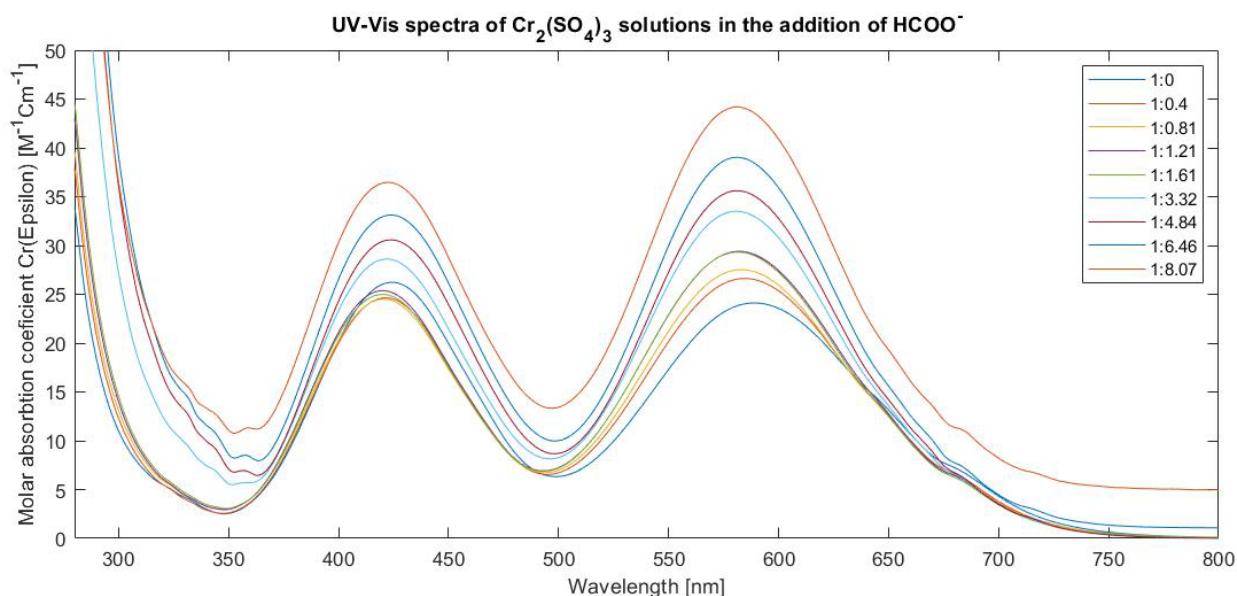


Figure 7.1: UV-Vis spectra of $\text{Cr}_2(\text{SO}_4)_3$ at pH 2.45 and room temperature, legend shows different ratios of $[\text{Cr}^{3+}]:[\text{HCOO}^-]$

It can be observed that with an increasing ratio of $[\text{Cr}^{3+}]:[\text{HCOO}^-]$, a hyperchromic shift

occurs in the molar absorption coefficient. Simultaneously, a hypsochromic (blue) shift, towards lower wavelength can be observed in the first transition peak. The shift in the second transition peak is also hypsochromic upon the addition of low concentration of $\text{Cr}^{3+}:\text{HCOO}^-$ until $[1]:[3.32]$. This shifts in the wavelength of UV-Vis data can be confirmed by an observed change in the the electrolyte's appearance, which has slightly changed from green towards a more blue appearance in the addition of formate. Two other observations that need to be mentioned are that the first peak becomes slightly more narrow, when the spectra without NaHCOO and with the addition of NaHCOO are observed. Transition peaks are characterised narrow if they are smaller than 100cm^{-1} (2 nm)[6], this is definitely not the case for the peaks visible in figure 7.1. However, a decrease in the peak width can indicate the following[47]:

- More species of the same energy are observed in a smaller range, so there is a smaller variation in the number different complexes
- The coordination of the complex is with only one type of ligand vs multiple types, since complexes with only one type of ligand should naturally have narrower peaks.
- The broader band has ligands situated further apart in the spectrochemical series.

It should be mentioned that both bands are not characterised narrow, but only that the transition peak becomes slightly more narrow in addition of NaHCOO . Secondly, the shape of both transition peaks is symmetrical. This can give an indication that similar ligands are present in the complex or not situated far apart in the spectrochemical series, since complexes with different ligands often produces less symmetrical transition bands[47].

The effect of the addition of formate on the locations of the maxima (λ_{Max}) is visualized by calculating and plotting the points in two separated graphs, figure 7.2 and 7.3.

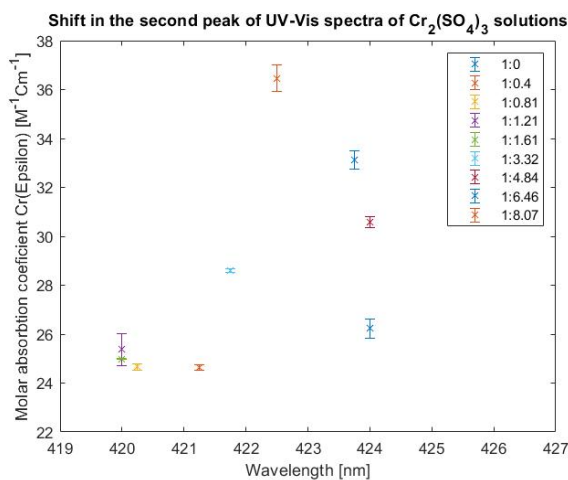


Figure 7.2: Shift in the position of λ_{Max} of the second transition peak in $\text{Cr}_2(\text{SO}_4)_3$ solutions. Legend shows different ratios of $[\text{Cr}^{3+}]:[\text{HCOO}^-]$

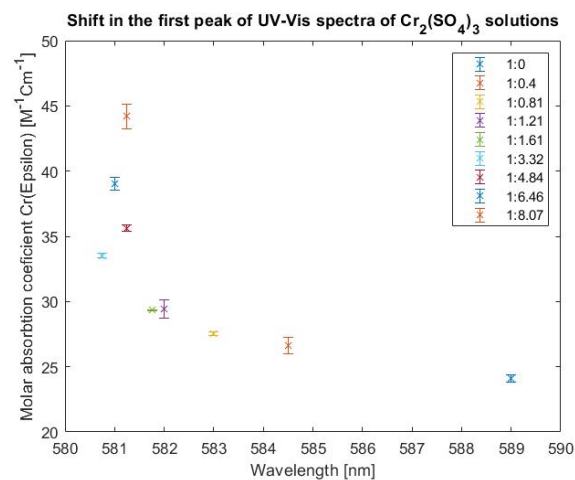


Figure 7.3: Shift in the position of λ_{Max} of the first transition peak in $\text{Cr}_2(\text{SO}_4)_3$ solutions. Legend shows different ratios of $[\text{Cr}^{3+}]:[\text{HCOO}^-]$

In figure 7.3 it can be observed that there is a clear hypsochromic (blue) shift to lower wavelengths in the first peak until the ratio of $[\text{Cr}^{3+}]:[\text{HCOO}^-] = [1]:[3.32]$. If the formate ion concentration is further increased, no significant effect in the shift of λ_{Max} can be observed, and the position of maximum λ_{Max} oscillates around 581 nm. A hyperchromic shift is visible in

the molar absorption coefficient, suggesting more light is absorbed by the newly formed complex.

Figure 7.2 visualizes the shift in the second transition peak, which shows a similar hypsochromic (blue) shift to lower wavelengths up to and including the ratio of $[\text{Cr}^{3+}]:[\text{HCOO}^-] = [1]:[1.61]$. Between the measurements of solutions with ratios $[\text{Cr}^{3+}]:[\text{HCOO}^-] = [1]:[1.61]$ and $[\text{Cr}^{3+}]:[\text{HCOO}^-] = [1]:[4.84]$ an opposite bathochromic shift occurs. Beyond the ratio of $[\text{Cr}^{3+}]:[\text{HCOO}^-] = [1]:[4.84]$, again a hypsochromic shift occurs.

It is suggested that the shift change is caused by an excess of HCOO^- ions in the electrolytes that is present at higher concentrations of NaHCOO . At the concentrations below $[\text{Cr}^{3+}]:[\text{HCOO}^-] = [1]:[1.61]$, it is expected that almost all HCOO^- will be bonded to the Cr(III) atom; this will be confirmed with ATR-FTIR. Therefore, only a small concentration of HCOO^- will be in the solutions as an excess. It is mentioned in chapter 2.3 that the second peak is correlated with the crystal field splitting Dq + the Racah parameter B and that the Racah parameter is a measure of the electron-electron interaction. It is expected that the shift in λ_{Max} past the concentration of $[\text{Cr}^{3+}]:[\text{HCOO}^-]$ is $[1]:[1.61]$ is caused mainly by more electron-electron interactions in the electrolytes as a result of the excess of HCOO^- . In the next section on ATR-FTIR results, more details on the bonding between HCOO^- and chromium or HCOO^- free in solution (excess) will be provided.

The similar behaviour of the first and second transition peak between the ratios $[\text{Cr}^{3+}]:[\text{HCOO}^-] = [1]:[0]$ and $[\text{Cr}^{3+}]:[\text{HCOO}^-] = [1]:[1.61]$ is attributed to the exchange of a ligand in the complex. According to equation 3 ($E = hc/\lambda$), the observed hypsochromic (blue) shift is related to a complex with higher energy. This increase in energy suggests that the ligand substituted in the complex should be higher in the spectrochemical series than the ligand initially present in the complex. It is expected that the ligand initially present in the chromium complex is SO_4^{2-} due to the green appearance of the electrolytes an availability of SO_4^{2-} from the chromium salt[41]. Therefore, the shift, especially in the first transition peak, indicates that SO_4^{2-} or H_2O is replaced by another ligand. Since the first peak is a direct measure of Dq the octahedral field splitting, the shift in this transition peak can be fully attributed to the ligand exchange.

There is a general agreement on the higher position of H_2O in the spectrochemical series than SO_4^{2-} . Therefore it is possible that SO_4^{2-} will be replaced by H_2O . However, it is suspected that the new complex formed will include HCOO^- , as a deposit from Cr(III) electrolytes with formate consist of chromium-carbides. Besides, if the order presented by Mandich[29] is considered, it can be expected that HCOO^- will be included in the complex.

To summarize all findings, it can be concluded that there is a change occurring in the investigated Cr(III) complexes' coordination structure, which is related to the addition of NaHCOO in the electrolytes. There are two main observations: There is a shift in the wavelengths at which the maximum absorption is measured, and secondly, there is an increase in the molar absorption coefficient at this wavelength for the first peak. The second peak first shows a slight decrease before it increases. The increase in the molar absorption coefficient means that more light is absorbed on a specific wavelength. In all solutions, the pH, temperature and concentration are kept constant. Therefore, this increase in molar absorption coefficient is likely caused by the formation of a new complex. However, it is expected that, for example, an excess of HCOO^- also affects the observed molar absorption coefficient.

The other main observation is a gradual shift visible towards lower wavelengths, related to a complex with higher energy. However, there are differences in the positions of λ_{Max} between the two transition peaks. The first peak, which is directly related to splitting in the d-orbitals (Dq), shows a total shift of c.a 8 nm until the ratio of $[\text{Cr}^{3+}]:[\text{HCOO}^-] - [1]:[3.32]$ is reached. Beyond

this ratio the position of λ_{Max} keep constant around 281 nm. On the other hand, the second peak only shows a significant shift till $[\text{Cr}^{3+}]:[\text{HCOO}^-] - [1]:[1.61]$, after which the shift is in the opposite direction and shows no clear trend at all. The second peak depends on the splitting of the d-orbitals (Dq) and the Racah parameter B, which describes the effects of electron-electron repulsion[69]. Since Dq's value should be equal in both peaks, the difference in the position of λ_{Max} can only be caused by the influence of Racah parameter B. Therefore, it is assumed that there is an excess of free formate in solution, which is expected start to be formed between the concentrations of $[\text{Cr}^{3+}]:[\text{HCOO}^-] - [1]:[1.61]$ and $[\text{Cr}^{3+}]:[\text{HCOO}^-] - [1]:[3.32]$ and that this excess affects the observed shift of λ_{Max} in the second peak.

It was observed by testing the two solutions of NaHCOO (1M) and Na₂SO₄ (1M) that an HCOO⁻ and SO₄²⁻ show no absorption peaks in the region of 280-800 nm. Therefore, an excess of HCOO⁻ and SO₄²⁻ cannot be measured unless it affects the chromium complex. Based on the UV-Vis data, it can be concluded that ligand exchange is occurring. However, to prove the presence of formate in the chromium complex, ATR-FTIR experiments will be conducted.

7.1.2 ATR-FTIR experiments

The collected ATR-FTIR spectra, visualised with Spectrograph software developed by Menges[105], can be observed in figure 7.4. In this figure, the four main areas of interest A, B, C and D, are selected with green rectangles. These regions will be addressed separately, in a magnified view.

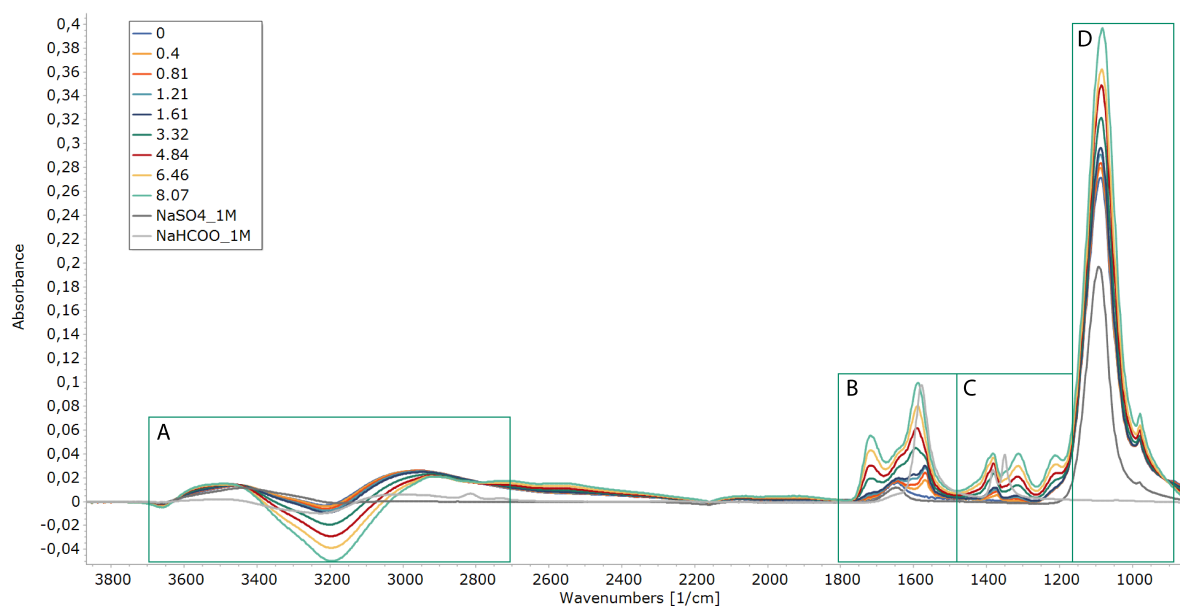


Figure 7.4: Collected ATR-FTIR spectra of Cr₂(SO₄)₃ solutions with four ranges

Figure 7.5 shows an magnified view of the 3900-2500 cm⁻¹ range A. It can be observed that with increasing concentration of HCOO⁻, the peak corresponding to the intermolecular O-H bond shifts to higher wavenumbers and becomes more symmetrical. The peak corresponding to the intramolecular H-O bond decreases in absorbance and shifts towards lower wavenumbers. At the ratio of $[\text{Cr}^{3+}]:[\text{HCOO}^-] = [1]:[3.32]$ and higher, a new maxima can be distinguished around 2975 cm⁻¹ corresponding to a different vibration than below this concentration. However, since the peaks in the spectra of HCOO⁻ 1M and the electrolytes spectra have no similar peak positions, no specific bond can be assigned. The shift is expected to be caused by the

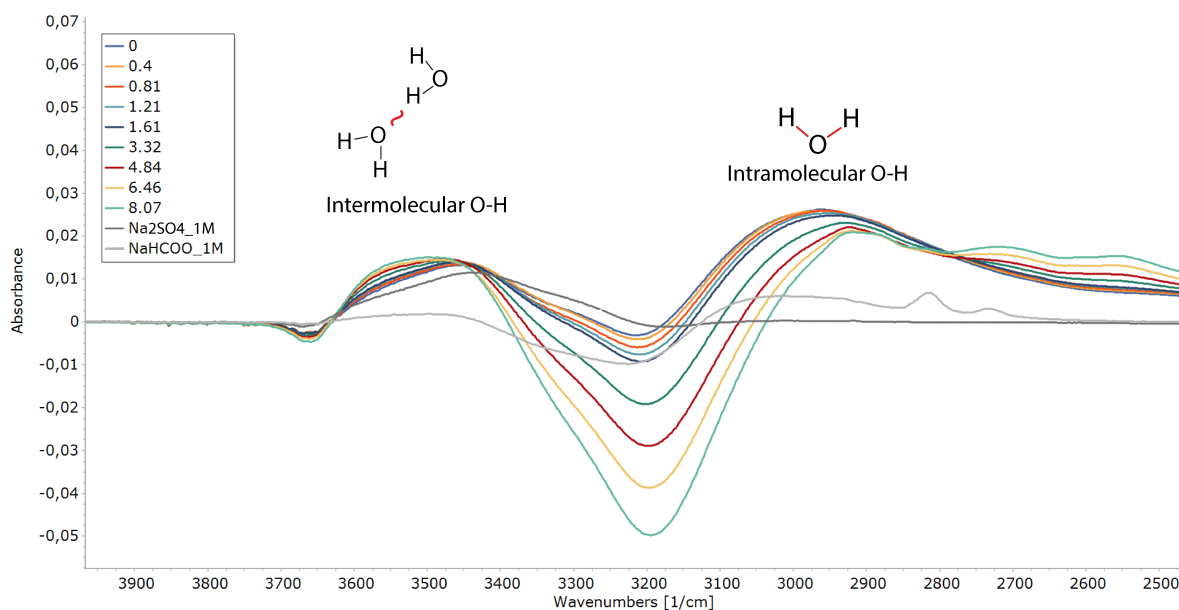


Figure 7.5: Expanded FTIR spectra of the 3900 - 2500 cm^{-1} range

blending of different peaks in this region due to the addition of NaHCOO.

Figure 7.6 shows an extended view of the 1800-1500 cm^{-1} range B. In this region, multiple peaks can be distinguished, and the following four observations are found:

- A peak at 1719 cm^{-1} arises corresponding to a vibration of the carbon-oxygen double bond of HCOOH. This vibration is also observed in the work of Lucks et al. on the vibrational spectra of HCOOH[3](see figure 2.5 for reference).
- In the electrolytes without the addition of sodium formate, only one peak is around 1648 cm^{-1} is observed. The spectra of the Na₂SO₄ 1M solution shows a similar shaped peak around 1648 cm^{-1} . Therefore, it is expected that both the absorption peaks around 1648 cm^{-1} are from the vibrations in the SO₄²⁻ anions. After the addition of formate, this peak at 1648 cm^{-1} blends in with the new rising peaks from the addition of NaHCOO. However, it does not disappear, and only a tiny shift (c.a 7 cm^{-1}) to lower wavenumbers can be observed. If this shift is caused by the exchange of SO₄²⁻ ligands or due to the appearance of new close laying peaks is undetermined yet.
- In the range of 1550-1600, with increasing formate ion concentration, a peak arises at 1567 cm^{-1} till the ratio [Cr³⁺]:[HCOO⁻] exceeds [1]:[1.61]. In the solutions with ratio [Cr³⁺]:[HCOO⁻] = [1]:[3.32], this peak at 1567 cm^{-1} is still visible, but a new peak at 1690 cm^{-1} has become dominant. The peak at 1567 cm^{-1} does not change in position. Therefore, it is expected that this peak corresponds one specific vibration in the chromium complex related to the attachment of a HCOO⁻ molecule to a chromium atom. The vibration at 1567 cm^{-1} is close to the asymmetrical vibration of COO⁻ in HCOO⁻. Therefore, the vibration at 1567 cm^{-1} is assigned to the asymmetrical COO⁻ vibration in the complex with HCOO⁻ ligand(s).
- It has been mentioned that a significant peak arises around 1600-1588 cm^{-1} . This peak starts to form from the ratio [Cr³⁺]:[HCOO⁻] = [1]:[0.81] & [Cr³⁺]:[HCOO⁻] = [1]:[1.21], and becomes larger with increasing HCOO⁻ concentration. As the position of this peak

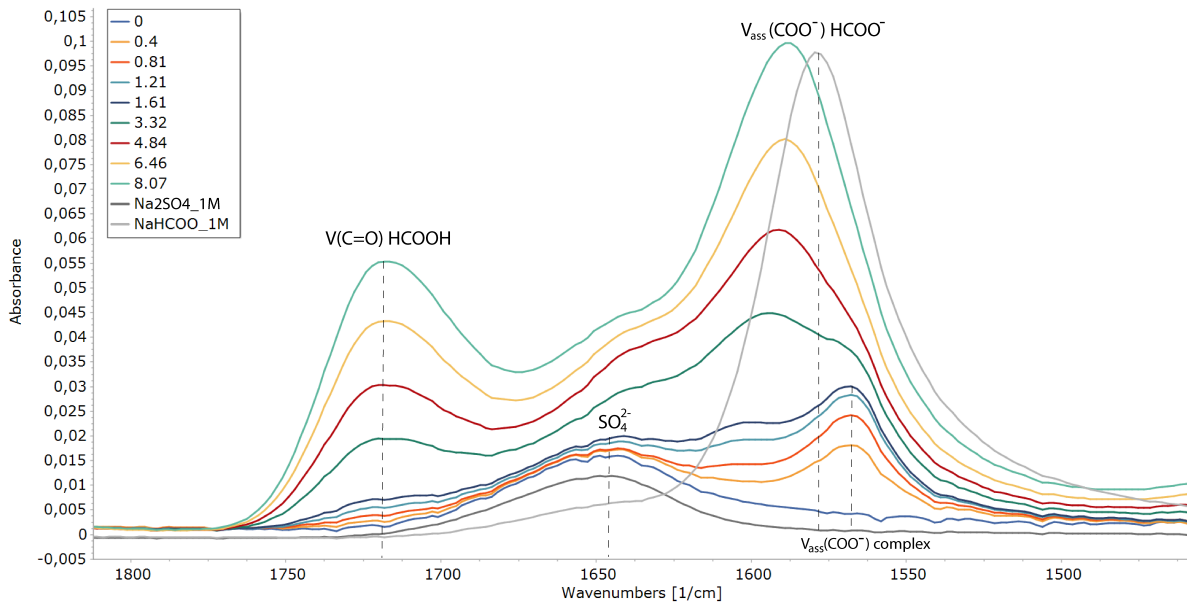


Figure 7.6: Expanded FTIR spectra of the 1800- 1500 cm^{-1} range

shifts with increasing HCOO^- concentration, it is expected that this peak is a mixture of different absorption peaks. The shape and absorbance of this peak at ratios of $[\text{Cr}^{3+}]:[\text{HCOO}^-]$ above $[1]:[6.46]$ shows similarities with the asymmetrical vibration of COO^- in HCOO^- . Therefore, this peak between 1600-1588 cm^{-1} is expected to be mainly caused by an excess of HCOO^- in the electrolytes. The observed peak difference in the position of the $V_{\text{ass}}(\text{COO}^-)\text{HCOO}^-$ and 1688 of cm^{-1} in $[\text{Cr}^{3+}]:[\text{HCOO}^-] = [1]:[8.07]$ (light green line) is caused by the mixing of close laying peaks.

Figure 7.7 shows an extended view of the 1500-1200 cm^{-1} region C. In this range, peaks corresponding to vibrations in HCOO^- , HCOOH and a formed complex are observed, and the following observations are found:

- At 1382 cm^{-1} a peak corresponding to the C-H vibration of HCOO^- can be observed in the spectra of NaHCOO 1M ($V(\text{C-H})\text{HCOO}^-$). Around this same wavenumber at 1380 cm^{-1} a peak with a shoulder can be observed in the spectra of the electrolytes at higher ratios of $[\text{Cr}^{3+}]:[\text{HCOO}^-]$. This peak around 1380 cm^{-1} can be observed from the ratio $[\text{Cr}^{3+}]:[\text{HCOO}^-] = [1]:[1.21]$ and becomes more clear at higher concentrations of HCOO^- . It is expected that the peaks at 1380 cm^{-1} can be attributed to excess of HCOO^- in the electrolytes. However, there is a clear difference between the peaks present in the spectra of NaHCOO 1M and the electrolytes' spectra at 1380 cm^{-1} . Therefore, the peak at 1380 cm^{-1} can not be attributed purely to the excess of HCOO^- and is expected to be a mixture of multiple vibrations, including $V(\text{C} - \text{H})\text{HCOO}^-$ at higher ratios of $[\text{Cr}^{3+}]:[\text{HCOO}^-]$.
- At low ratios of $[\text{Cr}^{3+}]:[\text{HCOO}^-]$ below $[1]:[1.61]$ an asymmetrical peak with a wide shoulder can be observed at 1370 cm^{-1} ($V_{\text{s}}(\text{COO}^-)$ -complex). It is expected that this peak corresponds to the merged vibrations of $V(\text{C} - \text{H})$ and the symmetrical vibration of (COO^-) in the formed complex. Since the peaks at 1382 and 1352 cm^{-1} corresponding to the vibrations in the solution of NaHCOO 1M solution have disappeared.
- Around 1352 cm^{-1} the peak assigned to $V_{\text{s}}(\text{COO}^-)\text{HCOO}^-$ can be observed. This peak position matches the experimental found data presented by Lucks et al. perfectly[42](see

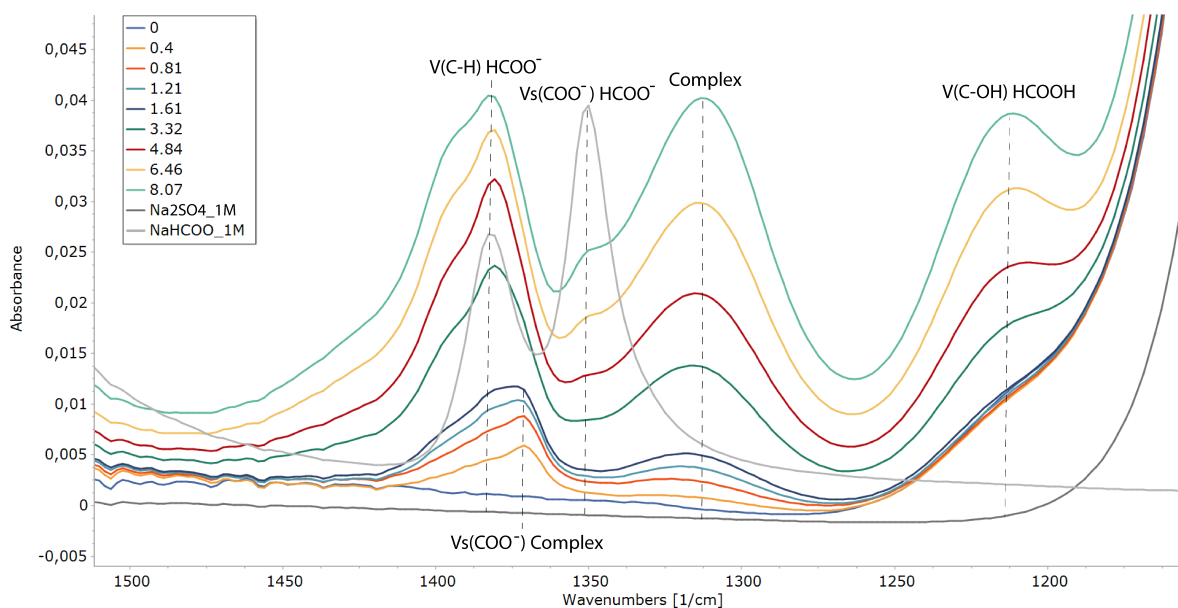


Figure 7.7: Expanded FTIR spectra of the 1500- 1200 cm^{-1} range

figure 2.5 for reference). The bump observed in the electrolytes' spectra with ratios $[\text{Cr}^{3+}]:[\text{HCOO}^-] = [1]:[4.84]$ and higher is assumed to be caused by the vibration of

- It can be observed that with increasing HCOO^- concentration, a peak arises at 1313 cm^{-1} . This peak can not be attributed to HCOO^- , HCOOH or SO_4^{2-} since it is not visible in the reference spectra and is not present without the addition of HCOO^- . Therefore, this peak assigned to the formed complex (complex).
- At 1214 cm^{-1} the peak corresponding to the vibration of $\text{V}(\text{C-OH})$ in HCOOH can be observed. The position of this peak matches the experimental found data presented by Lucks et al.[3](see figure 2.5 for reference). In the electrolytes, HCOOH will be dominant due to the low pH of 2.45 of the electrolytes. However, at low concentrations up to and including $[\text{Cr}^{3+}]:[\text{HCOO}^-] = [1]:[1.61]$ almost no HCOOH is observed, since there is no peak visible at 1214 cm^{-1} . This observation suggests that the bonding with HCOO^- is preferred above HCOOH . However, the evidence is not fully convincing, and the preferred bonding with HCOOH should be explored in further research.

Finally, figure 7.8 shows an extended view of the $1200\text{-}800 \text{ cm}^{-1}$ region D. In these region, the focus is only on assigning the large observed peak between $1100\text{-}1050 \text{ cm}^{-1}$.

From the reference spectra of Na_2SO_4 1M, it can be observed that the vibration at 1092 cm^{-1} can be assigned to the presence of SO_4^{2-} . Due to the addition of 100 g/l of SO_4^{2-} to the electrolytes, there is a significant constant amount of SO_4^{2-} ions in the electrolytes. However, a slight shift and increase in this peak around 1092 cm^{-1} to lower wavenumbers can be observed. It is possible that due to ligand exchange, more free SO_4^{2-} becomes present in the electrolytes if SO_4^{2-} is replaced by HCOO^- . However, the shift observed is smaller than 10 cm^{-1} and occurs even at high concentrations of NaHCOO . Therefore, it is expected that this shift is not caused by ligand exchange but is affected by the changing surrounding of the SO_4^{2-} molecules.

Based on observations in this section, the following conclusions are drawn:

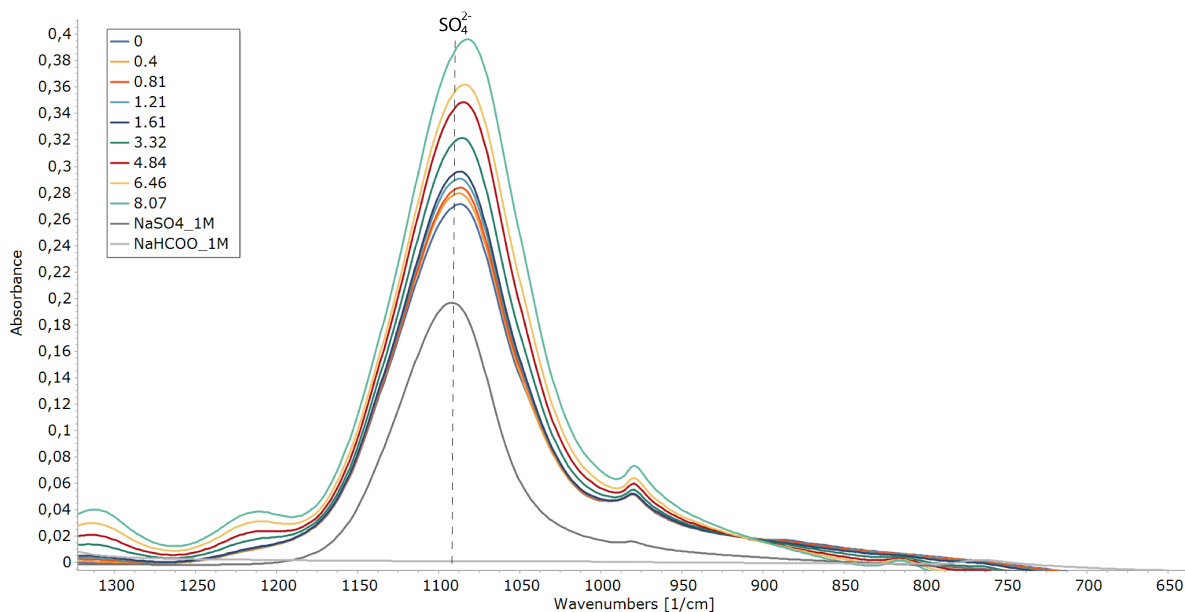


Figure 7.8: Expanded FTIR spectra of the 1200- 900 cm^{-1} range

- Firstly, the peak corresponding to the intermolecular hydrogen-oxygen bond shifts gradually to lower wavenumbers. Therefore, it is expected that there is a change in the molecules in which this bond is observed. The addition of NaHCOO clearly causes a shift in the intramolecular H-O bond, but this does not match the observed peaks of spectra from NaHCOO (1M). Therefore, it is not possible to assign the observed new maxima to the complex, as it is likely that a mixture of different vibrations is observed in the 3100- 2900 cm^{-1} range.
- Secondly, there is a clear shift visible in the peaks assigned to symmetrical and asymmetrical vibrations of COO^- in the complex compared to the symmetrical and asymmetrical vibrations of COO^- observed in HCOO^- . This shift in vibrational frequency indicates that HCOO^- molecules form a complex with the chromium atoms. Up to and including the ratio of $[\text{Cr}^{3+}]:[\text{HCOO}^-] = [1]:[1.61]$, mainly chromium-formate complexes are observed. Beyond the ratio of $[\text{Cr}^{3+}]:[\text{HCOO}^-] = [1]:[3.32]$ an strong increase in the peak around 1688 cm^{-1} indicates an excess of HCOO^- . Therefore, it is expected that the maximum amount of chromium-formate complexes is reached between the ratios of $[1]:[1.61]$ and $[1]:[3.32]$. Beyond the ratio of $[\text{Cr}^{3+}]:[\text{HCOO}^-] = [1]:[3.32]$ an excess of formate and formic acid is observed.
- Thirdly, the observed splitting between the peaks assigned to the symmetrical and asymmetrical vibration of COO^- in the complex found to be 197 cm^{-1} . This value is larger than 150 cm^{-1} , which confirms the monodentate binding of formate with the chromium ion.

7.2 Modelling of ligand substitution with DFT calculations

In this section, the results of the performed DFT calculations with ORCA are presented. Before conducting the calculations two, main assumptions are made. Firstly, it is assumed that the

initial structure before ligand substitution is the $[\text{Cr}(\text{H}_2\text{O})_6]^{3+}$ complex. There is an agreement on this complex's existence, especially in chromium salts solutions created from nitrate, chloride and perchlorate solutions[36, 78]. It is considered that this complex might be not the initial structure in chromium sulphate solutions. However, including SO_4^{2-} molecules in the complex makes the system more complicated, and the uncertainties on the chemical structure make the final results with these calculations unreliable.

Secondly, it is assumed that the ligands in the complexes studied are water molecules and that there are no hydroxide molecules present without the application of an external current. The pH of the solutions in this study is 2.45, which makes it more likely for H_2O molecules to be present in the complex than OH^- molecules. Therefore, the initial studied reactions are of the repeated ligand exchange of formate ions (HCOO^-) to a chromium complex with initially six H_2O ligands. An overview of the chromium-formate complexes used in this section is given in figure 7.9.

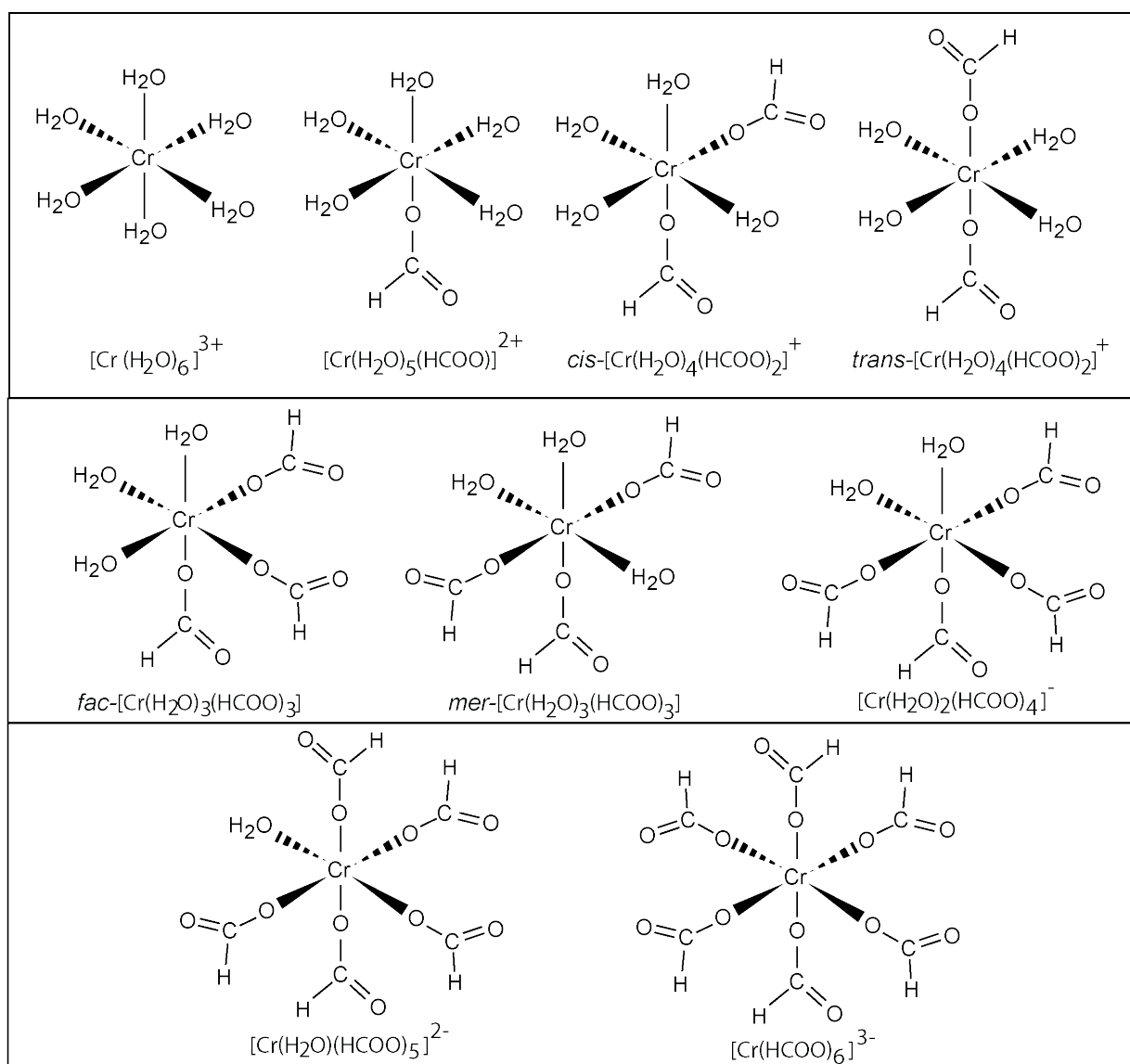
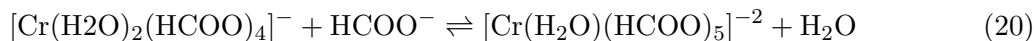
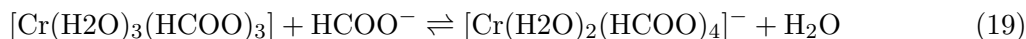
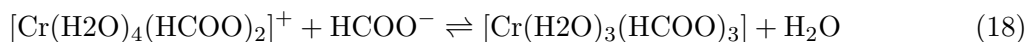
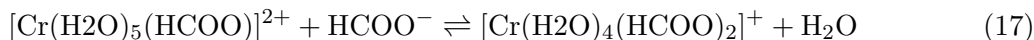
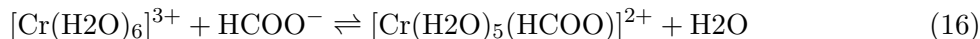


Figure 7.9: Overview chromium-formate complexes used in the DFT calculations

7.2.1 Point energy calculations

The following six ligand substitution reactions are studied first with DFT:



All calculations are performed at Def2-TZVP basis set[102] and with the CPCM or SMD solvation model and water as a medium. In this section only the results of PW91 are presented, the results with BP86 are comparable and can be found in appendix C. It is found that the ligand exchange is spontaneous up to and including the attachment of a fourth HCOO^- molecule. This can be observed in figure 7.10 and figure 7.11 or table C.1 and table C.2 in the appendix C.

The complexes with 2,3 and 4 HCOO^- groups have different isomers. Therefore, multiple results can be observed in figure 7.10 for complexes with 2,3 and 4 groups. The complexes with two HCOO^- groups have *cis*- $[\text{Cr}(\text{H}_2\text{O})_4(\text{HCOO})_2]^+$ and *trans*- $[\text{Cr}(\text{H}_2\text{O})_4(\text{HCOO})_2]^+$ as possible isomers. The complexes with three HCOO^- groups have *Mer*- $[\text{Cr}(\text{H}_2\text{O})_3(\text{HCOO})_3]$ and *Fac*- $[\text{Cr}(\text{H}_2\text{O})_3(\text{HCOO})_3]$ as possible isomers. Therefore, reaction 18 has four possible substitutions and reaction 17 and 19 have two possible substitutions.

It can be observed that the energy differences from the substitution of reaction 18 towards a third HCOO^- group is less spontaneous than the substitution of the first, second and fourth HCOO^- molecule in reactions 16,17 and 19. Between the isomers, there are only small variations in the energy difference. The substitution of a fifth and sixth HCOO^- molecule are unspontaneous. Similar results are found regardless of the solvation model or functionals (PW91, BP86, B3LYP) used in this study.

The results show that up to and including the substitution of a fourth HCOO^- molecule is spontaneous. However, the energy differences of the third ligand substitution reaction in equation 18 are considered too small (≈ 0.2 eV) to conclude that these are spontaneous. Since the observed differences between the functionals are also in this range. Therefore, it can only be concluded that the substitution of the first and second HCOO^- molecules is expected to be spontaneous, as these energy differences are clearly negative (>1 eV).

Due to the acidic environment, the initial complex is not expected to contain hydroxide groups. However, suppose an external voltage is applied during the electroplating process. In that case, it is mentioned that a diffusion layer with an increased pH can occur, and according to Wiberg, one of the H_2O molecules can become deprotonated[12]. It is not expected that this will occur in the experimentally studied electrolytes in this study since the pH is adjusted to 2.45, and no external voltage is applied. Therefore, the explained mechanism of section 4 where a negatively charged surface attracts positively charged complexes and a diffusion layer with increased pH can occur is not possible in the electrolytes used in this study since the conditions are different. However, the effect of an increased pH on the complexation is considered very relevant for implementing electroplating with Cr(III). Therefore, to investigate the possible

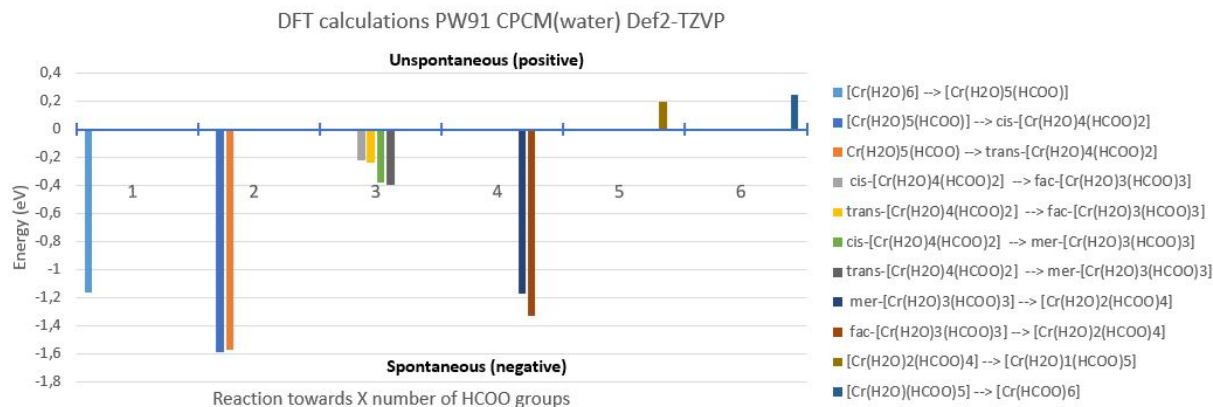


Figure 7.10: Results DFT point energy calculations PW91 and CPCM solvation model

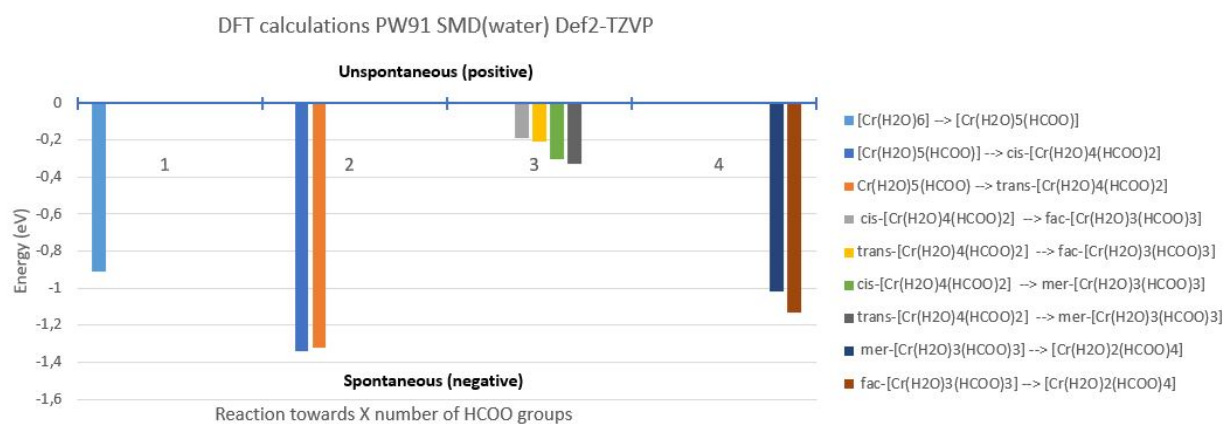
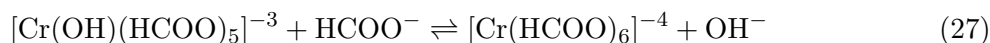
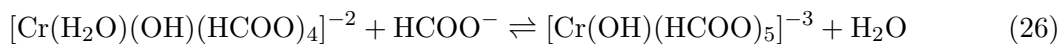
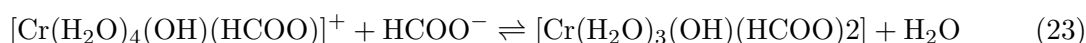
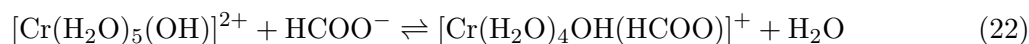


Figure 7.11: Results DFT point energy calculations PW91 and SMD solvation model

impact of a hydroxide group on the ligand substitution of the complex, the following set of reactions (22 till 27) are studied:



In figure 7.12 the results of the point energy calculations of the substitution of a water molecule in the complexes in the presence of a hydroxide group are visualized. It is found that in the presence of a hydroxide group, the substitution of an H_2O molecule by an HCOO^- molecule is still favourable. However, less favourable than without a presence of hydroxide group in the complex. One exception is the substitution of a third HCOO^- molecule towards $\text{Mer}-[\text{Cr}(\text{OH})(\text{HCOO})_3]^{-1}$ isomer. This is possibly the result of the presence of the hydroxide group, since this behaviour was not observed without the presence of a OH^- molecule. However,

it is considered out of this thesis's scope to go into depth on the hydroxide group's effect in this specific complex as there is no proof of its existence.

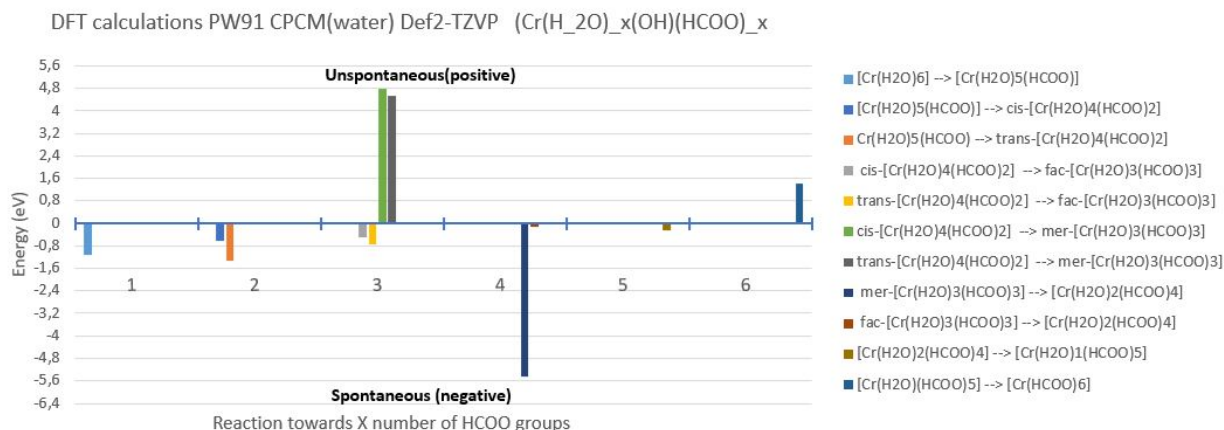
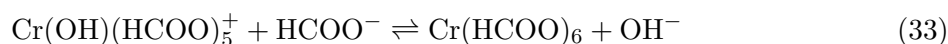
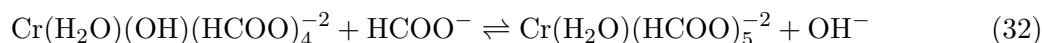
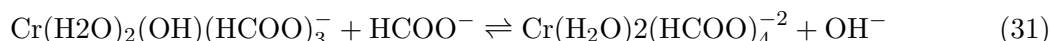
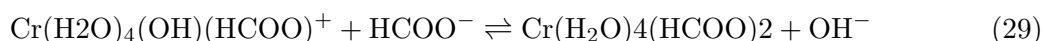
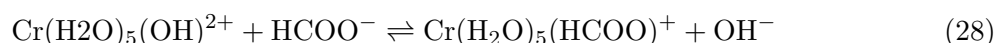


Figure 7.12: DFT point calculations of reactions 22 till 27 with PW91 and CPCM solvation model, in these reactions a hydroxide group is present in the complex, but a H₂O molecule will be substituted.

According to the results of figure 7.12, the substitution of an H₂O molecule by an HCOO⁻ molecule is spontaneous as long as H₂O molecules are present in the complex. The earlier observation where the substitution was favoured up to and including the fourth substitution of HCOO⁻ has disappeared. The unspontaneous character of equation 27, led to the assumption that it is not favourable to replace a hydroxide molecule by an HCOO⁻ molecule.

A new set of reactions with the substitution of a hydroxide molecule instead of water molecules is studied to investigate if the hypothesis of the hydroxide group's unspontaneous substitution is correct. The following set of reactions are studied where a hydroxide molecule is replaced with an HCOO⁻ molecule, equation 28 till equation 33:



It can be observed in figure 7.13 and table C.4 in the appendix C that all six reactions show an unspontaneous tendency towards hydroxide substitution by an HCOO⁻ molecule. This except for the replacement of the hydroxide group in the *Mer*-[Cr(H₂O)₃(HCOO)₃] complex. However, it is assumed that this is caused by the *Mer*-[Cr(H₂O)₃(HCOO)₃] complex being a very unfavourable isomer, as it is observed earlier that the substitution towards this complex is not spontaneous even if a H₂O molecule is replaced. Based on these results, it can be concluded that ligand exchange will be occurring with H₂O and not with OH⁻ when it is present in the complex. This conclusion is important for the interpretation of the ligand substitution reactions of the UV-Vis spectra, and for defining the relative positions of HCOO⁻, SO₄²⁻ and H₂O in the spectrochemical series.

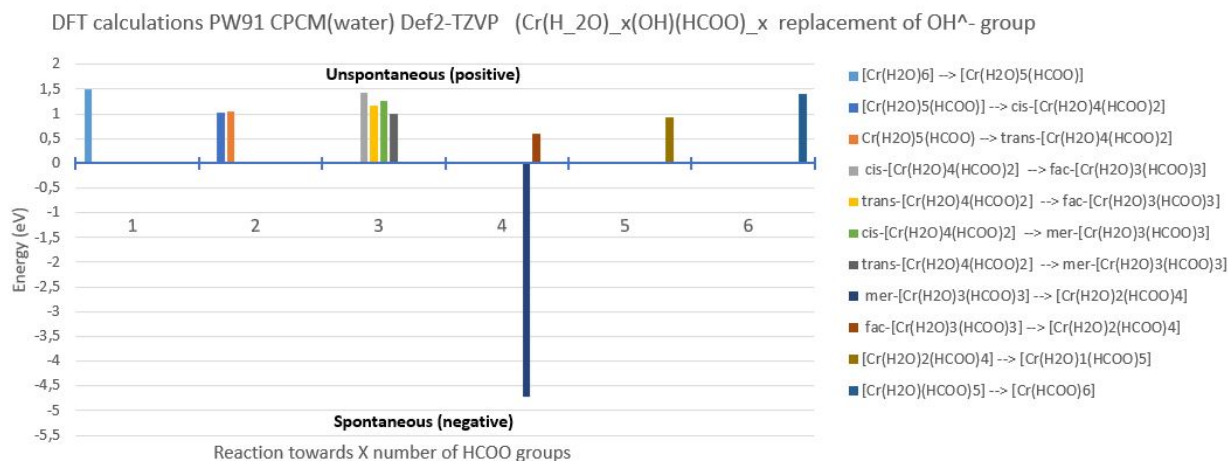


Figure 7.13: DFT point calculations of reactions 28 till 33 with PW91 and CPCM solvation model

In this study, an attempt is made on guessing the complexation structure with SO_4^{2-} . In a study by Fogel, the maximum ratio of $[\text{Cr}^{3+}] : [\text{SO}_4^{2-}]$ observed in complexes is found to be two[41]. Therefore, only the possibilities of having one or two SO_4^{2-} groups are considered in this study. It is found very difficult to successfully optimize the geometries where SO_4^{2-} was attached as monodentate. In most attempts, the SO_4^{2-} group separated at the S-O bond. Therefore, it is doubtful if this geometry will exist. When SO_4^{2-} is bonded as bidentate, some possible structures were calculated without an error. This might indicate that the binding of SO_4^{2-} is more likely to be as bidentate than monodentate. However, with this data, no conclusions can be drawn. At this moment, the structure of complexes from $\text{Cr}_2(\text{SO}_4)_3$ solutions is too uncertain to produce any valuable data with point energy calculations to predict ligand substitution with HCOO^- . However, the two successfully optimized complexes with SO_4^{2-} will be used comparing the bandgap properties.

Finally, from the DFT point energy calculations, it can be concluded that only H_2O participates in the ligand exchange and that OH^- can be excluded from the interpretation. It is found that the replacement of a hydroxide group in the presence of H_2O molecules in the complex was never spontaneous. It can be concluded that the substitution reactions of the first and second HCOO^- molecule are spontaneous even in the presence of a hydroxide group in the complex. The substitution reaction of the third and fourth HCOO^- molecules might be favourable. However, considering all the data, this can not be concluded due to the minor (c.a 0.2 eV) difference in energy or even positive values.

7.2.2 Molecular orbitals and bandgap

It is mentioned in chapter 3 that ligand exchange affects the splitting of the d-orbitals. Therefore, it is considered useful to study the effect of ligand exchange on the splitting of the molecular orbitals with DFT. In 2014, Liu et al. conducted a study on the change in the splitting of HOMO and LUMO as a result of ligand exchange[106]. In the DFT calculation of this study, all molecular orbitals are calculated and studied using the Avogadro software[101] to visualize the orbitals. In the complexes studied, the highest occupied molecular orbital (HOMO) is a d-orbital with the electron clouds orientated between the axes (d_{xy} , d_{yz} or d_{xz}). The lowest unoccupied molecular orbital (LUMO) is a d-orbital orientated along the axis ($dx^2 - y^2$ or dz^2).

Therefore, the studied bandgap in Cr(III) complexes is equal to the splitting in the d-orbitals. In figure 7.14, the splittings in $[\text{Cr}(\text{H}_2\text{O})_6]^{3+}$, $[\text{Cr}(\text{H}_2\text{O})(\text{HCOO})]^{2+}$, *cis*- $[\text{Cr}(\text{H}_2\text{O})_4(\text{HCOO})_2]^+$ and *trans*- $[\text{Cr}(\text{H}_2\text{O})_4(\text{HCOO})_2]^+$ are visualized.

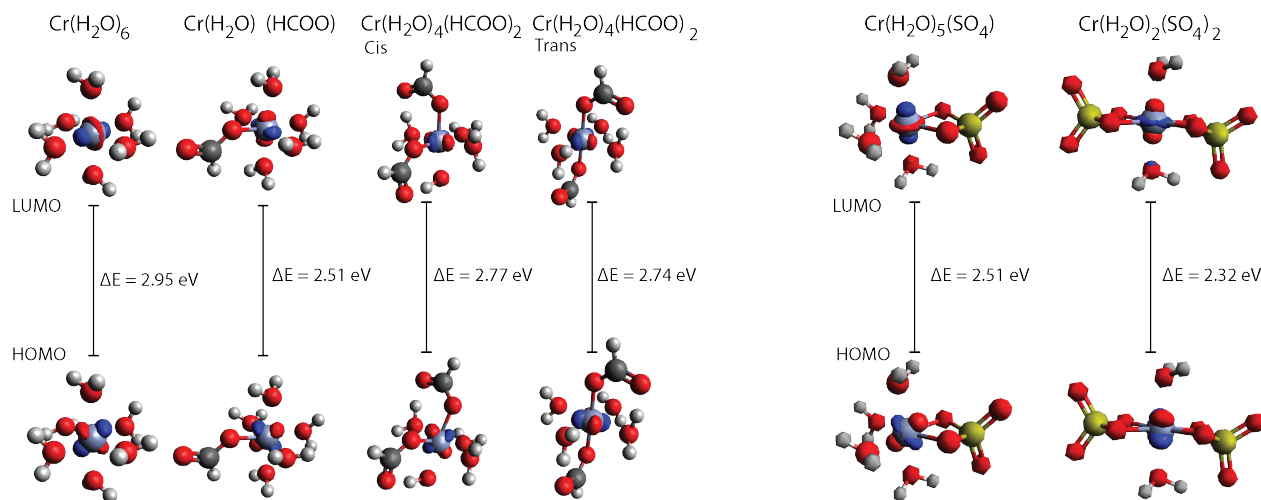


Figure 7.14: Difference between HOMO en LUMO in Cr^{3+} complexes, simulated with functional PW91 and SMD solvation model with medium water

It can be observed that the difference in HOMO en LUMO is largest for the $[\text{Cr}(\text{H}_2\text{O})_6]^{3+}$ complex and smallest for $[\text{Cr}(\text{H}_2\text{O})(\text{HCOO})]^{2+}$. The splitting in HOMO and LUMO of *cis*- $[\text{Cr}(\text{H}_2\text{O})_4(\text{HCOO})_2]^+$ and *trans*- $[\text{Cr}(\text{H}_2\text{O})_4(\text{HCOO})_2]^+$ is comparable and is smaller than observed splitting in $[\text{Cr}(\text{H}_2\text{O})_6]^{3+}$, but larger than the splitting in $[\text{Cr}(\text{H}_2\text{O})(\text{HCOO})]^{2+}$.

It is observed that with substitution of a H_2O molecule by HCOO^- , there is a higher distortion in the $[\text{Cr}(\text{H}_2\text{O})(\text{HCOO})]^{2+}$ complex. This distortion is visible in the bond lengths and angles being further deviated from an octahedral symmetry. Simultaneously, it can be observed that the bandgap is decreased from 2.95 eV to 2.51 eV. The bandgap change simulated with ORCA predicts a bathochromic (red) shift in a UV-Vis spectrum if HCOO^- substitutes H_2O . However, this does not agree with the experimental data observed in section 7.1.1. If $[\text{Cr}(\text{H}_2\text{O})_6]^{3+}$ is indeed the initial complex, all substitutions of a H_2O molecule by HCOO^- molecule will accommodate a bathochromic redshift, which contradicts the experimental data. Therefore, it is unlikely that $[\text{Cr}(\text{H}_2\text{O})_6]^{3+}$ is the initial complex before ligand substitution with HCOO^- occurs.

The simulated bandgaps of $\text{Cr}(\text{H}_2\text{O})_4(\text{SO}_4)$ and $\text{Cr}(\text{H}_2\text{O})_2(\text{SO}_4)_2$ are studied to look at the possible influence of a SO_4^{2-} ligand in the complex on the observed bandgap. It should be mentioned that the geometry of these complexes is guessed and can be different from reality. However, in both cases, the bandgap of Cr-complexes with SO_4^{2-} ligand(s) is smaller than the bandgap in complexes with HCOO^- ligand(s). Therefore, the substitution of SO_4^{2-} by HCOO^- in this complex will show a hypsochromic blue shift. This type of shift matches the experimentally observed data from section 7.1.1.

Although the geometry of these structures with SO_4^{-2} are not proven to exist, it can predict why the experimental data of $\text{Cr}_2(\text{SO}_4)_3$ solutions shows a hypsochromic blue shift instead of the bathochromic redshift, which was simulated with the $[\text{Cr}(\text{H}_2\text{O})_6]^{3+}$ as the initial complex.

7.2.3 Polarizability

In this subsection, the results of the ORCA calculations of the polarizability of the four molecules SO_4^{-2} , HCOO^- , HCOOH and H_2O are presented. The isotropic polarizabilities are calculated with PW91 using the Def2-TZVP basis set[102].

Molecule	Isotropic polarizability
SO_4^{-2}	71.5
HCOO^-	31.0
HCOOH	25.8
H_2O	7.9

Table 7.1: Isotropic polarizabilities of molecules in Cr(III) electrolytes of this study

In table 7.1 it can be observed that the polarizability of SO_4^{-2} is more than two times larger than the polarizability of HCOO^- and almost ten times larger than the polarizability of H_2O . Therefore, it is expected that a deviation in the number of free SO_4^{-2} molecules in the electrolytes can cause more significant electron-electron interactions in the UV-Vis spectra, in comparison to HCOO^- , HCOOH and H_2O molecules respectively.

7.2.4 Simulated IR-spectra

Vibrational frequencies are generated with ORCA 4.0.2[104] using the analytical frequency command in the input file. The Avogadro software[101] is used for visualizing the calculated vibrations and generalizing the infrared spectra. All spectra are calculated using the PW91 functional with a Def2-TZVP basis set[102]. Initially, the CPCM solvation model was implemented with water as a medium. However, it was observed that the CPCM solvation model often caused imaginary frequencies in the output file; this gave the assumption that the geometry was in a saddle point. Therefore, to be sure the calculated frequencies are realistic and the system is stable, the molecules' IR spectra without applying the solvent model are studied since these calculations show no imaginary frequencies. It is found that similar problems with imaginary frequencies occur more often if the CPCM solvation model is applied. However, the proposed solutions of the manual to tighten the SCF and grid did not solve this study's problems.

It is recommended to recalculate the spectra with a larger system of chromium, formate, sulphate and water molecules on a supercomputer with more computational power, to test if the presented system of only one complex might be unstable in a solvation model, causing imaginary frequencies to appear. However, this is not included in this study.

This section compares the IR spectra of the different complexes in a vacuum. It should be noted that the wavenumbers at which the vibrations occur in a vacuum are expected to be different from the experimentally observed data of the electrolytes. The difference observed between HCOOH and HCOO^- with and without the application of a solvation model in the 2000 - 1000 cm^{-1} range is found to be 75 cm^{-1} which is a significant difference. However, all the vibrations observed in the spectra with and without a solvation model are similar. Therefore,

it is assumed that the type vibrations observed in the IR spectra are comparable to vibrations in the spectra using a solvation model.

The generated IR-spectra of the complexes: $[\text{Cr}(\text{H}_2\text{O})_6]^{3+}$, $[\text{Cr}(\text{H}_2\text{O})(\text{HCOO})]^{2+}$, *cis*- $[\text{Cr}(\text{H}_2\text{O})_4(\text{HCOO})_2]^+$, *trans*- $[\text{Cr}(\text{H}_2\text{O})_4(\text{HCOO})_2]^+$, *Mer*- $[\text{Cr}(\text{H}_2\text{O})_3(\text{HCOO})_3]$, *Fac*- $[\text{Cr}(\text{H}_2\text{O})_3(\text{HCOO})_3]$, $[\text{Cr}(\text{H}_2\text{O})_2(\text{HCOO})_4]^-$, $[\text{Cr}(\text{H}_2\text{O})(\text{HCOO})_5]^{-2}$ and $[\text{Cr}(\text{HCOO})_6]^{-2}$ can be observed in figure 7.15-7.23. Figure 7.24 gives the ATR-FTIR spectra of $[\text{Cr}^{3+}]:[\text{HCOO}^-] = [1]:[1.21]$ as comparison with the three peaks assigned to the chromium-formate complex.

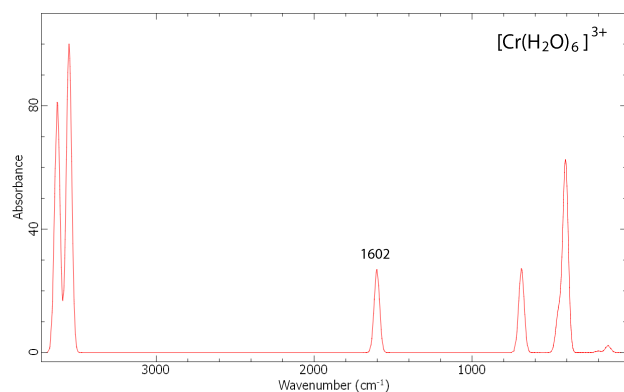


Figure 7.15: Simulated IR spectra PW91 CPCM(water)

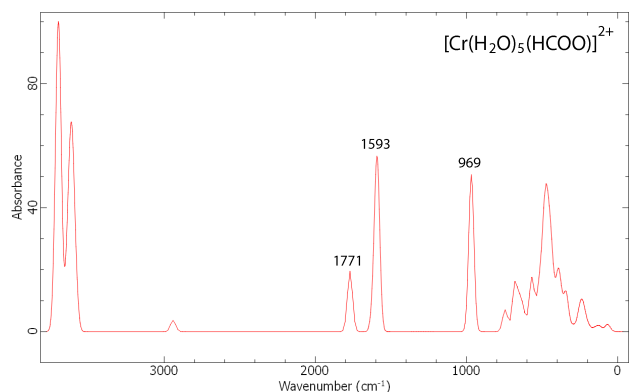


Figure 7.16: Simulated IR spectra PW91 CPCM(water)

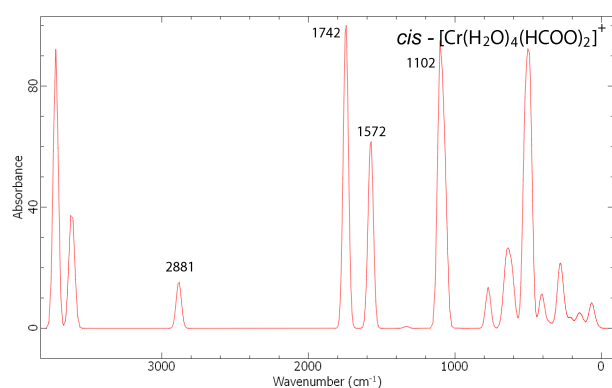


Figure 7.17: Simulated IR spectra PW91 CPCM(water)

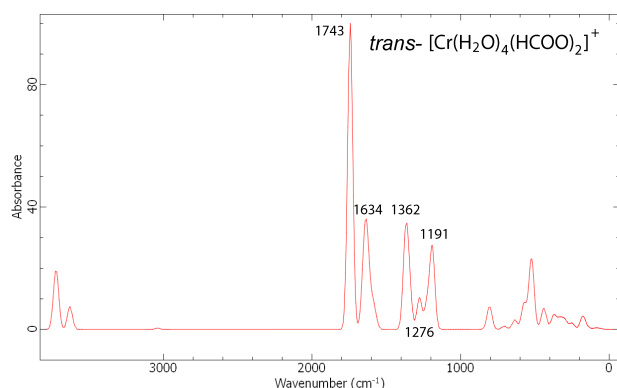


Figure 7.18: Simulated IR spectra PW91 CPCM(water)

As expected, the addition of a formate molecule in the complexes introduces more vibrations in the IR spectrum. The simulated IR spectra showed that when multiple HCOO^- groups are present in one complex, they could vibrate at different frequencies if there is a significant difference between the molecules. It is observed that HCOO^- molecules oriented close to each other have similar wavenumbers at which a specific vibration occurs compared to the HCOO^- groups, which are separated further apart in the complex, for example, in the *Mer*- $[\text{Cr}(\text{H}_2\text{O})_3(\text{HCOO})_3]$ isomer. Similar vibrations can be observed in the spectra of *Mer*- $[\text{Cr}(\text{H}_2\text{O})_3(\text{HCOO})_3]$ and *Fac*- $[\text{Cr}(\text{H}_2\text{O})_3(\text{HCOO})_3]$, however, the differences in the number of peaks are caused by the splitting of the vibrational modes of the HCOO^- molecules within the complex.

A possible explanation for this behaviour in the molecule is the interaction of the negatively

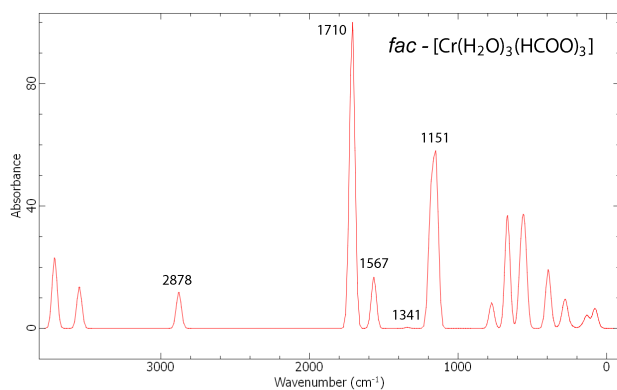


Figure 7.19: Simulated IR spectra PW91 CPCM(water)

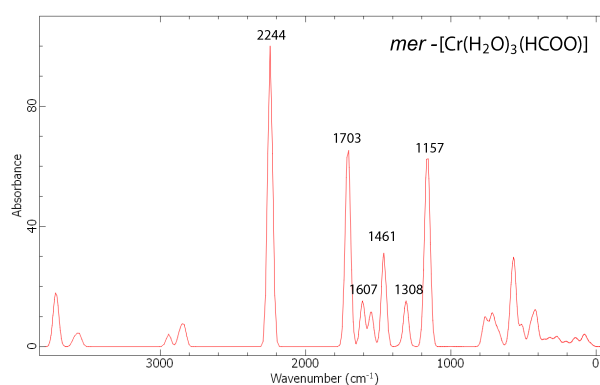


Figure 7.20: Simulated IR spectra PW91 CPCM(water)

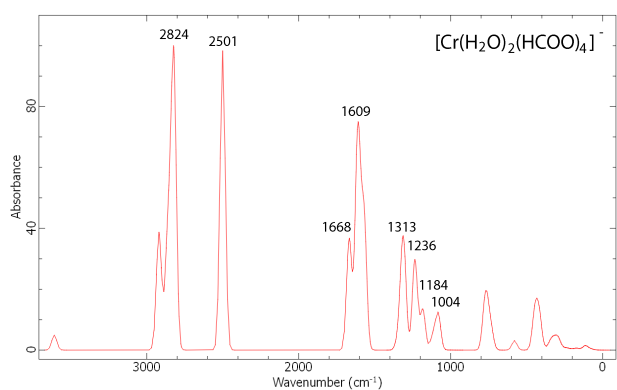


Figure 7.21: Simulated IR spectra PW91 CPCM(water)

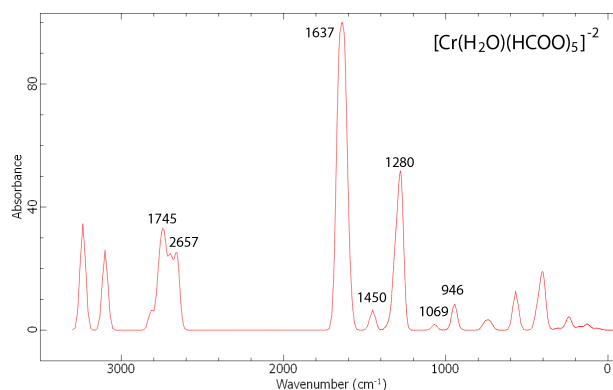


Figure 7.22: Simulated IR spectra PW91 CPCM(water)

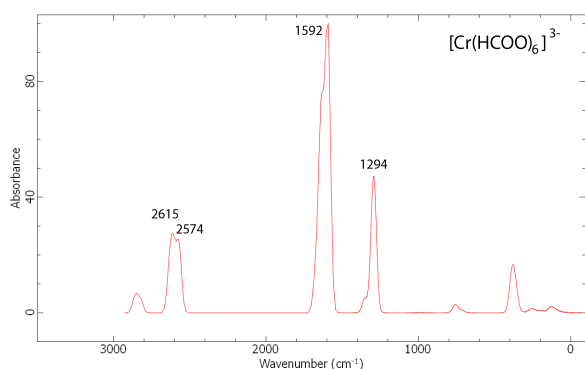


Figure 7.23: Simulated IR spectra PW91 CPCM(water)

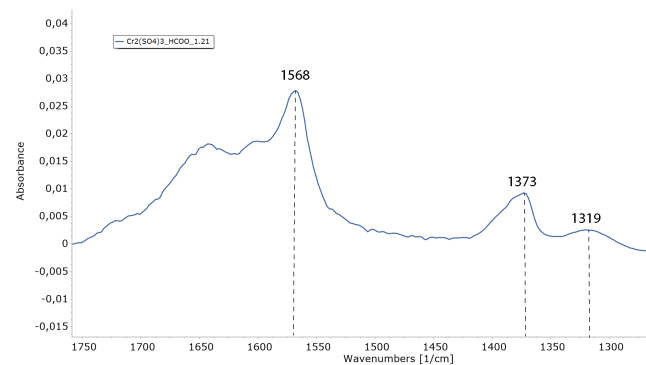


Figure 7.24: Experimental ATR-FTIR spectra of $[Cr^{3+}]:[HCOO^-] = [1]:[1.21]$

charged oxygen and positively charged hydrogen atom of the $HCOO^-$ molecule affecting each other by hydrogen bonding. As a result, broader peaks or multiple peaks are observed for the similar type of vibration in the spectra. This type of interaction is also expected to be present in the electrolytes, where $HCOO^-$, H_2O and SO_4^{2-} molecules will interact with the ligands of the Cr(III) ion by hydrogen bonding.

According to the simulated data, the vibrations that likely to occur in the range of 1100-3000 cm^{-1} are:

- Symmetric and asymmetric stretching of single C-O bond in HCOO^- groups (1150-1300 cm^{-1})
- In and out of the plane movement of hydrogen atoms in the HCOO^- -group (1300- 1360 cm^{-1}) (observed at low absorption values, compared to the other vibrations)
- Scissoring and wagging of the hydrogen atoms in the water molecules causing the double C=O bond to rotate (1400-1600 cm^{-1} , if H_2O molecules are present in the complex)
- Asymmetric and symmetric stretching of C=O bond in the HCOO^- molecules around c.a 1700-1800 cm^{-1} . However, except for $[\text{Cr}(\text{H}_2\text{O})_6]^{3+}$ which has no HCOO^- molecules and $[\text{Cr}(\text{H}_2\text{O})(\text{HCOO})_5]^{-2}$ & $[\text{Cr}(\text{HCOO})_6]^{-2}$ which show this vibration at c.a 1450-1600 cm^{-1})
- Separated asymmetric stretching of the hydrogen atoms in the HCOO^- groups (2800-3000 cm^{-1} , not in all complexes observed)

A more extensive overview of all vibrations addressed separately for the spectra of figures 7.15-7.23 can be found in appendix C.

To summarize all findings, there is no perfect match between the simulated IR spectra and the experimental data in section 7.1.2. From the experimental ATR-FTIR data it is concluded that there are three absorption peaks in the experimental spectra related to the newly formed complex, which can be observed in figure 7.24. Therefore, it seems logical that the simulated spectra would also show three peaks, since there is no excess of formate present in the simulated model.

If only the 1200-2000 cm^{-1} range is compared, the simulated spectra of *trans*- $[\text{Cr}(\text{H}_2\text{O})_4(\text{HCOO})_2]^+$ show the most similarities with the experimental spectra. These similarities are based on one absorption peak, which is connected to the vibrations of the H_2O molecules in the complex and three absorption peaks of almost similar absorbance values connected to the vibrations of the carbon-oxygen single bond, scissoring of the hydrogen atom and carbon-hydrogen double bond.

The spectra of $[\text{Cr}(\text{H}_2\text{O})(\text{HCOO})_5]^{-2}$ and *cis*- $[\text{Cr}(\text{H}_2\text{O})_4(\text{HCOO})_2]^+$ show a $\nu(\text{COO}^-)$ peak around 1593 and 1572, which are closer to the experimentally observed value of 1560. However, these spectra do not show the expected three peaks in the 1200-2000 cm^{-1} region. Since the absorption peaks' locations are expected to have a significant error caused by the execution of the calculations in a vacuum, comparing the number of vibrational peaks is considered more reliable in comparing the simulated and experimental spectra.

However, it has to be concluded that the simulation of the IR-spectra in this study has not been successful in predicting the experimentally observed spectra of the electrolytes. This is expected to be caused by too many differences between the experimental solutions and simulated data.

7.2.5 Simulated UV-Vis spectra

In the experimental part of this study, UV-Vis experiments are conducted on different chromium solutions. Therefore, an attempt is conducted on simulating the UV-Vis spectra of chromium formate complexes, which are expected to be present in the electrolytes. In this section, the results of the simulated absorption spectra with ORCA 4.0.2[104] are presented and visualized

with the Avogadro software[101]. The ORCA software is used for conducting Time-Dependent DFT (TD-DFT) calculations. These TD-DFT calculations can predict the neutral excitations of molecules, which can be used to predict the absorption properties of different molecules.

The earlier calculated optimized ground state geometries and molecular orbital configurations from this section are used as input for the TD-DFT calculations. The functional PW91 and basis set Def2-TZVP are used combined with the RIJCOXS approximation to reduce computational task. The RIJCOXS approximation is chosen as the ORCA input library suggested it would increase speed without effecting the results drastically[103]. Since all calculations are performed on a laptop and due to this study's time restrictions, reducing the computational cost is necessary. Figure 7.25-7.33 show the simulated absorption spectra calculated with ORCA 4.0.2[96] and visualized with the Avogadro software[101] using a Gaussian distribution with peak width 20.

The locations of λ_{Max} from the $\text{Cr}(\text{ClO}_4)_3$ solutions (407 nm & 576 nm) are used as comparison for the $[\text{Cr}(\text{H}_2\text{O})_6]^{3+}$ complex. These values are chosen as it is expected that the complex in $\text{Cr}(\text{ClO}_4)_3$ solutions is mainly $[\text{Cr}(\text{H}_2\text{O})_6]^{3+}$ due to the low tendency of ClO_4 to participate in ligand exchange. The other spectra are compared to the λ_{Max} values found in the spectra with $\text{Cr}_2(\text{SO}_4)_3$ of 581 nm and 420-422 nm. The specific value of 420 nm is chosen from the ratio of $[\text{Cr}^{3+}]:[\text{HCOO}^-] = [1]:[1.61]$ as it is expected that at this ratio the number of chromium-formate complexes is the largest without a huge excess of HCOO^- in the electrolytes.

In the figures 7.25 - 7.33 it can be observed that most simulated spectra are far off from the experimental values. This similar conclusion is found in the spectra simulated with B3LYP as functional, which can be found in appendix C. The results observed with B3LYP as functional are comparable to the spectra found with PW91, but the spectra of B3LYP in the appendix include 20 excitation instead of 10 excitations presented in this section with PW91. However, considering only 10 excitations in this section is enough to obtain the first two transition peaks. There are differences in the location of λ_{Max} between PW91 and B3LYP. The locations of λ_{Max} for the first transition peak are observed slightly higher wavelengths for B3LYP than PW91, but still different from the experimentally observed values.

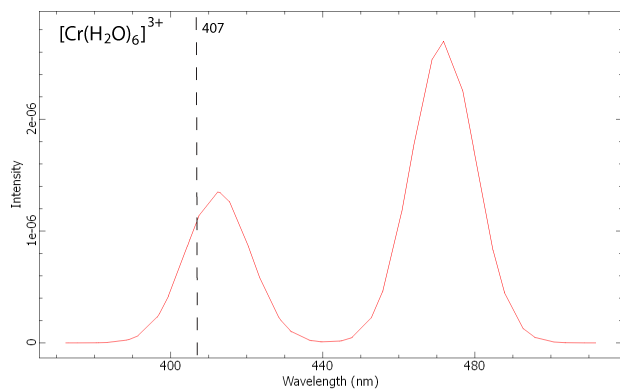


Figure 7.25: Simulated absorption spectra of $[\text{Cr}(\text{H}_2\text{O})_6]^{3+}$ with PW91 CPCM(water), without the presence of HCOO^- molecules.

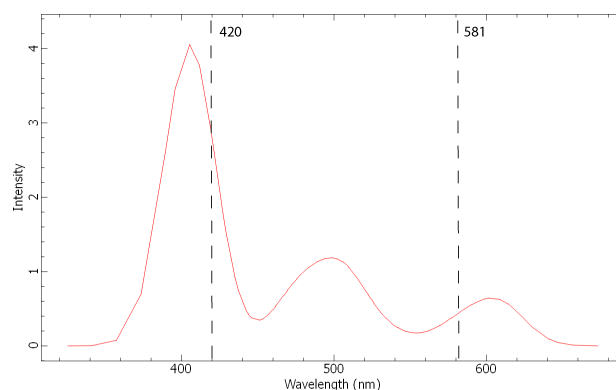


Figure 7.26: Simulated absorption spectra of $[\text{Cr}(\text{H}_2\text{O})_5(\text{HCOO})]^{2+}$ with PW91 CPCM(water)

Two absorption peaks can be observed in figure 7.25 for $[\text{Cr}(\text{H}_2\text{O})_6]^{3+}$. The second transi-

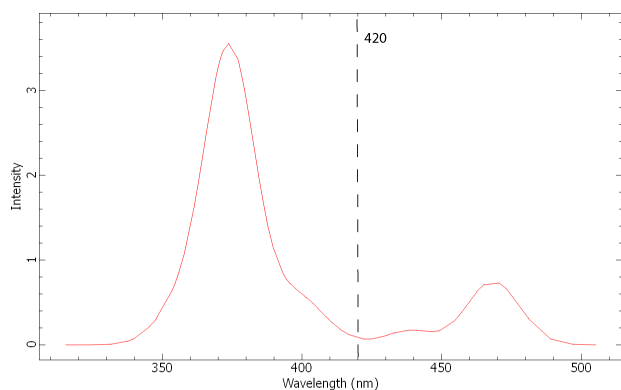


Figure 7.27: Simulated absorption spectra of cis - $[Cr(H_2O)_4(HCOO)_2]^+$ with PW91 CPCM(water)

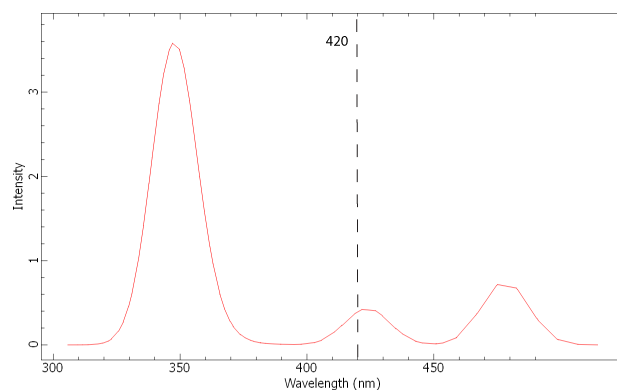


Figure 7.28: Simulated absorption spectra of $trans$ - $[Cr(H_2O)_4(HCOO)_2]^+$ with PW91 CPCM(water)

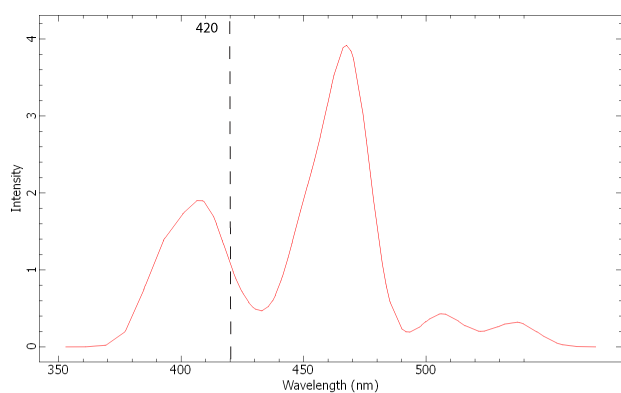


Figure 7.29: Simulated absorption spectra of mer - $[Cr(H_2O)_3(HCOO)_3]$ with PW91 CPCM(water)

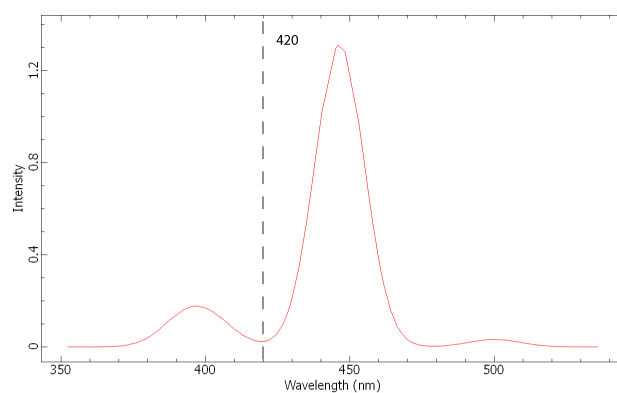


Figure 7.30: Simulated absorption spectra of fac - $[Cr(H_2O)_3(HCOO)_3]$ with PW91 CPCM(water)

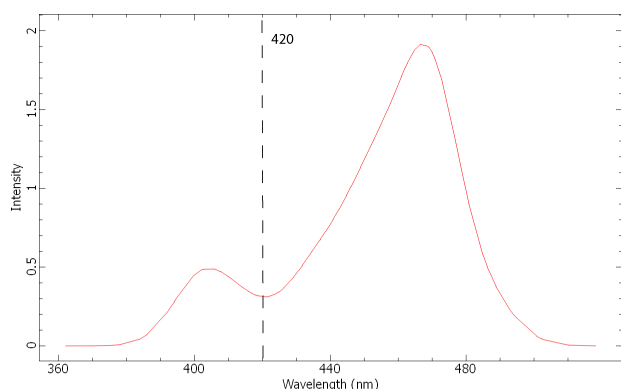


Figure 7.31: Simulated absorption spectra of $[Cr(H_2O)_2(HCOO)_4]$ with PW91 CPCM(water)

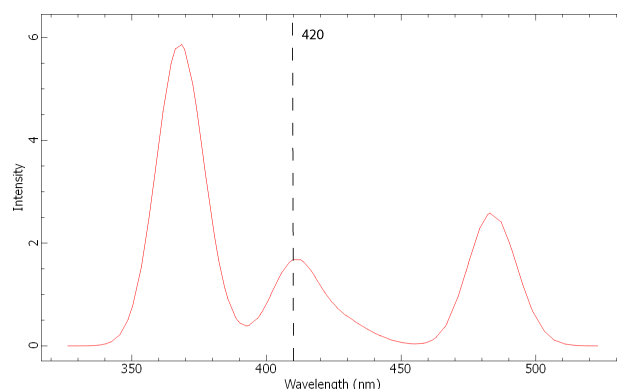


Figure 7.32: Simulated absorption spectra of $[Cr(H_2O)(HCOO)_5]$ with PW91 CPCM(water)

tion peak at 412 nm matches the experimentally found second transition peak of the $Cr(ClO_4)_3$ spectrum of 407 nm within a reasonable range. However, the first transition peak in the simulated spectra is far off from the experimentally observed first transition peak at 576 nm in

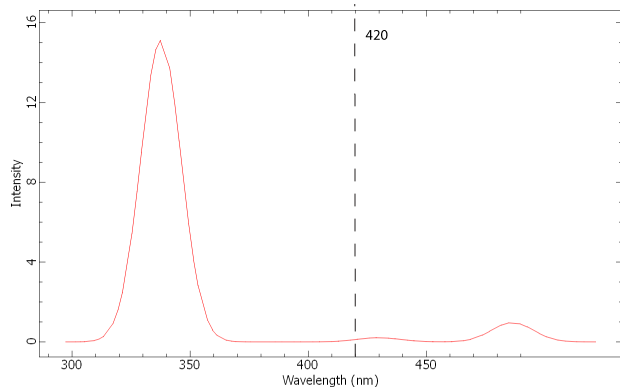


Figure 7.33: Simulated absorption spectra of $[\text{Cr}(\text{HCOO})_6]$ with PW91 CPCM(water)

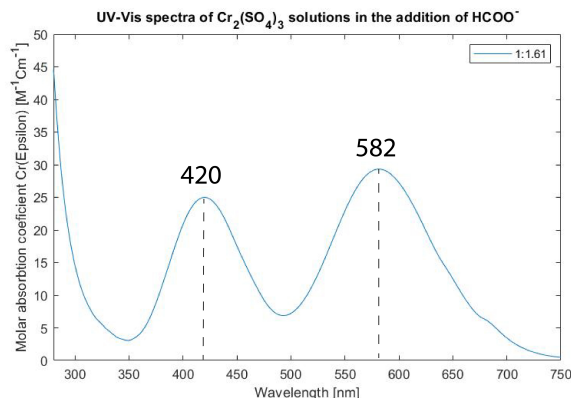


Figure 7.34: Experimental UV-Vis spectra of $[\text{Cr}^{3+}]:[\text{HCOO}^-] = [1]:[1.61]$

the spectra of $\text{Cr}(\text{ClO}_4)_3$. This similar conclusion can be found for the spectra of all other complexes, except $[\text{Cr}(\text{H}_2\text{O})_5(\text{HCOO})]^{2+}$ in figure 7.26, which is the only spectra showing a transition in the 600 nm range. None of the spectra in figures 7.25, 7.27-7.33 shows a transition peak in the experimentally observed range of 576-581 nm. This same problem is found using B3LYP as functional.

The shape of the transition curves observed in the spectra of $[\text{Cr}(\text{H}_2\text{O})_6]^{3+}$, $[\text{Cr}(\text{H}_2\text{O})_5(\text{HCOO})]^{2+}$, $\text{trans-}[\text{Cr}(\text{H}_2\text{O})_4(\text{HCOO})_2]^+$, $[\text{Cr}(\text{H}_2\text{O})_5(\text{HCOO})]^{-2}$ and $[\text{Cr}(\text{H}_2\text{O})_5(\text{HCOO})]^{-3}$ show similarities with the experimental found spectrum of figure 7.34, but they are far from perfect. In the spectra of figures 7.26, 7.27, 7.28, 7.29 and 7.32 two lower absorbance transition peaks can be distinguished at wavelengths of c.a >400 nm, followed by a third transition peak with a higher absorbance at wavelength of c.a <400 nm. This description of the shape is in agreement with the experimentally observed spectra. However, the positions of the transition peaks do not match and especially the first transition peaks shows values which are very far off.

The spectra which show the most similarities in shape and position of the transition peaks besides the spectra of $[\text{Cr}(\text{H}_2\text{O})_6]^{3+}$ are $\text{trans-}[\text{Cr}(\text{H}_2\text{O})_4(\text{HCOO})_2]^+$ and $[\text{Cr}(\text{H}_2\text{O})_5(\text{HCOO})]^{2+}$. However, the spectra are far from a perfect match and unreliable for predicting the complexation in $\text{Cr}_2(\text{SO}_4)_3$ electrolytes. A possible explanation for the observed differences between the simulated and experimental data is that TD-DFT is not suitable for predicting low energy Laporte forbidden transitions. Besides, it is also possible that the predicted transitions do not occur in the experimental solutions or that these complexes are not present in the experimental solutions.

In a study by Vlahović et al., similar difficulties are observed for $[\text{Cr}(\text{H}_2\text{O})_6]^{3+}$, especially the first two transitions could not be predicted accurately[95]. They conclude that TD-DFT provides satisfactory results only in the cases of d^2 , d^4 , and low-spin d^6 transition metals, but lacks in predicting transitions in d^3 structures[95]. The problems with TD-DFT for d^3 complexes is attributed to a lack of orbital relaxation in the calculations[95].

Besides TD-DFT calculations, Vlahović et al. used LF-DFT calculations to predict the spectra. LF-DFT's key feature is the explicit treatment of the near degeneracy effects using CI (configuration interaction) within Kohn-Sham orbitals' active space with a dominant transition metal ion d-electron character[95]. Therefore, LF-DFT takes dynamic and non-dynamic correlation effects into account with DFT XC potential (dynamical correlation) and by CI (non-dynamical correlation)[95].

On the contrary, successful spectra are obtained with LF-DFT for $[\text{Cr}(\text{H}_2\text{O})_6]^{3+}$. Therefore, it is expected that a method like LF-DFT might be more suitable for this section's calculations. However, a drawback of LF-DFT is that it can not be used for predicting the charge transfer transitions, which are also crucial in the spectra of transition metal compounds[95]. Therefore, the choice between LF-DFT or TD-DFT should be on what transitions need to be visualized. In this study, only the first two Laporte forbidden transitions are experimentally studied with UV-Vis. Therefore, LF-DFT might have been more suitable for predicting these transitions. However, if the experimental range of this study is extended, and charge transfer transitions that occur below 300 nm are studied, using TD-DFT to predict these Laporte allowed transitions might be suitable after all. However, more background research should be executed on how to implement these calculations for our system.

Finally, it has to be concluded that there are substantial errors between the experimental and simulated values at which λ_{Max} is observed. Although TD-DFT successfully simulates the correct shape of some of the complexes' UV-Vis spectra, the large error between the experimental and simulated data limits the final conclusions that can be drawn. The data from this section is not considered convincing enough to conclude the presence of a specific complex.

7.3 Effect of formate and sulphate on $[\text{Cr}(\text{H}_2\text{O})_6]^{3+}$

This section presents the experimental results with UV-Vis of electrolytes created with $\text{Cr}(\text{ClO}_4)_3$ solutions. Solutions of 15 g/L Cr in addition of sulphate in the ratios [1]:[1] up to and including [1]:[6] are tested.

In figure 7.35, it can be observed that the differences between the solution with and without the addition of sulphate are small. The largest differences observed are in the 300-350 nm range. However, this part cannot be used for the interpretation as the third transition peaks is out of the experimental range of 280-800 nm.

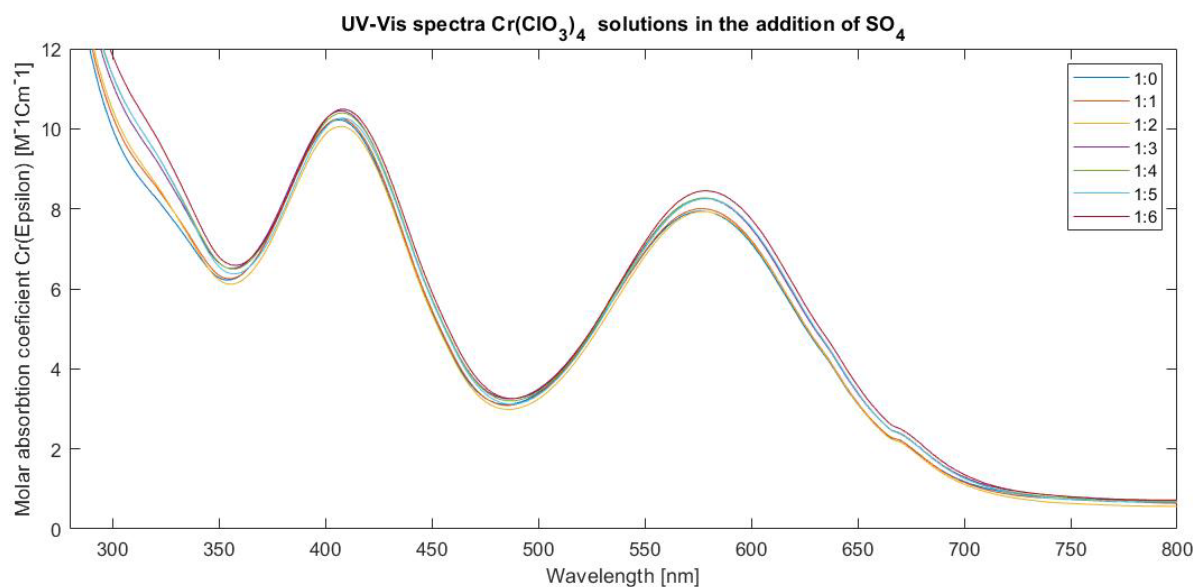


Figure 7.35: UV-Vis spectra of $\text{Cr}(\text{ClO}_4)_3$ in addition of SO_4^{-2} (no pH adjustment), legend defines the ratio of $[\text{Cr}^{3+}]:[\text{SO}_4^{2-}]$

In figure 7.36 and 7.37 the maximum absorbance values λ_{Max} are plotted for the $\text{Cr}(\text{ClO}_4)_3$

solutions in addition of SO_4^{2-} . A bathochromic (red) shift towards higher wavelengths can be observed in addition of sulphate to $\text{Cr}(\text{ClO}_4)_3$ solutions. A similar but slightly larger shift is observed in the addition of formate to SO_4^{2-} . However, the execution of these experiments are not of this thesis study. According to equation 3, a bathochromic shift corresponds to a complex with lower energy. This observed shift is in the opposite direction than the shift observed in $\text{Cr}_2(\text{SO}_4)_3$ solutions in the addition of formate.

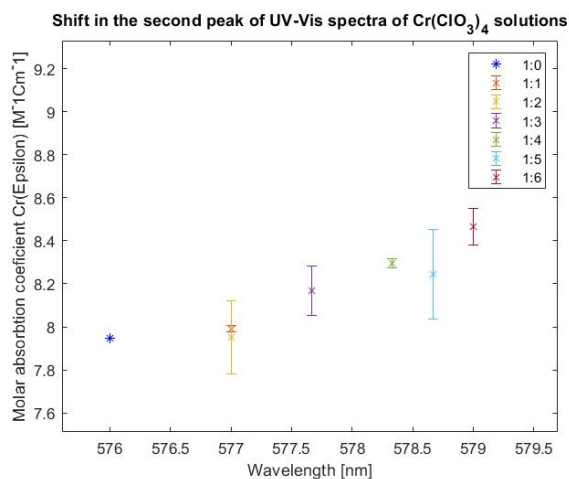


Figure 7.36: Shift in the position of λ_{Max} of the second transition peak in $\text{Cr}(\text{ClO}_4)_3$ solutions, legend defines the ratio of $[\text{Cr}^{3+}]:[\text{SO}_4^{2-}]$

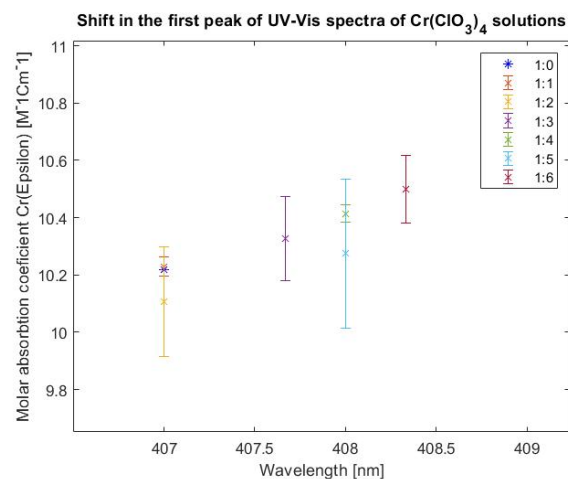


Figure 7.37: Shift in the position of λ_{Max} of the first transition peak in $\text{Cr}(\text{ClO}_4)_3$ solutions, legend defines the ratio of $[\text{Cr}^{3+}]:[\text{SO}_4^{2-}]$

The behaviour observed in the positions of λ_{Max} of both peaks is different. In figure 7.37, only a shift of c.a. 1 nm can be observed. This shift is initiated from the ratio $[\text{Cr}^{3+}]:[\text{SO}_4^{2-}]=[1]:[3]$ or higher. This indicates that there is a minimum amount of SO_4^{2-} needed before a difference in wavelength can be observed.

According to Bennett[69] the first absorption peak is a direct measure of the splitting in the d-orbitals and the second absorption peak corresponds $Dq + \text{Racah parameter}$. The shift observed in the first absorption peak is minimal, and it is doubtful if ligand substitution of H_2O by SO_4^{2-} even has occurred. It is expected that SO_4^{2-} is still free in solution or has formed an outer-sphere complex by attaching to the water molecules present in the complex.

In figure 7.36, a shift is visible immediately after the addition of sulphate. With increasing sulphate concentration, λ_{Max} continues to shift towards higher wavelengths. Since no significant shift in the spectra's first absorption peak is observed, it is expected that the shift in the second absorption peak is mainly caused by electron-electron interaction (Racah parameter B). The polarizability of sulphate is higher than the polarizability of the other species in the solution. It is mentioned earlier, that molecules with significant dipole moments or anions with larger polarizabilities must bring more significant depressions and cause a larger shift in the spectra[47]. It is expected that anions in a solution with higher polarizability, which is a measurement of ease to distort the electron cloud of an atom, will have more overlap of electron clouds and cause more electron-electron interactions. This could explain the constant shift with increasing sulphate concentration.

In the $\text{Cr}(\text{ClO}_4)_3$ solutions in addition of formate, the results also only show a small shift of a few nm. Therefore, it is expected that HCOO^- is also not able to replace a H_2O ligand with

HCOO⁻ within the give time period of this study (2-3 weeks at elevated temperature). However, the addition of HCOO⁻ produces a larger shift in the band gap than the addition of SO₄²⁻.

To conclude, it is expected that in the electrolytes created with Cr(ClO₄)₃, the ligand substitution reactions occur slower than in the solutions created with Cr₂(SO₄)₃. This conclusion is based on the differences in observed time and shift of the UV-Vis spectra. Besides, it concluded that the substitution reactions with sulphate take more time than the substitution reactions with formate. However, this seems reasonable considering the tendency to participate in ligand exchange presented by Mandich[29].

When the ligand substitutions occurring in Cr(ClO₄)₃ solutions are compared to the ligand substitutions occurring in Cr₂(SO₄)₃ solutions. It can be concluded that the presence of sulphate in the complex accelerates the ligand exchange of formate. This faster ligand exchange could be beneficial for the deposition process, as the chromium-formate complexes in the plating bath will be formed more quickly in solutions created from Cr₂(SO₄)₃ than from Cr(ClO₄)₃.

8 Conclusions

The work performed in this project has led to several findings regarding the effect of formate (HCOO^-) concentration on electrolytes created with $\text{Cr}(\text{SO}_4)_3$ as chromium salt. At the end of this study, three research questions have been addressed. The conclusion on each question will be presented here.

1. What is the effect of formate ion concentration on the possible complexation and ligand substitution in Cr(III) electrolytes?

By adding sodium formate to electrolytes made with $\text{Cr}_2(\text{SO}_4)_3$ as chromium salt, a ligand substitution occurs even in a small concentration of the formate ion. The amount of chromium-formate complexes in the electrolyte keeps increasing with an increasing concentration of NaHCOO . However, a transition point is observed between the concentrations $[\text{Cr}^{3+}]:[\text{HCOO}^-] = [1]:[1.61]$ and $[\text{Cr}^{3+}]:[\text{HCOO}^-] = [1]:[3.32]$. Beyond the ratio $[\text{Cr}^{3+}]:[\text{HCOO}^-] = [1]:[1.61]$, a clear excess of formate and formic acid is observed in the ATR-FTIR spectra. As a result, it is concluded that the maximum possible coordination of HCOO^- to the Cr-ion occurring in $\text{Cr}_2(\text{SO}_4)_3$ electrolytes at pH 2.45 is three. However, this study does not prove this complex's existence. It is possible that the coordination with one or two HCOO^- molecules is favoured.

From the UV-Vis and ATR-FTIR data, it can be concluded that up to and including the concentration of $[\text{Cr}^{3+}]:[\text{HCOO}^-] = [1]:[1.61]$ nearly no excess of formate is present in the electrolytes. This conclusion is based on the ATR-FTIR and UV-Vis results presented in this study. The second UV-Vis absorption peak in $\text{Cr}_2(\text{SO}_4)_3$ solutions shows a hypsochromic shift to lower wavelengths with increasing concentration up to and including the ratio of $[\text{Cr}^{3+}]:[\text{HCOO}^-] = [1]:[1.61]$. Since HCOO^- shows no transition peaks in the 280-800 nm range, it seems that beyond this ratio the Racah parameter, which contains electron-electron interactions, influences the position of λ_{max} in the second absorption peak. Therefore, it is expected that the electron clouds of the HCOO^- molecules that are within the chromium complexes' close laying solvation shells influence the electrons transitions by providing extra repulsion. In the ATR-FTIR data, the absence of the $\nu(\text{COO}^-(\text{HCOO}^-))$ peak at low concentrations of HCOO^- also indicate that there is almost no excess of formate present in the electrolytes until the ratio of $[\text{Cr}^{3+}]:[\text{HCOO}^-] = [1]:[1.61]$. It is mentioned, that below $[\text{Cr}^{3+}]:[\text{HCOO}^-] = [1]:[1.61]$ almost no excess of HCOO^- is observed. However, even at the ratio of $[\text{Cr}^{3+}]:[\text{HCOO}^-] = [1]:[0.8]$ a slight excess of HCOO^- is observed. Only in the spectra with ratio $[\text{Cr}^{3+}]:[\text{HCOO}^-] = [1]:[0.4]$, this excess is not observed. From this it can be concluded that at concentrations up to and including $[\text{Cr}^{3+}]:[\text{HCOO}^-] = [1]:[0.4]$, all formate is used to form chromium-formate complexes.

Between the ratios of $[\text{Cr}^{3+}]:[\text{HCOO}^-] = [1]:[1.61]$ and $[\text{Cr}^{3+}]:[\text{HCOO}^-] = [1]:[3.32]$ a larger increase in the peak corresponding to $\nu(\text{COO}^-(\text{HCOO}^-))$ can be observed. In addition, the shift in the first transition peak of the UV-Vis spectra of $\text{Cr}_2(\text{SO}_4)_3$ solutions does not shift significantly above the ratio of $[\text{Cr}^{3+}]:[\text{HCOO}^-] = [1]:[3.32]$. Therefore, the concentration with the most chromium-formate complexes is expected to be within the range of $[\text{Cr}^{3+}]:[\text{HCOO}^-] = [1]:[1.61]$ and $[\text{Cr}^{3+}]:[\text{HCOO}^-] = [1]:[3.32]$.

The UV-Vis and ATR-FTIR data presented in the report's main structure originate from solutions created in two-fold, which show the same trends. In addition, a different batch of solutions was initially used, which was later on excluded from the data due to the possible presence of additional compounds. However, even in this excluded batch, similar trends are found, for example, the transition point around the ratio of $[\text{Cr}^{3+}]:[\text{HCOO}^-]$ is c.a $[1]:[3]$ in the

ATR-FTIR data. These results are promising for the reproducibility of this studies ATR-FTIR data.

The peaks in the ATR-FTIR data assigned to the chromium-formate complex do not change their width and shape at increasing NaHCOO concentrations in the range of ratios of 0.4 - 1.61. Therefore, it is expected that the composition of complexes present in the electrolytes is not influenced by the increasing concentration of NaHCOO. Besides, the peaks assigned to the chromium-formate complex at 1667 cm^{-1} show no signs that this peak is a mixture of different ATR-FTIR peaks, based on the symmetrical shape and width of c.a 20 cm^{-1} . This could indicate that only one type of complex is formed. However, based on the data presented in this study, this can not be confirmed.

The pKa value of 3.45 for HCOOH/HCOO⁻ indicates that there should be a higher concentration of HCOOH at low pH values below 3.45. However, the ATR-FTIR data shows that up to and including the ratio of [Cr³⁺]:[HCOO⁻] = [1]:[1.61], almost no HCOOH is observed in the ATR-FTIR spectra around 1212 cm^{-1} . However, there is a slight excess of HCOO⁻ observed. This observation is also found in the earlier conducted experiments of rejected batch in the appendix B. This observation provides a strong indication that the ligand substitution with HCOOH is more likely occur than HCOO⁻, and mainly HCOOH is used in during the complexation reaction with chromium. This preference could also indicate that above the pH of 3.45, where more HCOO⁻ is present than HCOOH, the ligand substitution mechanism is different.

Finally, the observed splitting between the peaks of $\nu(\text{COO}^-)$ symmetrical and $\nu(\text{COO}^-)$ asymmetrical is investigated. The observed splitting between these peaks is 197 cm^{-1} , which is larger than 150 cm^{-1} . Therefore it can be concluded that formate forms a monodentate bond with the chromium ion at the analysed concentrations. In addition, from the observed splitting, it can be concluded that formate does not participate as bridging ligand. Therefore, the only possibility for Cr(III) to form clusters, is with SO₄²⁻, a hydroxide group or hydrogen bonding of the water molecules.

The limited excess of HCOO⁻ or HCOOH at the ratio of [Cr³⁺]:[HCOO⁻] = [1]:[1.61], gives a strong indication that the complex formed contains two or three HCOO⁻ molecules. However, the large increase of free HCOO⁻ between [Cr³⁺]:[HCOO⁻] = [1]:[1.61] and [Cr³⁺]:[HCOO⁻] = [1]:[3.32] makes the option of two HCOO⁻ molecules more likely. When the DFT point energy calculations are considered, it is suspected that the complex formed includes one or two HCOO⁻ molecules as the substitution reactions towards these complexes were clearly negative. However, based on the significant differences between λ_{Max} (424 nm, 420 nm and 407 nm) in the UV-Vis spectra of Cr₂(SO₄)₃ without the addition of HCOO⁻, Cr₂(SO₄)₃ with the addition of HCOO⁻ and Cr(ClO₄)₃ respectively, and the observed differences in band gap in the HOMO LUMO simulations, the presence of [Cr(H₂O)₄(HCOO)₂]⁺ in the electrolytes would explain the significant shift in wavelengths better. Since the large difference between 424 nm, 420 nm and 407 nm, indicate a larger difference in band gap between complexes in Cr(ClO₄)₃ (expected to be [Cr(H₂O)₆]³⁺) and the other two Cr₂(SO₄)₃ solutions with and without HCOO⁻.

To conclude, based on all the findings in this study, the complexation with one or two HCOO⁻ groups is considered most likely. Besides, the transition point in the complex formation is found to be between the ratio of [Cr³⁺]:[HCOO⁻] is respectively [1]:[1.61] and [1]:[3.32]. Finally, the bonding of HCOO⁻ to chromium is as monodentate at all analysed concentrations

concentrations.

2. Can DFT computational studies be used in predicting complexation and substitution reactions?

In this study, DFT successfully predict a red bathochromic or blue hypsochromic shift in UV-Vis spectra. This conclusion is based on the studied molecular orbitals and changes in the bandgap affected by ligand exchange, which match the experimental data found in this study. As a result, the following order of the spectrochemical species of the species HCOO^- , SO_4^{2-} and H_2O is concluded:

- $\text{SO}_4^{2-} < \text{HCOO}^- < \text{H}_2\text{O}$

In this order, H_2O will produce the largest splitting of the d-orbitals and SO_4^{2-} the smallest.

Next, it is considered that performing point energy calculations on the ligand substitution reactions can provide indicative data on the most likely complexation and ligand exchange. However, it is required to test multiple functionals to determine whether there is a general agreement on the spontaneous character of the ligand substitution. Besides, it is considered necessary that the energy difference between both sides of the equation is significantly (larger than 0.5 eV) to be certain that the reaction is spontaneous. In this study, only the substitutions up to and including the second formate molecule are considered significant enough to conclude this reaction's spontaneous character.

Simulation of IR spectra in this study has not been successful in reproducing the experimental data. In this study, the simulated IR spectra can not be used to predict the complexation of Cr(III) complexes due to the too large difference between experimentally observed data and simulated data. However, if calculations can be performed that include solvent effects, without creating imaginary frequencies, the data is expected to be more realistic.

Finally, it is found that the simulated UV-Vis spectra have not been successful in reproducing the experimental found UV-Vis data. There are too large differences in the observed values of λ_{Max} and the simulated values for λ_{Max} . The simulated spectra of some complexes are successful in predicting a similar shape as the experimental found data of $\text{Cr}_2(\text{SO}_4)_3$ electrolytes. However, this information is already available in other studies, which makes these experiments redundant. From these results, it has to be concluded that TD-DFT is not suitable for predicting the correct positions λ_{Max} of the low energy Laporte forbidden transitions in Cr(III) complexes. TD-DFT is especially unsuitable for the prediction of the location in the first transition peak, which only depends on the ligand field splitting parameter Dq .

3. Is the effect of formate concentration different in the presence of sulphate in the electrolytes?

The effect of sodium formate is indeed different in the presence of sulphate, but not in the way it was initially expected. The solutions created with $\text{Cr}_2(\text{SO}_4)_3$ are stored at 70 degrees for two days and studied with UV-Vis and ATR-FTIR. The UV-Vis and ATR-FTIR data shows that ligand substitution with HCOO^- occurs within 2 days at elevated temperature (and within 11 days at room temperature). A shift of 8 nm is observed in the first transition peak, showing a clear sign of ligand exchange.

In the experiments with $\text{Cr}(\text{ClO}_4)_3$, no ligand substitution occurs after one week. Subsequently, the solutions are stored at elevated temperatures to accelerate ligand substitution. After two weeks at elevated temperatures, still, no significant shifts (only 1 nm in UV-Vis) are visible in the UV-Vis spectra between the solutions of $\text{Cr}(\text{ClO}_4)_3$ in addition to sulphate or formate. There are small shifts visible in the second transition peak of the UV-Vis spectra, which can be caused by the more extensive electron-electron interaction in addition to sulphate. However, no significant shifts in the first peak are observed. Therefore, it is expected that no ligand exchange with sulphate has occurred due to the earlier mentioned high stability and inertness of the $[\text{Cr}(\text{H}_2\text{O})_6]^{3+}$ complex. It is expected that the presence of SO_4^{-2} in the chromium complex enhances ligand substitution of HCOO^- . As a result, it would be beneficial to choose for $\text{Cr}_2(\text{SO}_4)_3$ salts as those accelerates the ligand substitution. This insight into the enhanced ligand exchange from $\text{Cr}_2(\text{SO}_4)_3$ solutions could also help control the number of chromium-formate complexes in the solution in electroplating at an industrial scale. This, however, would be a recommendation for further research.

9 Recommendations

Based on the results of this thesis, the following recommendations for further research are suggested. The suggestions are organized in different categories:

Formate concentration

- To define the mechanism of Cr(III) deposition, correlations between the concentration of complexes in the electrolyte and the deposit's quality need to be made. However, to be able to conclude the effect of an excess of HCOO^- or a high concentration of chromium-formate complexes on the coating quality, plating experiments need to be conducted. The implementation a rotating electrode set-up is considered critical to ensure that no pH increase occurs in the diffusion layer. However, the implementation of a rotating electrode set-up was not possible in this study due to the limitations in equipment. Therefore, it is recommended for future studies to conduct plating experiments to test the deposit quality and composition in a specific range of concentrations. From this work, the ratios between $[\text{Cr}^{3+}]: [\text{HCOO}^-] = [1]:[0.4]$ and $[\text{Cr}^{3+}]: [\text{HCOO}^-] = [1]:[3.32]$ are considered most promising. The ratios until $[\text{Cr}^{3+}]: [\text{HCOO}^-] = [1]:[0.81]$ have the most complexes with only a slight excess of HCOO^- or HCOOH . Secondly, the ratio of c.a. $[\text{Cr}^{3+}]: [\text{HCOO}^-] = [1]:[3]$, is expected to have the highest concentration of chromium-formate complexes, but a larger degree of free HCOO^- in the electrolytes.
- The solutions created from $\text{Cr}_2(\text{SO}_4)_3$ formed a layer of solid deposit at the bottom of the bottles after a certain amount of time (expected is 3-4 weeks). This deposit made the solution unuseful for further experiments. This problem was only observed in electrolytes with a high concentration of NaHCOO . For further research, it is recommended to store the solutions at elevated temperatures to extend the lifetime. Besides, it is also recommended to include effects of temperature on the electrolytes since during electroplating at an industrial scale, the plating bath will also be at an elevated temperature.
- It is found that the use of $\text{Cr}_2(\text{SO}_4)_3$ as chromium salt shows a faster ligand exchange with formate than solutions created with $\text{Cr}(\text{ClO}_4)_3$. It is considered useful for further studies to investigate the effect of formate ion concentration on the electroplating efficiency in different chromium salts solutions. It is also considered useful to investigate mixtures of different chromium salt in addition of NaHCOO . As it is expected that a mixture of chromium salts might provide a more gradual supply of chromium-formate complexes in the electrolyte.
- The increase of pH in the diffusion layer is detrimental for the plating process of Cr-metal. However, in this study is suggested that when formate is present in a inner-sphere complex the process of olation could be slowed down due to the presence of formate groups in the complex. This is expected, since it could be more difficult to produce two hydroxo bridges between between the chromium complexes, visible in figure 4.2. Therefore, it is recommended to perform electroplating experiments at high chromium-formate complex concentrations with increased pH values, to test if a high concentration of chromium-formate complexes might have a beneficial effect on the plating bath efficiency. In the experiments presented in this study at pH 2.45 no bridging with HCOO^- is observed due to the large splitting between the COO^- modes.

Density functional theory

- It was observed that the application of solvation models in ORCA often resulted in the appearance of imaginary frequencies. Therefore, this data is expected to be unreliable. The following two possibilities are recommended to overcome these problems: 1) Running the calculations with an extreme tight SCF, a very large grid on a computer with large computational power. However, this is no guaranty the imaginary frequencies will disappear, as it is possible the system is unstable. 2) Instead of using a solvent model, the system can be built from different solvation shells of SO_4^{2-} , H_2O and HCOO^- molecules surrounding the Cr-atom(s), an example of this kind of system with multiple solvation shells is visualized in figure A.2 in appendix B. This type of calculation will require a large computational power, but is expected to mimic the experimental system better, as the system proposed in this study of only one chromium complex could be unstable.
- In this study is is concluded that TD-DFT is not successful in prediction the low energy Laporte forbidden transitions in this studies chromium complexes. This conclusion is based on the unsuccessful prediction of both locations of λ_{max} of the experimental spectra. Since these two transitions, are the only UV-Vis transitions studied in the experimental part of this study, the simulated and experimental data can not be compared. In literature, similar problems in the simulated spectra are observed by Vlahović et al. However, they successfully predict the peak positions of $[\text{Cr}(\text{H}_2\text{O})_6]^{3+}$ with LF-DFT (Ligand field DFT) which is part of the Ligand field theory. According to Vlahović et al. [95] LF-DFT is observed to give realistic data for the excitations of d^3 transition metal complexes. The dependence of the first low energy Laporte forbidden transition on only the splitting in the d-d orbitals and the double excitation character of $[\text{Cr}(\text{H}_2\text{O})_6]^{3+}$ are aspects of the system which makes it difficult to predict the system correctly.

The observed results with LF-DFT of Vlahović et al. on the $[\text{Cr}(\text{H}_2\text{O})_6]^{3+}$ complex is promising for the improvement of this studies results. Therefore, it is recommended to perform LF-DFT in stead of TD-DFT calculations for the specific Cr(III) complexes used in this study. It is expected that LF-DFT, is a more suitable calculation for the complexes in presented in this study, as TD-DFT could have a lack of orbital relaxation[95]. However, LF-DFT is not implemented in the ORCA software and a different software needs to be searched for these calculations. The TD-DFT calculations of this work can be of use if the experimental UV-Vis range can be extended to wavelengths below 280 nm.

- Finally, it is recommended to perform spectroscopic measurements in the lower ultra violet range of the light spectrum <280 nm. In this region the Laporte allowed transitions between metal and ligand can be studied. The results of these experiments can be compared to the simulated UV-Vis data of this study. However, the range of studied excitations need to be extended from 10 (used with PW91) to 20 (used with B3LYP in appendix C). It can be observed that the this region below 300 nm, the transitions in the simulated spectra so clear difference in the absorption peaks. These transitions are expected to be predicted more accurately with TD-DFT since the transitions are allowed and show no double excitation character.

Additional research techniques

- In the ATR-FTIR experiments, a Germanium crystal is used, which has a small penetration depth into the sample. As a result, the data corresponds to mainly the interface area

between the sample and crystal. However, for the data's reproducibility and correctness, it is recommended to conduct similar experiments with a crystal with a smaller refractive index, for example diamond, providing a larger penetration depth. As a result, a larger influence of the bulk of the sample is included in the measurement.

- In this study, the initial composition of complexes is studied without the application of a potential. As the main goal of this study was to investigate the effect of formate ion concentration in the initial composition of electrolytes. However, since electroplating is conducted under the application of potential, it is recommended to investigate the effect of applied potential on the solution chemistry. Therefore, for further study the following research techniques are recommended. Cyclic voltammetry experiments could be used to study the reduction reactions at the concentration range presented in this study. Subsequently, plating experiments can be conducted, after which secondary electron microscope (SEM) and X-ray photoelectron spectroscopy (XPS) experiments can be used for characterizing the deposit. However, for further studies, electrochemistry atomic force microscopy (EC-AFM) experiments of in-situ monitoring of the chromium(III) electrodeposition process is also considered very useful for determining the reduction mechanism. As this technique can be used to study the solid electrolyte interface area.

References

- [1] Zeng Z, Sun Y, Zhang J. The electrochemical reduction mechanism of trivalent chromium in the presence of formic acid. *Electrochemistry Communications*. 2009;11(2):331–334. Available from: <http://dx.doi.org/10.1016/j.elecom.2008.11.055>.
- [2] Kumar CSSR. *Nanotechnology Characterization Tools for Biosensing and Medical Diagnosis*. Springer; 2018.
- [3] Lucks C, Rossberg A, Tsushima S, Foerstendorf H, Fahmy K, Bernhard G. Formic acid interaction with the uranyl(vi) ion: Structural and photochemical characterization. *Dalton Transactions*. 2013;42(37):13584–13589.
- [4] Lancashire RJ. *Crystal Field Stabilization Energy*; 2020. Available from: [https://chem.libretexts.org/Bookshelves/Inorganic%20Chemistry/Modules%20and%20Websites%20\(Inorganic%20Chemistry\)/Crystal%20Field%20Theory/Crystal%20Field%20Stabilization%20Energy%20#:~:text=Definition%20of%20Crystal%20Field%20Stabilization%20Energy,configurationintheisotropicfield](https://chem.libretexts.org/Bookshelves/Inorganic%20Chemistry/Modules%20and%20Websites%20(Inorganic%20Chemistry)/Crystal%20Field%20Theory/Crystal%20Field%20Stabilization%20Energy%20#:~:text=Definition%20of%20Crystal%20Field%20Stabilization%20Energy,configurationintheisotropicfield).
- [5] Townsend T. *Electronic Spectroscopy: Interpretation*; 2020. Available from: [https://chem.libretexts.org/Bookshelves/Physical%20and%20Theoretical%20Chemistry%20Textbook%20Maps/Supplemental%20Modules%20\(Physical%20and%20Theoretical%20Chemistry\)/Spectroscopy/Electronic%20Spectroscopy/Electronic%20Spectroscopy%20%203A%20Interpretation](https://chem.libretexts.org/Bookshelves/Physical%20and%20Theoretical%20Chemistry%20Textbook%20Maps/Supplemental%20Modules%20(Physical%20and%20Theoretical%20Chemistry)/Spectroscopy/Electronic%20Spectroscopy/Electronic%20Spectroscopy%20%203A%20Interpretation).
- [6] Lever ABP. *Physical inorganic chemistry*. Amsterdam, Londen, New York: Elsevier; 1968.
- [7] Richens DT. Ligand substitution reactions at inorganic centers. *Chemical Reviews*. 2005;105(6):1961–2002.
- [8] Westerstrand M. *Process Water Geochemistry and Interactions With Magnetite at the Kiirunavaara Iron Mine , Northern Sweden Magnus Westerstrand*. September; 2015.
- [9] Burns RG. Crystal field effects in chromium and its partitioning in the mantle. *Geochimica et Cosmochimica Acta*. 1975;39(6-7):857–864.
- [10] Robert J Lancashire AA. *Crystal field theory*. Chemistry Libretexts. 2020. Available from: [https://chem.libretexts.org/Bookshelves/Inorganic%20Chemistry/Modules%20and%20Websites%20\(Inorganic%20Chemistry\)/Crystal%20Field%20Theory/Crystal%20Field%20Theory](https://chem.libretexts.org/Bookshelves/Inorganic%20Chemistry/Modules%20and%20Websites%20(Inorganic%20Chemistry)/Crystal%20Field%20Theory/Crystal%20Field%20Theory).
- [11] Johnson WR, Bart A H. Safety assesment of formic acid. *International journal of toxicology*. 2016.
- [12] Wiberg E, Wiberg N, Holleman AF. *Inorganic chemistry_ The chromium group*; 2001.
- [13] Jäger M, Freitag L, González L. Using computational chemistry to design Ru photosensitizers with directional charge transfer. *Coordination Chemistry Reviews*. 2015;304-305:146–165. Available from: <http://dx.doi.org/10.1016/j.ccr.2015.03.019>.
- [14] Chemguide. *Orbital Polarization Terms in Basis Sets*; 2020. Available from: <https://chem.libretexts.org/Courses/Pacific%20Union%20College/Quantum%20Chemistry/11%20%203A%20Computational%20Quantum%20Chemistry/11.04%20%203A%20Orbital%20Polarization%20Terms%20in%20Basis%20Sets>.

- [15] Chen J. Implicit solvent general principles. Kansas state univeristy. 2009. Available from: <https://www.k-state.edu/bmb/labs/jc/teaching/mdlectures/implicit-solvent.pdf>.
- [16] Kulig W. Introduction into solvation models - Organic chemistry Slides computational chemistry. HELSINKI, FINLAND; 2016. Available from: https://events.prace-ri.eu/event/455/attachments/369/551/solvation{_}models.pdf.
- [17] Daberdaku S. UCSF ChimeraX User Guide: Surface; 2021. Available from: <https://www.cgl.ucsf.edu/chimerax/docs/user/commands/surface.html>.
- [18] Vijayalaxmi Kinhal. Popularity of Metal Packaging is Increasing; 2018. Available from: <https://www.desjardin.fr/en/blog/popularity-of-metal-packaging-is-increasing>.
- [19] Insitution APEAL. Steel for packaging REACH compliant and in transfer to passivation.
- [20] Hagelüken C. The EU circular economy and its relevance to metal recycling. 2016;242–253.
- [21] Beck K. Properties & Uses of Steel; 2020. Available from: <https://sciencing.com/properties-uses-steel-7271721.html>.
- [22] view research G. Metal Packaging Market Size, Share & Trends Analysis Report By Application, Regional Outlook, Competitive Strategies, And Segment Forecasts, 2019 To 2025;. Available from: [grandviewresearch.com/industry-analysis/metal-packaging-market](https://www.grandviewresearch.com/industry-analysis/metal-packaging-market).
- [23] Richard Coles MJK. Food and beverage technologies; 2011.
- [24] Wijenberg. Method for electrodeposition of chromium containing coatings from trivalent chromium based electrolytes; 2014.
- [25] Zhang X, Boelen B, Beentjes P, Mol JMC, Terryn H, de Wit JHW. Influence of uniaxial deformation on the corrosion performance of pre-coated packaging steel. *Progress in Organic Coatings*. 2007;60(4):335–342.
- [26] Edy JE, McMurray HN, Lammers KR, DeVoos ACA. Kinetics of corrosion-driven cathodic disbondment on organic coated trivalent chromium metal-oxide-carbide coatings on steel. *Corrosion Science*. 2019;157(January):51–61. Available from: <https://doi.org/10.1016/j.corsci.2019.04.037>.
- [27] Wijenberg JHOJ, Steegh M, Aarnts MP, Lammers KR, Mol JMC. Electrodeposition of mixed chromium metal-carbide-oxide coatings from a trivalent chromium-formate electrolyte without a buffering agent. *Electrochimica Acta*. 2015;173:819–826. Available from: <http://dx.doi.org/10.1016/j.electacta.2015.05.121>.
- [28] Lindsay JH. Decorative & hard chromium plating. *Plating and Surface Finishing*. 2007;94(11):46–48.
- [29] Mandich BNV. *Chemistry & Theory of Chromium Deposition*:108–115.
- [30] Rengman S. When is it best to use, formic acid or sodium formate?; 2017. Available from: [https://www.perstorp.com/en/news{_}center/news/2017/20171114{_}formic{_}acid{_}vs{_}sodium{_}formate{_}#:~:text=Assodiumformateisvery,asformicacid\(HCOOH\)](https://www.perstorp.com/en/news{_}center/news/2017/20171114{_}formic{_}acid{_}vs{_}sodium{_}formate{_}#:~:text=Assodiumformateisvery,asformicacid(HCOOH).).

- [31] Lu CE, Pu NW, Hou KH, Tseng CC, Ger MD. The effect of formic acid concentration on the conductivity and corrosion resistance of chromium carbide coatings electroplated with trivalent chromium. *Applied Surface Science*. 2013;282:544–551. Available from: <http://dx.doi.org/10.1016/j.apsusc.2013.06.008>.
- [32] Chien CW, Liu CL, Chen FJ, Lin KH, Lin CS. Microstructure and properties of carbon-sulfur-containing chromium deposits electroplated in trivalent chromium baths with thiosalicylic acid. *Electrochimica Acta*. 2012;72:74–80. Available from: <http://dx.doi.org/10.1016/j.electacta.2012.03.168>.
- [33] Danilov FI, Protsenko VS, Gordiienko VO, Kwon SC, Lee JY, Kim M. Nanocrystalline hard chromium electrodeposition from trivalent chromium bath containing carbamide and formic acid: Structure, composition, electrochemical corrosion behavior, hardness and wear characteristics of deposits. *Applied Surface Science*. 2011;257(18):8048–8053. Available from: <http://dx.doi.org/10.1016/j.apsusc.2011.04.095>.
- [34] Song YB, Chin DT. Current efficiency and polarization behavior of trivalent chromium electrodeposition process. *Electrochimica Acta*. 2002;48(4):349–356.
- [35] Song YB, Chin DT. Pulse plating of hard chromium from trivalent baths. *Plating and Surface Finishing*. 2000;87(9):80–87.
- [36] Del Pianta D, Frayret J, Gleyzes C, Cugnet C, Dupin JC, Le Hecho I. Determination of the chromium(III) reduction mechanism during chromium electroplating. *Electrochimica Acta*. 2018;284:234–241.
- [37] Zeng Z, Zhang Y, Zhao W, Zhang J. Role of complexing ligands in trivalent chromium electrodeposition. *Surface and Coatings Technology*. 2011;205(20):4771–4775. Available from: <http://dx.doi.org/10.1016/j.surfcoat.2011.04.019>.
- [38] de Vooy ACA, Wijenberg JHOJ, Koper MTM. Cyclic voltammetry study of trivalent basic chromium sulphate electrolytes contaminated with sulphite. *Electrochimica Acta*. 2018;269:700–705.
- [39] Ghaziof S, Golozar MA, Raeissi K. Characterization of as-deposited and annealed Cr-C alloy coatings produced from a trivalent chromium bath. *Journal of Alloys and Compounds*. 2010;496(1-2):164–168. Available from: <http://dx.doi.org/10.1016/j.jallcom.2010.02.101>.
- [40] Protsenko, Gordiienko VO, Danilov FI, Kwon SC. Thick chromium electrodeposition from trivalent chromium bath containing carbamide and formic acid: An investigation into current efficiency, electrodeposition rate and surface morphology. *Metal Finishing*. 2011;109(4-5):33–37.
- [41] Fogel BN, Tai JMJ, Yarborough J. Chromium (III) Sulfate in Acid Sulfate Solutions. *Journal of the American Chemical Society*. 1962;84(7):1145–1151.
- [42] Lucks C, Rossberg A, Tsushima S, Foerstendorf H, Scheinost AC, Bernhard G. Aqueous uranium(VI) complexes with acetic and succinic acid: Speciation and structure revisited. *Inorganic Chemistry*. 2012;51(22):12288–12300.
- [43] Xu L, Pi L, Dou Y, Cui Y, Mao X, Lin A, et al. Electroplating of Thick Hard Chromium Coating from a Trivalent Chromium Bath Containing a Ternary Complexing Agent: A Methodological and Mechanistic Study. *ACS Sustainable Chemistry & Engineering*. 2020.

- [44] Reddy SL, Endo T, Reddy GS. Electronic (Absorption) Spectra of 3d Transition Metal Complexes; 2012.
- [45] Chemguide. UV-Vis visible absorbtion spectra;. Available from: <https://www.chemguide.co.uk/analysis/uvvisible/theory.html>.
- [46] Mehta A. Ultraviolet-Visible (UV-Vis) Spectroscopy – Limitations and Deviations of Beer-Lambert Law; 2012. Available from: <https://pharmaxchange.info/2012/05/ultraviolet-visible-uv-vis-spectroscopy-â–limitations-and-deviations-of-beer-lambert>
- [47] Tsuchida R. Absorption Spectra of Co-ordination Compounds. II. Bulletin of the Chemical Society of Japan. 1938;13(6):436–450.
- [48] Mead A. Absorption Spectra , in Aqueous Solution ,. Transactions of the faraday Society. 1934;30:1052–1058.
- [49] Chris P Schaller PD. B.2. Spectrochemical Series; 2019. Available from: chem.libretexts.org/Courses/Saint_Marys_College_Notre_Dame_IN/CHEM_342%3A_Bio-inorganic_Chemistry/Readings/Purgatory/Chapter_3%3A_Introduction_to_Advanced_Bonding_Theories/3.2_Ligand_Field_Theory/B._Ligand_Field_Theory/B.2._Spectrochemical_Series.
- [50] Shimadzu. Spectral Characteristics Dependent on ATR Crystal Selection – Differences in Properties (Shape, Hardness, Refractive Index). Application News. 2015;A485.
- [51] Topala CM. Temperature effects on the FTIR spectra of ribavirin. Revista de Chimie. 2013;64(2):132–135.
- [52] Nandiyanto ABD, Oktiani R, Ragadhita R. How to read and interpret ftir spectroscopie of organic material. Indonesian Journal of Science and Technology. 2019;4(1):97–118.
- [53] Nara M, Morii H, Tanokura M. Coordination to divalent cations by calcium-binding proteins studied by FTIR spectroscopy. Biochimica et Biophysica Acta - Biomembranes. 2013;1828(10):2319–2327. Available from: <http://dx.doi.org/10.1016/j.bbamem.2012.11.025>.
- [54] Nara M, Torii H, Tasumi M. Correlation between the vibrational frequencies of the carboxylate group and the types of its coordination to a metal ion: An ab initio molecular orbital study. Journal of Physical Chemistry. 1996;100(51):19812–19817.
- [55] Mizuguchi M, Nara M, Kawano K, Nitta K. FT-XR study of the Ca²⁺-binding to bovine α -lactalbumin. Relationships between the type of coordination and characteristics of the bands due to the Asp COO⁻ groups in the Ca²⁺-binding site. FEBS Letters. 1997;417(1):153–156. Available from: [http://dx.doi.org/10.1016/S0014-5793\(97\)01274-X](http://dx.doi.org/10.1016/S0014-5793(97)01274-X).
- [56] Phuong NV, Kwon SC, Lee JY, Lee JH, Lee KH. The effects of pH and polyethylene glycol on the Cr(III) solution chemistry and electrodeposition of chromium. Surface and Coatings Technology. 2012;206(21):4349–4355. Available from: <http://dx.doi.org/10.1016/j.surfcoat.2012.04.025>.
- [57] Paunovic M. Fundamentals of electrochemical deposition; 1998.

- [58] Börgel J, Campbell MG, Ritter T. Transition Metal d-Orbital Splitting Diagrams: An Updated Educational Resource for Square Planar Transition Metal Complexes. *Journal of Chemical Education*. 2016;93(1):118–121.
- [59] Lancashire R.J. Selection Rules for Electronic Spectra of Transition Metal Complexes; 2020. Available from: [chem.libretexts.org/Bookshelves/Physical_and_Theoretical_Chemistry_Textbook_Maps/Supplemental_Modules_\(Physical_and_Theoretical_Chemistry\)/Spectroscopy/Electronic_Spectroscopy/Selection_Rules_for_Electronic_Spectra_of_Transition_Metal_Complexes](https://chem.libretexts.org/Bookshelves/Physical_and_Theoretical_Chemistry_Textbook_Maps/Supplemental_Modules_(Physical_and_Theoretical_Chemistry)/Spectroscopy/Electronic_Spectroscopy/Selection_Rules_for_Electronic_Spectra_of_Transition_Metal_Complexes).
- [60] Hill H. *Physical Methods in Advanced Inorganic Chemistry*. John Wiley & Sons, Inc.; 1968.
- [61] Crabtree R. *The organometallic chemistry of the transition metals*. 4th ed. John Wiley and Sons; 2005.
- [62] CC-BY-SA. Ligand Substitution Reactions; 2020. Available from: https://chem.libretexts.org/Bookshelves/Inorganic_Chemistry/Book%3A_Introduction_to_Inorganic_Chemistry/05%3A_Coordination_Chemistry_and_Crystal_Field_Theory/5.03%3A_Ligand_Substitution_Reactions.
- [63] Cerar J. Reaction between Chromium (III) and EDTA Ions : an Overlooked Mechanism of Case Study Reaction. 2015;(Iii):538–545.
- [64] Dalal M. *A Textbook of Inorganic Chemistry – Volume 1 Chapter 3*. Dalal Institute; 2017.
- [65] Begel S, Illner P, Kern S, Puchta R, Van Eldik R. Mechanistic studies on fast ligand substitution reactions of Pt(II) in different ionic liquids: Role of solvent polarity and ion-pair formation. *Inorganic Chemistry*. 2008;47(16):7121–7132.
- [66] van Eldik R, Erdik T, le Noble WJ. Activation and Reaction Volumes in Solution. *Chemical Reviews*. 1989;89(8):1981.
- [67] Dei JK, Pasupalak NN, Mohanty P. Kinetics and mechanism of the reaction of aquachromium(III) with L-ascorbic acid in aqueous media. *Transition Metal Chemistry*. 1997;22(5):516–520.
- [68] Creutz C, Ford PC, Meyer TJ. Henry taube: Inorganic chemist extraordinaire. *Inorganic Chemistry*. 2006;45(18):7059–7068.
- [69] Bennett MA, Clark RJH, Goodwin ADJ. Electronic and Infrared Spectral Study of Chromium (III) Derivatives of The Type $[\text{Cr}(\text{NCS})_4(\text{Ligand})_2]$ -. *Inorganic Chemistry*. 1967;6(9):1625–1631.
- [70] Lancashire R.J. Geometric Isomers in Transition Metal Complexes; 2020. Available from: [https://chem.libretexts.org/Bookshelves/Inorganic_Chemistry/Modules_and_Websites_\(Inorganic_Chemistry\)/Coordination_Chemistry/Structure_and_Nomenclature_of_Coordination_Compounds/Isomers/Stereoisomers%3A_Geometric_Isomers_in_Transition_Metal_Complexes](https://chem.libretexts.org/Bookshelves/Inorganic_Chemistry/Modules_and_Websites_(Inorganic_Chemistry)/Coordination_Chemistry/Structure_and_Nomenclature_of_Coordination_Compounds/Isomers/Stereoisomers%3A_Geometric_Isomers_in_Transition_Metal_Complexes).
- [71] Alan J Jircitano. An Evaluation of The Spectrochemical Series: The Preparation and Spectroscopy of Chromium(III) Complexes. 2015;(Iii):4. Available from: <http://chemistry.bd.psu.edu/jircitano/Spectrochemical.pdf>.

- [72] Danilov FI, Protsenko VS, Butyrina TE, Krasinskii VA, Baskevich AS, Kwon SC, et al. Electrodeposition of nanocrystalline chromium coatings from cr(iii)-based electrolyte using pulsed current. *Protection of Metals and Physical Chemistry of Surfaces*. 2011;47(5):598–605.
- [73] Dalius Sagatys AGTBHLJBBCMPWSL. *Chemistry: The Central Science*. New York: Pearson; 2013.
- [74] Mandich NV, Fellow A. pH , Hydrogen Evolution & Their Significance In Electroplating Operations;(4):2–5.
- [75] Novinson E. The Effect of pH in Electroplating; 2017. Available from: <https://sciencing.com/the-effect-of-ph-in-electroplating-13636685.html>.
- [76] Su X, Qiang C. Influence of pH and bath composition on properties of Ni-Fe alloy films synthesized by electrodeposition. *Bulletin of Materials Science*. 2012;35(2):183–189.
- [77] MicroChemicals. Electroplating basics - Basics of microstructuring. *MicroChemicals Basics of Microstructuring*. 2020;1:17. Available from: https://www.microchemicals.com/technical{_}information/plating{_}theory.pdf.
- [78] Mandich NV, Snyder DL. Electrodeposition of Chromium. *Modern Electroplating: Fifth Edition*. 2011:205–248.
- [79] Tu Z, Yang Z, Zhang J. Cathode polarization in trivalent chromium plating. *Plating and Surface Finishing*. 1993;80(November):79–82. Available from: <http://infohouse.p2ric.org/ref/25/24554.pdf>.
- [80] institute of biomedical imaging, Bioengineering N. *Computational Modeling*; 2020. Available from: <https://www.nibib.nih.gov/science-education/science-topics/computational-modeling>.
- [81] Kohn W, Becke AD, Parr RG. Density functional theory of electronic structure. *Journal of Physical Chemistry*. 1996;100(31):12974–12980.
- [82] Truhlar DG. *Density Functional Theory*. Minnesota: Department of Chemistry, University of Minnesota; 2014.
- [83] Cramer C. *University of Minnesota Chem 4021/8021 Computational Chemistry*. Minnesota: University of Minnesota; 2014. Available from: http://pollux.chem.umn.edu/8021/Lectures/DFT{_}10.pdf.
- [84] Rappoport D, Crawford NRM, Furche F, Burke K. Approximate Density Functionals: Which Should I Choose? *Encyclopedia of Inorganic and Bioinorganic Chemistry*. 2011.
- [85] Comba P, Hausberg S, Martin B. Calculation of exchange coupling constants of transition metal complexes with DFT. *Journal of Physical Chemistry A*. 2009;113(24):6751–6755.
- [86] Qi SC, Hayashi JI, Zhang L. Recent application of calculations of metal complexes based on density functional theory. *RSC Advances*. 2016;6(81):77375–77395.
- [87] Jensen F. *Introduction to Computational chemistry*. John Wiley & Sons, Inc.; 2016.
- [88] Weigend F, Ahlrichs R. Balanced basis sets of split valence, triple zeta valence and quadruple zeta valence quality for H to Rn: Design and assessment of accuracy. *Physical Chemistry Chemical Physics*. 2005;7(18):3297–3305.

- [89] Jensen F. Polarization consistent basis sets . VIII . The transition metals Sc-Zn Polarization consistent basis sets . VIII . The transition metals Sc-Zn. 2013;014107(December 2012).
- [90] Zinola CF. Density functional theory. Electrocatalysis: Computational, Experimental, and Industrial Aspects. 2010:117–138.
- [91] Zhang J, Zhang H, Wu T, Wang Q, Spoel DVD. Comparison of Implicit and Explicit Solvent Models for the Calculation of Solvation Free Energy in Organic Solvents. 2017.
- [92] Tomasi J, Mennucci B, Cammi R. Quantum mechanical continuum solvation models. Chemical Reviews. 2005;105(8):2999–3093.
- [93] Barone V, Cossi M. Quantum calculation of molecular energies and energy gradients in solution by a conductor solvent model. Journal of Physical Chemistry A. 1998;102(11):1995–2001.
- [94] Marenich AV, Cramer CJ, Truhlar DG. Universal solvation model based on solute electron density and on a continuum model of the solvent defined by the bulk dielectric constant and atomic surface tensions. Journal of Physical Chemistry B. 2009;113(18):6378–6396.
- [95] Vlahović F, Perić M, Gruden-Pavlović M, Zlatar M. Assessment of TD-DFT and LF-DFT for study of d - D transitions in first row transition metal hexaaqua complexes. Journal of Chemical Physics. 2015;142(21):14. Available from: <http://dx.doi.org/10.1063/1.4922111>.
- [96] Neese F, Wennmohs F, Aravena D, Atanasov M, Becker U, Bykov D. Orca 4.0.1. Wiley Interdiscip Rev: Comput Mol Sci. 2012;2(1):73–78.
- [97] Liu Y, Sun X, Gahungu G, Qu X, Wang Y, Wu Z. DFT/TDDFT Investigation on the electronic structures and photophysical properties of phosphorescent Ir (III). 3700–3709. 2013:3700–3709.
- [98] Jornet-somoza J, Lebedeva I. Real-Time Propagation TDDFT and Density Analysis for Exciton Coupling Calculations in Large Systems. 2019;(ii).
- [99] Grimme S. A simplified Tamm-Dancoff density functional approach for the electronic excitation spectra of very large molecules. Journal of Chemical Physics. 2013;138(24).
- [100] Grimme S, Parac M. Substantial errors from time-dependent density functional theory for the calculation of excited states of large π systems. ChemPhysChem. 2003;4(3):292–295.
- [101] Hanwell MD. Avogadro: an open-source molecular builder and visualization tool; 2012.
- [102] Weigend F, Ahlrichs R. Balanced basis sets of split valence, triple zeta valence and quadruple zeta valence quality for H to Rn: Design and assessment of accuracy. Physical Chemistry Chemical Physics. 2005;7(18):3297–3305.
- [103] Bjornsson R. ORCA Input Library; 2020. Available from: <https://sites.google.com/site/orcainputlibrary/dft>.
- [104] Neese F. The ORCA program system. Wiley Interdiscip.; 2012.
- [105] Menges F. Spectragryph - optical spectroscopy software; 2020.

- [106] Liu W, Christian JH, Al-Oweini R, Bassil BS, Van Tol J, Atanasov M, et al. Synthesis, detailed characterization, and theoretical understanding of mononuclear chromium(III)-containing polyoxotungstates with exceptionally large magnetic anisotropy. *Inorganic Chemistry*. 2014;53(17):9274–9283.

A Appendix: Background figures

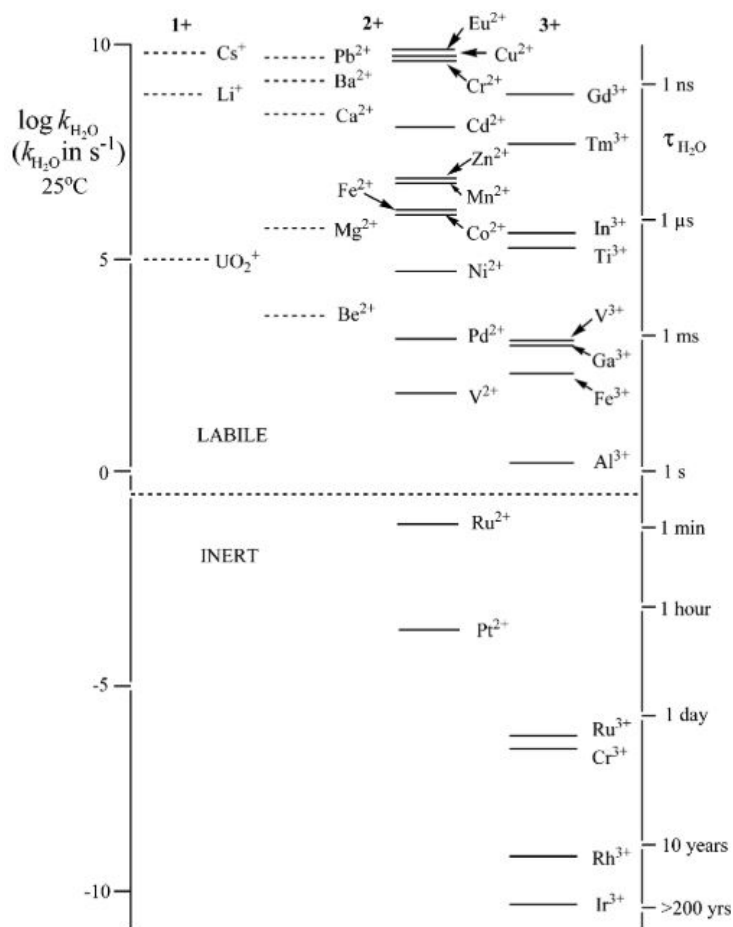


Figure A.1: Range of water exchange rate constants and mean lifetime (H_2O) for primary shell water molecules on aqua metal ions at 25 °C (the dotted line represents Taube's inert/labile boundary[7])

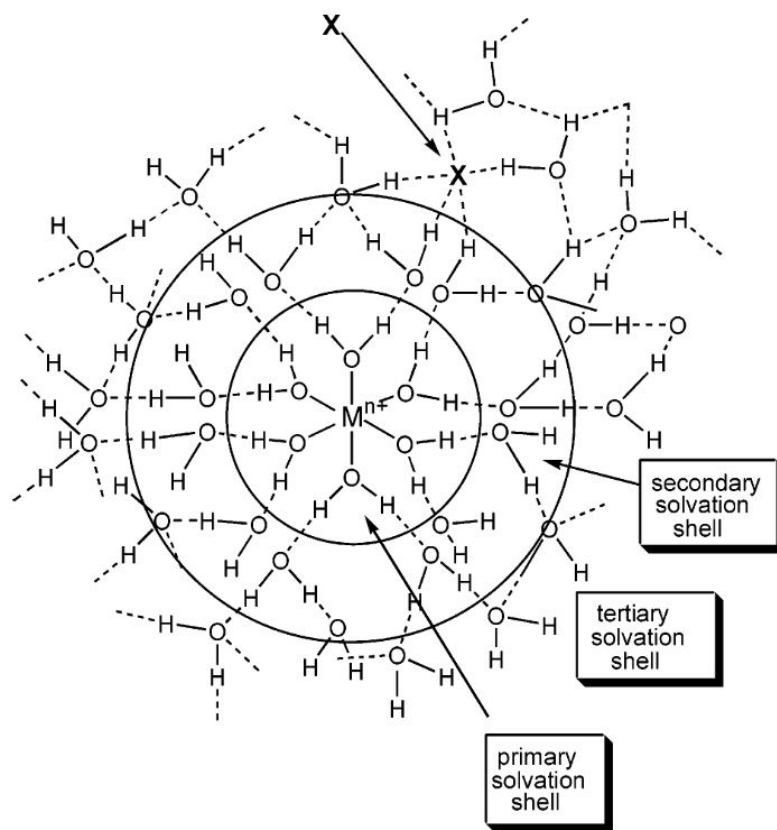


Figure A.2: Visualisation of solvation-shells around metal-ion[7], X can be an example of additional compounds introduced in the system

B Appendix: ATR-FTIR results

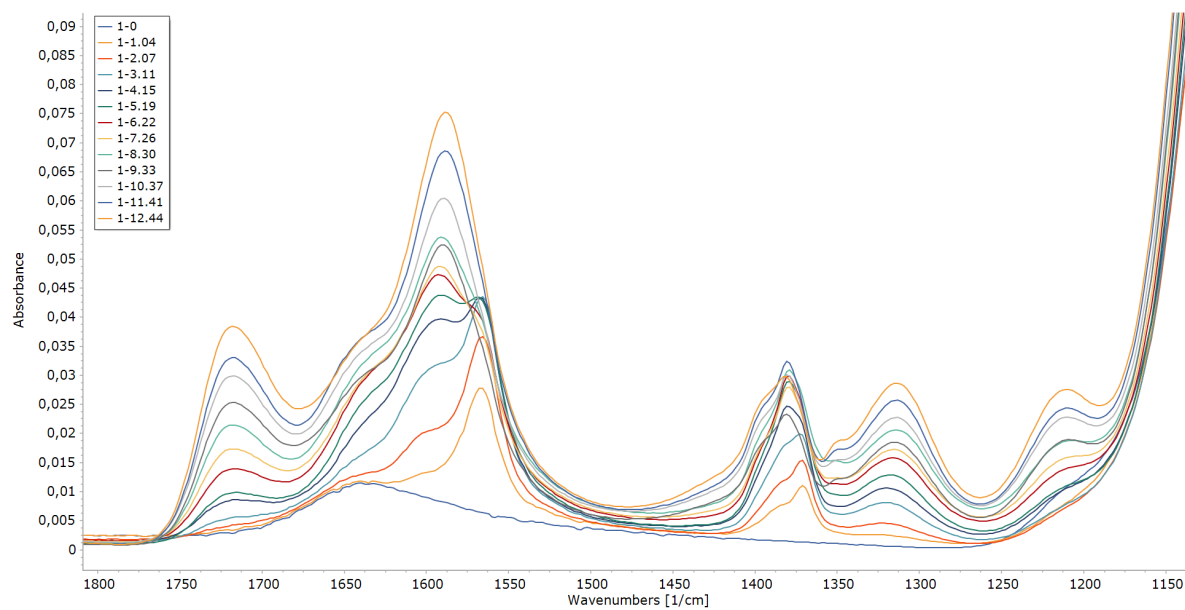


Figure B.1: ATR-FTIR Data of (incorrect) first batch Cr(OH)SO₄ solutions in addition of NaHCOO for comparison of similar results

C Appendix: DFT results

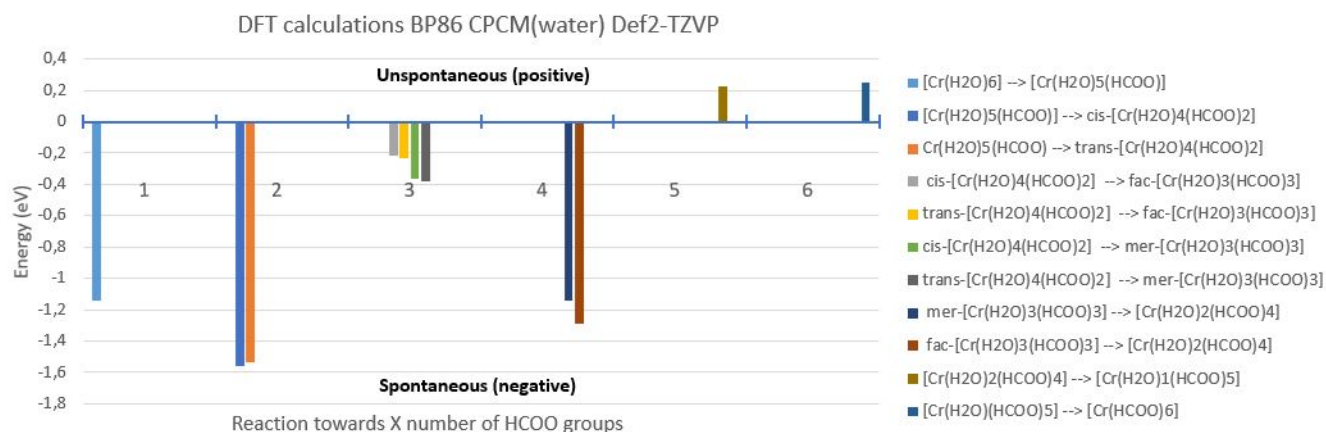


Figure C.1: Results DFT point energy calculations BP86 reaction 16 till 21

Equation	PW91 ΔE in eV	PB86 Δ in eV	Tendency
16	-1,160	-1,143	Spontaneous
17	-1,567(Trans) ; -1,588(Cis)	-1,539(Trans) ; -1,557(Cis)	Spontaneous
18	-0,216(Cis-Fac) -0,237(Trans-Fac) -0,395(Trans-Mer) -0,375(Cis-Mer)	-0,214(Cis-Fac) -0,232(Trans-Fac) -0,384(Trans-Mer) -0,365(Cis-Mer)	Spontaneous
19	-1,328 (Fac) ; -1,170 (Mer)	-1,292 (Fac) ; -1,141 (Mer)	Spontaneous
20	0,200	0,224	Unspontaneous
21	0,243	0,252	Unspontaneous

Table C.1: DFT point calculations of reactions 16 till 21 with PW91 and PB86 and CPCM solvation model

Equation	PW91 ΔE in eV	PB86 ΔE in eV	Tendency
16	-0,912	-0,900	Spontaneous
17	-1,319(Trans) ; -1,344(Cis)	-1,309(Trans) ; -1,283(Cis)	Spontaneous
18	-0,186(Cis-Fac) -0,211(Trans-Fac) -0,326(Trans-Mer) -0,301(Cis-Mer)	-0,290(Cis-Fac) -0,315(Trans-Fac) -0,172(Trans-Mer) -0,198(Cis-Mer)	Spontaneous
19	-1,018 (Fac) ; -1,133 (Mer)	-0,989 (Fac) ; -1,107 (Mer)	Spontaneous

Table C.2: DFT point calculations of reactions 16 till 19 with PW91 and PB86 and SMD solvation model

Equation	PW91 ΔE in eV	PB86 Δ in eV	Tendency
22	-1,120	-1,070	Spontaneous
23	-0,624(Cis) ; -0.357(Trans)	-0,583(Cis) ; -0.377(Trans)	Spontaneous
24	-0,485(Cis-Fac) -0.758(Trans-Fac) 4.537(Trans-Mer) 4.804(Cis-Mer)	-0,489(Cis-Fac) -0.695(Trans-Fac) 4.636(Trans-Mer) 4.842(Cis-Mer)	Spontaneous/ Unspontaneous
25	-0,142 (Fac) ; -5.431 (Mer)	-0,132(Fac) ; -5.488 (Mer)	Favourable
26	-0,229	-0,216	Spontaneous
27	1,391	1,084	Unspontaneous

Table C.3: DFT point calculations of reactions 22 till 27 with PW91 and PB86 and CPCM solvation model

Equation	PW91 ΔE in eV	PB86 Δ in eV	Tendency
28	1,486	1,467	Unspontaneous
29	1,018 Cis ; 1.018 Trans	0,981 Cis ; 0.999 Trans)	Unspontaneous
30	1,425(Cis-Fac) 1.158(Trans-Fac) 0.999(Trans-Mer) 1.266(Cis-Mer)	1,350(Cis-Fac) 1.144(Trans-Fac) 0.993(Trans-Mer) 4.842(Cis-Mer)	Unspontaneous
31	0,588 (Fac) ; -4.707 (Mer)	0,572(Fac) ; -4.784 (Mer)	Unspontaneous/ Spontaneous
32	0,924	0,928	Unspontaneous
33	1,396	1,084	Unspontaneous

Table C.4: DFT point calculations of reactions 28 till 33 with PW91 and PB86 and CPCM solvation model

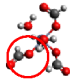
Cr(H ₂ O) ₆ (cm ⁻¹)	Vibration	Cr(H ₂ O) ₅ (HCOO) (cm ⁻¹)	Vibration
1600-1624	Symmetric and asymmetric scissoring and wagging of water molecules	1301	Scissoring and wagging of the hydrogen atom in the HCOO molecule
3552	Symmetrical stretching of hydrogens in water molecules	1568-1598	Scissoring and wagging of the hydrogen atoms in the water molecules causing the double C=O bond to rotate.
3626	Asymmetrical stretching of hydrogens in water molecules	1770.9	Stretching of the double C=O bond in the HCOO molecule
		3586-3639	Symmetrical stretching of hydrogens in water molecules
		3690- 3716	Asymmetrical stretching of hydrogens in water molecules
Trans (cm ⁻¹)	Type of vibration	Cis (cm ⁻¹)	Type of vibration
1016	Symmetric and asymmetric wagging and scissoring of the hydrogen atoms at the HCOO groups	1068, 1102	Asymmetric and symmetric stretching of C-O bonds in the HCOO groups, also affecting the O-Cr and C=O bonds in the groups
1191-1226	Hydrogen atoms in the water molecules close to double C=O bond interacting with it	1329-1333	In and out of plane scissoring of the hydrogen atoms at the HCOO groups
1276-1345	Asymmetric and symmetric stretching of C-O bonds in the HCOO groups	1570-1587	Symmetric and asymmetric scissoring and wagging of water molecules
1577-1597	In and out of plane scissoring of the hydrogen atoms at the H ₂ O groups	1741	Asymmetric stretching of the C=O bond
3000	Stretching of the hydrogen atom at the carbon	1749	Symmetric stretching of the C=O bond
1742-1752	Asymmetric stretching of the C=O bond	2881-2889	Scissor and wagging of the hydrogen atoms in the HCOO groups
3600-3700	Scissoring of the hydrogen atoms in the water molecules coupled to the double rotation of the C=O bond in HCOO		
Fac (cm ⁻¹)	Type of vibration	Mer (cm ⁻¹)	Type of vibration
1148-1182	Symmetric and asymmetric stretching of single O-C bonds of the HCOO groups	1170-1311	Separated asymmetric stretching vibrations of single O-C bonds of the HCOO groups and a small stretching in the Cr-O bond.
1341	In and out of plane movement of hydrogen atoms in the HCOO group	1345-1354	In and out of plane movement of hydrogen atoms in the HCOO group
1565-1571	Scissoring of the hydrogen atoms in the water molecules coupled to the double rotation of the C=O bond in the HCOO molecules	1445-1543	Scissoring of the hydrogen atoms in the water molecules. Only effecting one HCOO group with C=O bond in the direction of the water molecule movement.
1709-1723	Symmetric and asymmetric stretching in the HCOO group of C=O bond	1607	Stretching of the C=O bond in the HCOO group orientated farther away than the other two. 

Figure C.2: Vibrational spectra analysis of chromium-formate complexes

2877-2881	Symmetric and asymmetric stretching of the hydrogen atoms in the HCOO groups	1709-1725	Symmetric and asymmetric stretching in other two of the HCOO group of C=O bond
		2748-2943	Separated asymmetric stretching of the hydrogen atoms in the HCOO groups
Cr(H ₂ O) ₂ (HCOO) ₄ (cm ⁻¹)	Vibrations	Cr(H ₂ O)(HCOO) ₅ (cm ⁻¹)	Vibrations
1089.9	H ₂ O molecules interacting with the double-bonded oxygen	1068	H ₂ O molecule rotating
1235-1329	Separated combinations of symmetric and asymmetric stretching of single C-O bond in HCOO groups	1273-1318	Separated combinations of symmetric and asymmetric stretching of single C-O bond in HCOO groups
1349-1358	In and out plane bending of hydrogen atoms at the HCOO groups (low absorption)	1348-1358	In and out plane bending of hydrogen atoms at the HCOO groups (low absorption)
1566-1575	Stretching of the double C=O bond in three HCOO molecules orientated towards each other	1450	H ₂ O molecule affecting the stretching of double C=O bond in the surrounding HCOO groups
1602-1615	Scissoring of the water molecules affecting the stretching of the double bond of the close laying HCOO group	1593-1670	Asymmetric stretching of the C-O and C=O bonds in the HCOO groups
1668	Stretching of the forth HCOO group orientated away from the others	2657-2815	Separated stretching of the hydrogen atoms at the HCOO groups
2501, 2828, 2916	Stretching of hydrogen atoms in H ₂ O and HCOO molecules affecting double C=O bond in HCOO groups	3100, 3237	Symmetric and asymmetric stretching in the H ₂ O molecule

Figure C.3: Vibrational spectra analysis of chromium-formate complexes

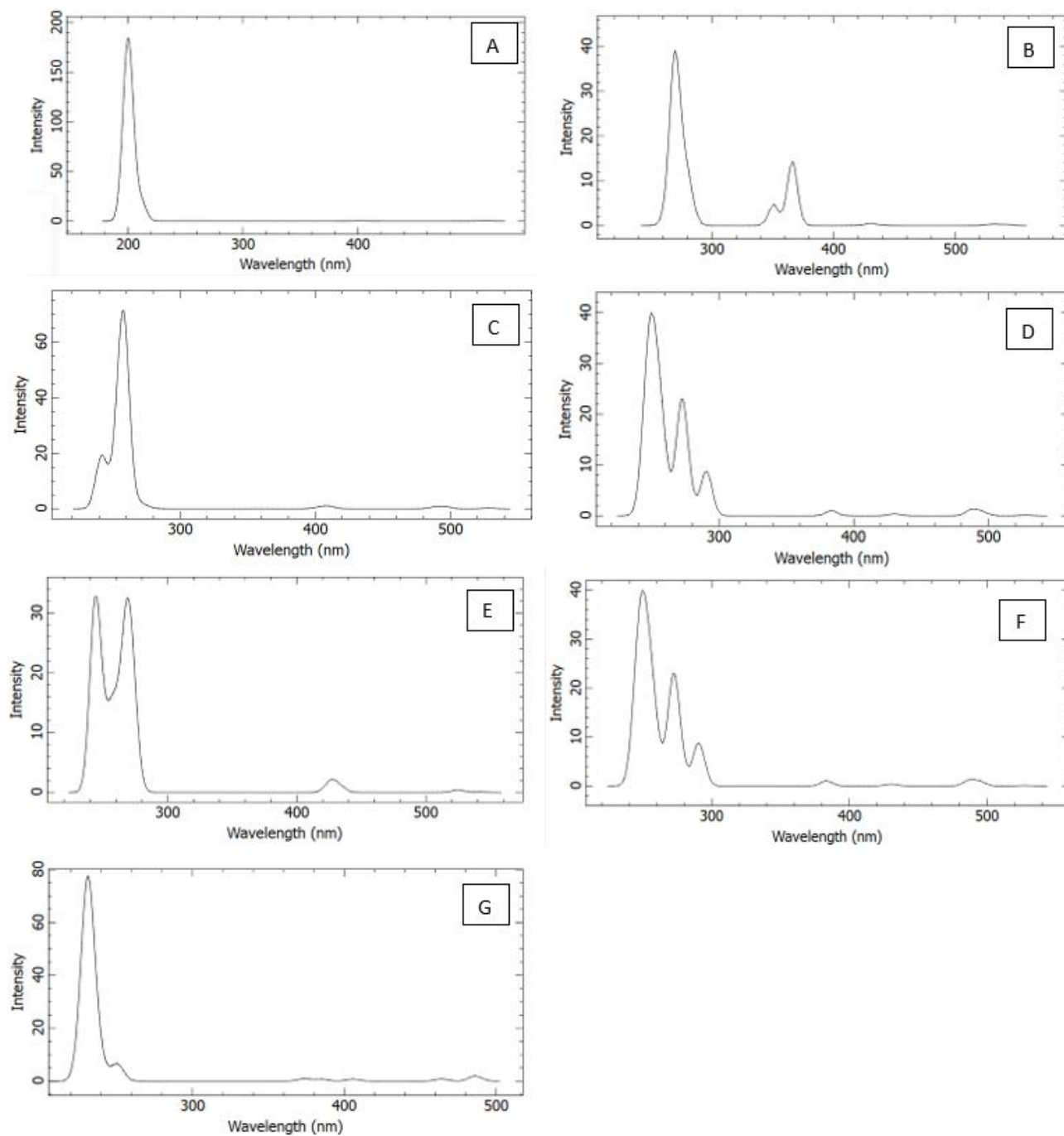


Figure C.4: Results TD-DFT with B3LYP of **a)** $[\text{Cr}(\text{H}_2\text{O})_6]^{3+}$ **b)** $[\text{Cr}(\text{H}_2\text{O})_5(\text{HCOO})]^{2+}$ **c)** *trans*- $[\text{Cr}(\text{H}_2\text{O})_4(\text{HCOO})_2]^+$ **d)** *cis*- $[\text{Cr}(\text{H}_2\text{O})_4(\text{HCOO})_2]^+$ **e)** *fac*- $[\text{Cr}(\text{H}_2\text{O})(\text{HCOO})_3]$ **f)** *mer*- $[\text{Cr}(\text{H}_2\text{O})(\text{HCOO})_3]$ **g)** $[\text{Cr}(\text{H}_2\text{O})_2(\text{HCOO})_4]^-$